Dissertation

submitted to the

Combined Faculties of the Natural Sciences and Mathematics

of the Ruperto-Carola-University of Heidelberg, Germany

for the degree of

Doctor of Natural Sciences

Put forward by

Sven Ahrens, M.Sc.

born in Erfurt

Oral examination: 14.11.2012

Investigation of the Kapitza-Dirac effect in the relativistic regime

Referees: Honorarprof. Dr. Christoph H. Keitel
Priv.-Doz. Dr. Andrey Surzhykov

Zusammenfassung

Quantenmechanische Beugungseffekte sind von besonderem Interesse, da sie unserer Alltagserfahrung widersprechen. Diese theoretische Arbeit befasst sich mit der Beugung von Elektronen an stehenden Lichtwellen, dem sogenannten Kapitza-Dirac Effekt. Ein besonderer Fokus wird dabei auf eine spezielle Variante des Kapitza-Dirac Effektes gelegt, in welcher das Elektron mit drei Photonen wechselwirkt. Eine besondere Eigenschaft dieses 3-Photonen Kapitza-Dirac Effektes ist, dass in diesem Fall der Spin des Elektrons bei der Beugung am optischen Gitter gedreht wird.

Die theoretischen Rechnungen in dieser Arbeit basieren auf verschiedenen relativistischen und nicht-relativistischen quantenmechanischen Wellengleichungen, die im Impulsraum formuliert werden. Einerseits wird die quantenmechanische Dynamik der gebeugten Elektronen numerisch im Impulsraum gelöst, um die Eigenschaften des 3-Photonen Kapitza-Dirac Effektes detailliert herauszuarbeiten. Andererseits werden die Gleichungen mit zeitabhängiger Störungstheorie gelöst und den numerischen Ergebnissen gegenüber gestellt.

Im Gegensatz zu der von Kapitza und Dirac vorgeschlagenen Elektronenbeugung unter Beteiligung zweier Photonen, ist die Anzahl der vom Elektron absorbierten und emittierten Photonen beim 3-Photonen Kapitza-Dirac Effekt nicht gleich groß. Aus diesem Grund findet der in dieser Arbeit diskutierte Beugungsvorgang nur für Elektronen mit einem relativistischen Impuls in Laserpropagationsrichtung statt. Zudem sind sehr hohe Laserfeldstärken nötig, um den Übergang mit einer messbaren Übergangswahrscheinlichkeit zu treiben. Der Spin des Elektrons wird beim Beugungsvorgang um die Magnetfeldachse des Laserstrahls gedreht, mit einem Drehwinkel, der vom Elektronenimpuls in Laserpolaristationsrichtung abhängt. Die Wahrscheinlichkeit für das Umklappen des Elektronenspins lässt sich durch die Wahl des Elektronenimpulses in Laserpolaristationsrichtung gezielt einstellen. Eine experimentelle Untersuchung der Vorhersagen kann mit zukünftigen Röntgenlasern erreicht werden.

Summary

Quantum mechanical diffraction is of particular interest, because it contradicts our everyday life experience. This theoretical work considers the diffraction of electrons at standing waves of light, referred to as the Kapitza-Dirac effect. The work focuses on a special version of a Kapitza-Dirac effect in which the electron interacts with three photons. The particular property of this 3-photon Kapitza-Dirac effect is, that the electron spin is rotated.

This work considers different relativistic and non-relativistic quantum mechanical wave equations which are described in momentum space. On one hand, the quantum dynamics of the diffracted electrons is solved numerically in momentum space and the properties of the 3-photon Kapitza-Dirac effect are investigated in detail. On the other hand, the quantum dynamics is solved via time-dependent perturbation theory and is compared with the numerical results.

In contrast to the originally proposed Kapitza-Dirac effect with two interacting photons, the number of absorbed and emitted photons by the electron is not equal for the 3-photon Kapitza-Dirac effect. Therefore, the diffraction process only appears for relativistic electron momenta in laser propagation direction. Furthermore, a very high field strength of the laser beam is required for driving the Kapitza-Dirac effect with a measurable diffraction probability. The electron spin is rotated along the axis of the magnetic field of the laser beam, when it undergoes the diffraction process. The rotation angle of the spin rotation depends on the electron momentum component in laser polarization direction. Therefore, the probability for flipping the electron spin can be tuned by choosing the electron momentum in the direction of the laser polarization. An experimental investigation may by established by utilizing future X-ray laser facilities.

In connection with this thesis, the following article has been published in a refereed journal:

- Sven Ahrens, Heiko Bauke, Christoph H. Keitel, and Carsten Müller. Spin dynamics in the Kapitza-Dirac effect. *Physical Review Letters*, 109(4):043601, (2012)

Contents

1 Introduction and Motivation **11**
- 1.1 The Kapitza-Dirac effect . . . 11
- 1.2 Recent progress in laser technology . . . 12
- 1.3 Synopsis . . . 15
  - 1.3.1 State of knowledge . . . 15
  - 1.3.2 New aspects treated in my work . . . 15
  - 1.3.3 Applied methods . . . 16
  - 1.3.4 Structure of the thesis . . . 16

2 Basic concepts related to the Kapitza-Dirac effect **17**
- 2.1 Physical setup, geometry and notation . . . 17
- 2.2 Conservation of energy and momentum . . . 18
  - 2.2.1 Diffraction of photons . . . 19
  - 2.2.2 Diffraction of electrons . . . 19
  - 2.2.3 Energy-momentum conservation by graphical considerations . . . 20
  - 2.2.4 Analytic derivation . . . 21
  - 2.2.5 The number of absorbed and emitted photons . . . 22
  - 2.2.6 The limit of small laser frequencies . . . 23

3 Theoretical framework: Quantum wave equations **25**
- 3.1 Schrödinger equation . . . 25
- 3.2 Pauli equation . . . 26
- 3.3 Klein-Gordon equation . . . 26
- 3.4 Dirac equation . . . 28

4 Quantum wave equations in momentum space **31**
- 4.1 Exemplification by the Schrödinger equation . . . 31
- 4.2 Pauli equation . . . 34
- 4.3 Klein-Gordon equation . . . 36
- 4.4 Dirac equation . . . 39

5 Properties of the 2-photon Kapitza-Dirac effect **41**
- 5.1 Setup . . . 41
- 5.2 Rabi oscillations . . . 42
- 5.3 Realistic pulse shape . . . 43

6 Electron spin dynamics: Conceptual considerations **47**
- 6.1 The propagator . . . 47
- 6.2 Spin dependence of the diffraction pattern . . . 48
- 6.3 Spin rotation in Pauli theory . . . 49
- 6.4 Spin rotation in Dirac theory . . . 50

7 Electron spin dynamics: Analytical small-time behavior **53**
7.1 General procedure . . . 53
7.2 Perturbation Theory for the Pauli equation . . . 54
7.2.1 Derivation . . . 54
7.2.2 Interpretation . . . 59
7.3 Perturbation Theory for the Dirac equation . . . 61
7.3.1 Derivation . . . 61
7.3.2 Interpretation . . . 66

8 Electron spin dynamics: Numerical results **69**
8.1 Setup . . . 69
8.2 Spin properties of the 3-photon Kapitza-Dirac effect . . . 71
8.3 Variation of the spin rotation . . . 75
8.4 The beam envelope in the 3-photon Kapitza-Dirac effect . . . 75
8.5 The resonance peak . . . 78
8.6 Rabi frequency of the 3-photon Kapitza-Dirac effect . . . 80

9 Conclusions and Outlook **85**
9.1 Conclusions . . . 85
9.2 Outlook . . . 86

A Bi-scalar matrix relations **87**

B Bi-spinor matrix relations **89**
B.1 Calculation of bi-spinor contractions . . . 89
B.2 Verification of spinor properties . . . 91

C Energy-momentum conservation **93**
C.1 Non-relativistic energy-momentum conservation . . . 93
C.2 Relativistic energy-momentum conservation . . . 94

Chapter 1

Introduction and Motivation

1.1 The Kapitza-Dirac effect

The diffraction of light has been known since the 17^{th} century [1] and gives evidence for the wave nature of light. Light diffraction was also observed at a double slit by Young [2] in 1803 and at a grating by Gregory [3] in 1673. The nature of light was under heavy dispute and with the advent of quantum mechanics at the beginning of the 20^{th} century it was realized that light ought to be described by a duality of particle and wave. In 1926 Davisson, Germer [4] and Thomson [5] showed that also electrons are subject to diffraction and therefore, subject to particle wave duality as well. The attribute, that matter has the same diffraction properties as light leads unavoidably to the question:

May the roles of light and matter be interchanged in a diffraction experiment? Which means: Can electrons be diffracted by a grating of light as it is shown in figure 1.1?

Since the superposition of two counter-propagating, monochromatic, coherent light waves of equal intensity forms a wave which has periodical nodes and anti-nodes in space, light may act as grating. The question, if electrons may be diffracted by a grating of light was first discussed by Pyotr Kapitza and Paul Dirac in 1933 [6]. The corresponding expression "Kapitza-Dirac effect" became a synonym for the diffraction of electrons, atoms and molecules at a standing wave of light [7]. Kapitza and Dirac considered electron diffraction by using the standing wave of light of an "ordinary mercury arc lamp" and concluded a tiny diffraction probability of 10^{-14} in their publication in 1933. It seems, that electron diffraction has not been tackled because of this small probability, until the availability of lasers in the 1960s. A few years after the invention of the laser, attempts for observing the Kapitza-Dirac effect have been made [8, 9, 10], but these early experiments were not able to prove the existence of electron diffraction by light. The enormous progress in laser technology in recent years permitted for light beams of very high intensities (see next section) and new experiments have been set up. The first confirmation of the Kapitza-Dirac effect of atoms was published in 1986 [11, 12]. The Kapitza-Dirac effect in the case of electrons was first observed by Bucksbaum in 1988 in the so-called diffraction regime [13]. The terms diffraction regime and also the complementary Bragg regime are introduced in chapter 5. The identification of single diffraction orders could be achieved the first time by Freimund, Aflatooni and Batelaan in 2001 [14] in a precise experimental setup based on improved technological devices.

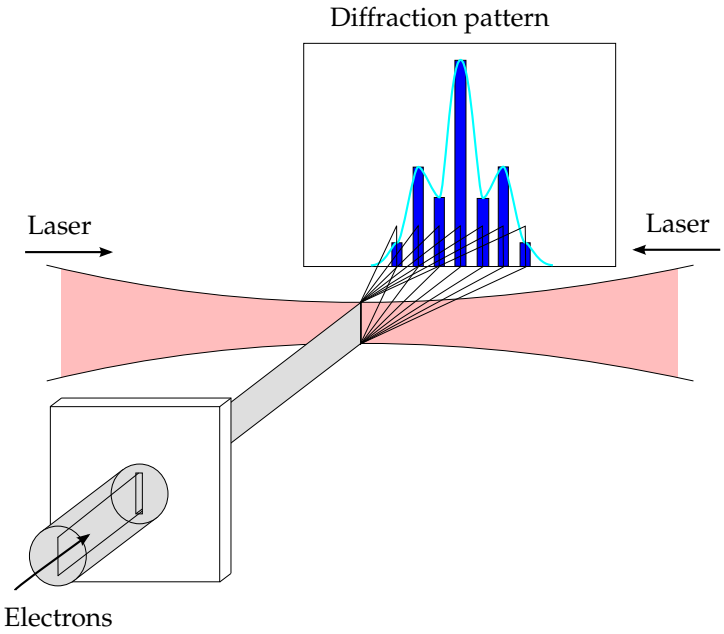

Figure 1.1: This is a schematic sketch of the Kapitza-Dirac effect. The two counter-propagating laser beams form a standing light wave. An electron beam crosses the standing light wave and is diffracted at the light. A diffraction pattern can be observed by placing a screen behind the interaction point.

1.2 Recent progress in laser technology

Since the invention of the laser in the 1960s [15], huge progress was made by increasing the laser intensity. Techniques like chirped pulse amplification [16] allow for laser facilities with intensities of $2 \cdot 10^{22}\,\mathrm{W/cm^2}$ at wavelengths of 800 nm (HERCULES laser [17]). Laser facilities with similar intensities exist, for example the "petawatt high energy laser for heavy ion experiments" (PHELIX) with a peak intensity of $10^{21}\,\mathrm{W/cm^2}$ [18]. Table top laser systems reach intensities of $10^{18}\,\mathrm{W/cm^2}$. Even stronger laser facilities are planned for the future, as it is the case for the "extreme light infrastructure" (ELI) [19] which will provide an intensity of $10^{25}\,\mathrm{W/cm^2}$ in the optical regime.

Coherent light beams with short wavelengths are of particular interest in this thesis, because the Kapitza-Dirac effect is investigated at very short wavelengths. The wavelength of laser light can be shortened by nonlinear laser-matter interaction, yielding higher harmonics of the laser light. This technique of high harmonic generation (HHG) may be realized by a plasma mirror. An example of an experimental realization is given in [20]. The authors report extreme ultra violet radiation with wavelengths of 50 nm up to 100 nm at intensities of $1 \cdot 10^{11}\,\mathrm{W/cm^2}$. Even higher intensities may be reached, as it is proposed in [21]. This publication claims attosecond pulses with a duration of 84 as and 10^{16} photons per pulse. The photon's energy ranges from 20 eV to 70 eV. Assuming an average photon energy of 45 eV yields a pulse energy of 0.072 J and therefore, a pulse power of $8.6 \cdot 10^{14}$ W. An intensity of $1.1 \cdot 10^{23}\,\mathrm{W/cm^2}$ would be accessible if one was able to focus this laser down to a beam spot diameter of 1 µm without any losses due to optical components.

Another source of coherent X-ray light of high intensity are free electron lasers. For example, the linac coherent light source (LCLS) at the Stanford linear accelerator center (SLAC) provides 2 keV X-ray laser light at intensities of $10^{18}\,\mathrm{W/cm^2}$ [22]. The European X-ray free-electron laser (European XFEL) [23] will provide a coherent X-ray beam of even higher intensity in the near future. The projected peak power of the European XFEL is 80 GW at a maximum photon energy of 17.5 keV. The laser will reach a peak intensity of $5.2 \cdot 10^{18}\,\mathrm{W/cm^2}$ at the intended beam spot diameter of 70 µm.

The properties of the mentioned laser systems are listed in table 1.1 and illustrated in the wavelength-

intensity diagram of figure 1.2.

Table 1.1: This table shows the properties of existing and prospective lasers. The intensities of the listed lasers may be even higher if one was able to narrow the beam focus.

laser type	intensity	wavelength	photon energy
existing lasers			
optical laser (HERCULES)	$2 \cdot 10^{22}\,\mathrm{W/cm^2}$	800.0 nm	1.5 eV
optical laser (PHELIX)	$1 \cdot 10^{21}\,\mathrm{W/cm^2}$	1064.0 nm	1.2 eV
optical tabletop	$1 \cdot 10^{18}\,\mathrm{W/cm^2}$	800.0 nm	1.5 eV
plasma mirror HHG	$1 \cdot 10^{11}\,\mathrm{W/cm^2}$	72.9 nm	17.0 eV
free electron laser (LCLS at SLAC)	$1 \cdot 10^{18}\,\mathrm{W/cm^2}$	0.6 nm	2.0 keV
proposed lasers			
optical laser (ELI)	$1 \cdot 10^{25}\,\mathrm{W/cm^2}$	800.0 nm	1.5 eV
plasma mirror HHG	$1 \cdot 10^{23}\,\mathrm{W/cm^2}$	27.6 nm	45.0 eV
free electron laser (European XFEL)	$5 \cdot 10^{18}\,\mathrm{W/cm^2}$	70.9 pm	17.5 keV
observed 2-photon Kapitza-Dirac effect [13]			
optical laser [24]	$1{\cdot}10^{11}\,\mathrm{W/cm^2}$	532.0 nm	2.3 eV
proposed 3-photon Kapitza-Dirac effect (section 8)			
free electron laser [25]	$2{\cdot}10^{23}\,\mathrm{W/cm^2}$	0.4 nm	3.1 keV

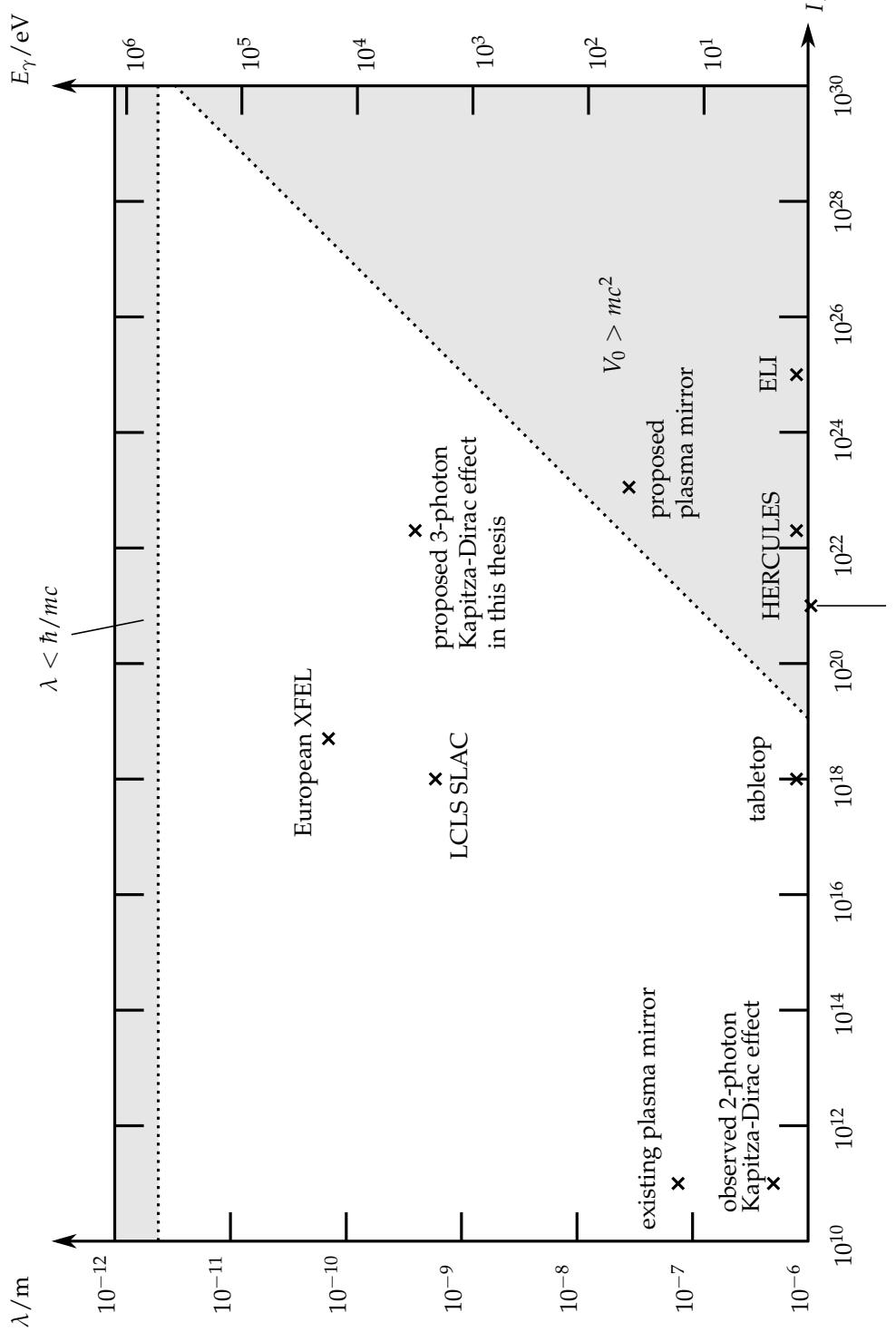

Figure 1.2: This figure shows the laser parameters of table 1.1 on a wavelength versus intensity chart. Laser wavelengths shorter than the reduced Compton wavelength ($\lambda < \hbar/mc$) are located in the upper gray region. Laser intensities whose amplitude of the ponderomotive potential (see section 5) is larger than the electron restmass energy $V_0 > mc^2$ are located in the lower right gray region. Relativistic effects are assumed to be large in the gray regions.

1.3 Synopsis

1.3.1 State of knowledge

Most of the theory of the Kapitza-Dirac effect is based on non-relativistic quantum mechanics with a ponderomotive potential (introduced in chapter 2.1) [26, 27]. The resulting differential equation can be solved in the diffraction regime using Bessel functions. Furthermore, an adiabatic laser-electron interaction of the Kapitza-Dirac effect is considered by Fedorov [28]. The Kapitza-Dirac effect in the Bragg regime is solved in detail by Efremov and Fedorov by using second order time-dependent perturbation theory [29, 30]. Gush and Gush account for even higher orders of time-dependent perturbation theory [31]. A non-perturbative treatment of the Kapitza-Dirac effect, which employs Volkov states of the Schrödinger equation, is presented in [32, 33, 34]. The Kapitza-Dirac effect is also discussed in a relativistic treatment by employing the Klein-Gordon equation [35, 36]. Particle statistics (Bosons or Fermions) in the case of the Kapitza-Dirac effect is considered by Sanco [37].

Freimund and Batelaan consider a spin-dependent interaction in the Kapitza-Dirac effect [38] and treat the electron as a point-like, non-relativistic particle with a magnetic moment and investigate its trajectory in two counterpropagating plane waves of different wavelengths. A quantum mechanical, non-relativistic treatment of spin-flips in the Kapitza-Dirac effect is presented by Leonard Rosenberg in 2004 [39]. The author solves the quantum dynamics of a non-relativistic particle in a quantized external laser field by using time-dependent perturbation theory and an approximation in the diffraction regime consisting of Bessel functions. Both studies find negligible small spin-effects in the interaction regime considered.

1.3.2 New aspects treated in my work

In my work, I investigate the Dirac equation, and I in particular exploit the electron spin, which is an intrinsic property of the Dirac equation.

I discuss a general condition for absorption and emission of a certain number of photons by requiring energy and momentum conservation of classical particles. The condition's analytical description is combined with geometric considerations, which – so far – cannot be found in such a detail in literature. Furthermore, the quantum dynamics of the electron-light interaction is solved numerically without applying approximations. The numerical results are exact in this sense. The quantum dynamics of the full time-dependent Pauli equation and the full time-dependent Dirac equation is also solved with the method of time-dependent perturbation theory. The comparison of both – the numerical and the analytical solution – features two advantages: First, even though reasoned approximations are assumed in time-dependent perturbation theory, the validity of the perturbative results can be checked by comparison with the numerical results. Second, one can easily provide scaling laws for the numerical results from perturbation theory. In view of the tremendous progress of available laser intensities and frequencies, the question arises which properties of the Kapitza-Dirac effect appear in these extreme fields. The methods appearing in this thesis (numerical simulations and perturbation theory) can compare the full and exact relativistic and non-relativistic properties of the Kapitza-Dirac effect. In particular, the newly introduced 3-photon Kapitza-Dirac effect is a quantum mechanical setup, which is a relativistic setup by its intrinsic properties (which has no non-relativistic limit) that demands for very high field strengths of the external X-ray laser field.

Additionally, the spin-flip of the diffraction process is described by the electron wave-function propagator and facilitates the conclusion, that the spin of the electron is rotated. I point out, that the resonance condition from energy and momentum conservation allows to tune the quantum dynamics, such that the spin-dependent coupling terms, which are usually weak, can be amplified by a suitable choice of parameters.

1.3.3 Applied methods

I derive a resonance condition from energy and momentum conservation, which can be utilized for determining laser and electron parameters, such that the electron will undergo a diffraction process, in which it absorbs and emits a certain number of photons in a classical interaction picture. I transform the Schrödinger-, Pauli-, Klein-Gordon- and Dirac equation into momentum space, such that each of them reduces into a system of coupled, ordinary differential equations. I implement these differential equations in a numeric code and investigate in this way the electron quantum dynamics. I derive the short-time quantum dynamics of the 3-photon Kapitza-Dirac effect by applying time-dependent perturbation theory to the Pauli- and Dirac equation and identify characteristic properties of the diffraction process from this analytic solution. In particular, I identify an $\mathcal{SU}(2)$ representation of the propagator of the quantum dynamics and compare it with the numerical results.

1.3.4 Structure of the thesis

The second chapter introduces the external laser field of the standing wave of light and considers classical energy and momentum conservation of the electron by graphical means. The third chapter introduces the quantum mechanical wave equations, namely the Schödinger equation, the Pauli equation, the Klein-Gordon equation and the Dirac equation. All four equations are transformed into momentum space in chapter 4. The resulting system of coupled differential equations is of relevance in this work, since the numerical and perturbative results are based on these equations. The fifth chapter discusses the original 2-photon Kapitza-Dirac effect and demonstrates, that the numerical implementation of the wave equations in chapter 4 reproduce the theoretically known and experimentally realized quantum dynamics of the 2-photon Kapitza-Dirac effect well. The sixth chapter infers general properties about the spin dependence of the diffraction pattern and the rotation of the electron spin from the propagator of the electron wave function. The seventh chapter calculates the perturbative short-time solutions of the Dirac equation and the Pauli equation with the method of time-dependent perturbation theory. Characteristic properties of the diffraction process, like the Rabi frequency and the spin-flip probability are derived. The eighth chapter applies the numerical implementation of the Dirac equation to the quantum dynamics of the 3-photon Kapitza-Dirac effect. The $\mathcal{SU}(2)$ property of the propagator and the properties from time-dependent perturbation theory are verified. The resonance peak of the transition is also discussed. The appendix contains the derivation of bi-scalar properties of the Klein-Gordon equation, bi-spinor properties of the mode expanded Dirac equation, and the constraint equations resulting from energy- and momentum conservation.

Chapter 2

Basic concepts related to the Kapitza-Dirac effect

The first part of this chapter introduces the vector potential of the external laser field, which is used throughout this thesis. The corresponding electric and magnetic fields of the laser beam are discussed as well as the effective ponderomotive potential.

The second part of this chapter considers energy and momentum conservation of classical particles, in a graphical and intuitive picture. Even though these conservation laws are pure classical properties, they are a useful criterion for determining laser frequency and initial electron momenta, such that quantum dynamics undergoes an n-photon Kapitza-Dirac effect (see chapters 5, 7 and 8). The geometrical origin of the corresponding resonance condition is elaborately discussed.

2.1 Physical setup, geometry and notation

In the Kapitza-Dirac effect, the electron moves in a standing wave of light (see figure 2.1), which can be described by an infinitely extended vector potential of the form

$$\vec{A}(\vec{x},t) = -\frac{\vec{A}_0}{2}\sin(\vec{k}_L\cdot\vec{x}-\omega t)+\frac{\vec{A}_0}{2}\sin(\vec{k}_L\cdot\vec{x}+\omega t) \tag{2.1a}$$

$$= \vec{A}_0\cos(\vec{k}_L\cdot\vec{x})\sin(\omega t)\,, \tag{2.1b}$$

where ω is the angular frequency of the wave and $\vec{k}_L$ is its wave vector. Note, that a small arrow is placed on top of each vector in this thesis. The vacuum Maxwell equations imply, that ω equals ck_L, with $k_L = |\vec{k}_L|$ and $\lambda_L = 2\pi/k_L$. In some parts of this thesis, the wave vector $\vec{k}_L$ is considered to be parallel to the x_1 axis, which is the case for the numerical chapters 5, 8, the sections, which discuss the resonance condition from energy and momentum conservation 2.2.4, 2.2 and the low laser frequency approximation of the perturbative calculations at the end of the subsections 7.2.1 and 7.3.1. A general $\vec{k}_L$ is used everywhere else. The names 'left' and 'right' are used for the $-x_1$ and x_1 direction for convenience in section 2.2. The polarization direction and amplitude of the external vector potential of the laser beam is denoted by the vector $\vec{A}_0$. The vacuum Maxwell equations also imply, that $\vec{A}_0$ and $\vec{k}_L$ are always orthogonal to each other. Apart from this orthogonality constraint, the vectors $\vec{k}_L$ and $\vec{A}_0$ can be chosen freely. Note, that line (2.1a) explicitly denotes the two counter-propagating laser beams with their vector potential amplitude, whereas line (2.1b) shows the combined potential, in which time and space dependence factorizes in a product of two trigonometric functions.

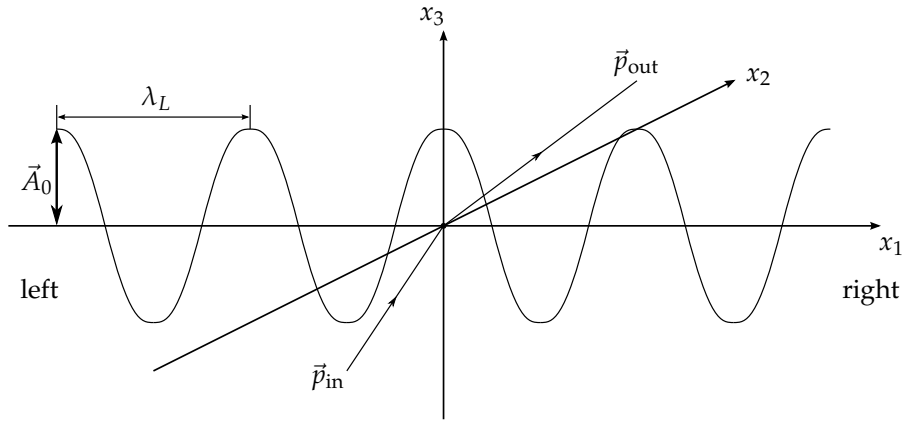

Figure 2.1: This figure shows the coordinate system, which we use for the description of the Kapitza-Dirac effect. The laser beam has the vector potential amplitude $\vec{A}_0$ and wavelength λ_L. The electron beam has the initial momentum $\vec{p}_{in}$ and may be detected with the final momentum $\vec{p}_{out}$.

The vector potential (2.1) results in the electric and magnetic fields

$$\vec{E}(\vec{x},t) = \vec{E}_0 \cos(\vec{k}_L \cdot \vec{x}) \cos(\omega t) \tag{2.2a}$$

$$\vec{B}(\vec{x},t) = \vec{B}_0 \sin(\vec{k}_L \cdot \vec{x}) \sin(\omega t)\,, \tag{2.2b}$$

with electric and magnetic field amplitude vectors

$$\vec{E}_0 = -\vec{A}_0 k_L \tag{2.3a}$$

$$\vec{B}_0 = -\vec{k}_L \times \vec{A}_0\,. \tag{2.3b}$$

In a quantum mechanical description of the Kapitza-Dirac effect the vector potential (2.1) enters into the corresponding wave equation of the electron motion. The solution of this equation is, in general, demanding because of the separate space and time dependencies of the standing wave potential. For non-relativistic electron dynamics based on the Schrödinger equation, it has been shown that the effect of the vector potential can be well approximated by a static scalar potential [40, 41]. This so-called ponderomotive potential originates from a separation of fast and slow motion of a classical electron in the electro-magnetic fields (2.2) and a time average over the fast motion. The ponderomotive potential is given by

$$V(\vec{x},t) = V_0 \cos^2\left(\vec{k}_L \cdot \vec{x}\right) \tag{2.4}$$

with the amplitude

$$V_0 = \frac{e^2 \vec{A}_0^2}{4mc^2}\,, \tag{2.5}$$

following the notion of [27]. The potential (2.4) varies periodically in laser propagation direction with spacial period $\lambda_L/2$. This periodic structure allows to interpret the standing light wave naturally as an optical grating.

2.2 Conservation of energy and momentum

The electron has the initial momentum $\vec{p}_{\text{in}}$ and the final momentum $\vec{p}_{\text{out}}$. The vector $\vec{k} = \vec{p}_{\text{in}}/\hbar$ is used later in favor of a compact notation.

This section considers the conservation of energy and momentum in the Kapitza-Dirac effect, by making the assumption that the electron with initial momentum $\vec{p}_{\text{in}}$ absorbs an integer number of

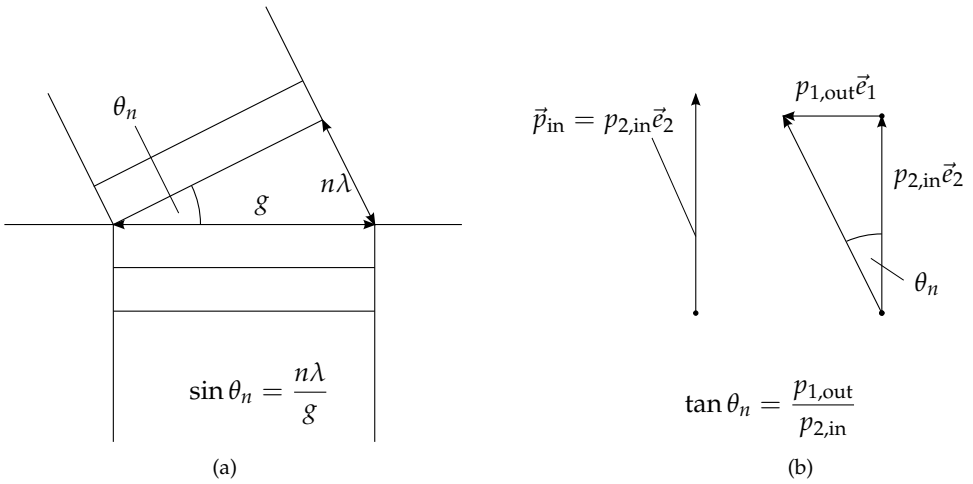

Figure 2.2: The left subfigure shows the geometric condition for light of wavelength λ being diffracted at the angle θ_n at a grating with spacing period g. The right figure shows the the same diffraction process in momentum space.

electrons and emits an integer number of photons, yielding the final electron momentum $\vec{p}_{\text{out}}$. It is worth to start with a general consideration on light diffraction first.

2.2.1 Diffraction of photons

If light of wavelength λ impinges at a grating with spacial period g, it is diffracted at angles, which fulfill the condition (see figure 2.2(a))

$$\sin\theta_n = n\lambda/g\,, \tag{2.6}$$

for wavelengths λ, which are much smaller than the grating spacing g. The Compton effect [42] tells, that the in-falling photon has a momentum of

$$p_{2,\text{in}} = 2\pi\hbar/\lambda\,. \tag{2.7}$$

If the light was detected at a small angle θ_n, when it passes the grating, it must have gathered the momentum

$$p_{1,\text{out}} = p_{2,\text{in}}\tan\theta_n \approx p_{2,\text{in}}\theta_n \approx 2\pi n\hbar/g \tag{2.8}$$

in the direction of the grating spacing (see figure 2.2(b)). Therefore, it stands to reason, that a grating with period g imposes multiples of momenta $2\pi\hbar/g$ at in-falling photons.

2.2.2 Diffraction of electrons

Figure 2.2 also holds for electrons and equation (2.7) is just de Broglie's relation for the wave-particle duality of a massive particle [43]. Therefore, a standing light wave with period λ_L is supposed to transfer multiples of momenta

$$\frac{2\pi\hbar}{\lambda_L} = \hbar k_L \tag{2.9}$$

as well. In fact, Freimund and Batelaan observed a diffraction pattern at multiples of $2\hbar k_L$ in their experiment [14]. The same property shows up for the discrete momenta $\hbar k_L$ in the mode expansion in chapter 4. Kapitza and Dirac also assumed a transfer of two photon momenta $\hbar k_L$ in their proposal [6] of the Kapitza-Dirac effect (see figure 2.3). According to that publication, the electron should incline at the Bragg angle, which means that the incident electron should have a momentum of one $\hbar k_L$ in laser propagation direction. The electron is reflected when it interacts with the laser, yielding an outgoing momentum of $\hbar k_L$ in the opposite laser propagation direction.

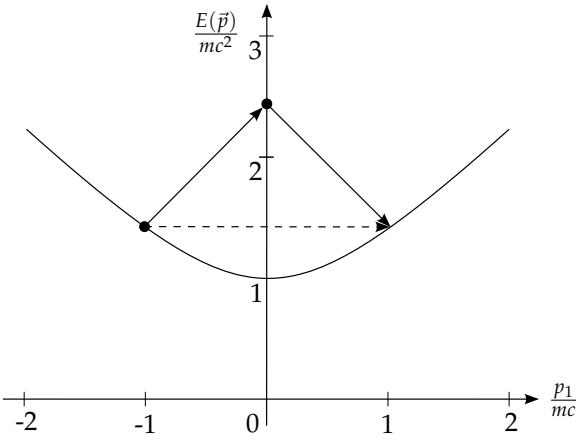

Figure 2.3: This figure shows the Kapitza-Dirac effect in an electron energy over the electron momentum diagram, which is already conceived in [27]. In the case of the original publication of the Kapitza-Dirac effect [6], one photon is absorbed from the laser field and one photon is emitted to the laser field. The bended line shows the relativistic energy-momentum relation (2.11) of the electron. The interacting photons transfer an energy of $c\hbar k_L$ and a momentum of $\hbar k_L$ and therefore appear as diagonal lines in the figure. The total exchange of energy and momentum of the electron with the laser is represented by the dashed arrow.

The electron interacts with two photons in the case of the originally published Kapitza-Dirac effect. Therefore, this originally published Kapitza-Dirac effect is referred to as 2-photon Kapitza-Dirac effect in this work. The question occurs, if other numbers of interacting photons are allowed by energy and momentum conservation. And, if this generalized version of the Kapitza-Dirac effect was possible: For what initial electron momenta and what laser frequencies does it occur? What are the final momenta of the electrons after the Kapitza-Dirac effect?

2.2.3 Energy-momentum conservation by graphical considerations

These questions can be answered by a simple geometric argument. For simplicity, this geometric argument is discussed with an electron moving in x_1 direction first. This means p_2 and p_3 are assumed to be zero. The general case, which includes non-vanishing momenta in x_2 and x_3 direction requires a minor modification of the geometric argument, which is discussed at the end of this subsection.

Assume, the electron absorbed n_a photons from the left laser beam and emits n_e photons into the right laser beam, with $n_a, n_e \in \mathbb{Z}$. Negative n_a corresponds to photon emission to the left and negative n_e corresponds to photon absorption from the right. Since a photon has the energy $c\hbar k_L$ and the momentum $\hbar k_L$, the total transferred energy is $\Delta E = c\hbar k_L(n_a - n_e)$ and the total transferred momentum is $\Delta p = \hbar k_L(n_a + n_e)$. In case of figure 2.3, n_a and n_e are 1. Therefore the dashed arrow, which illustrates the totally transferred energy and momentum in figure 2.3 is horizontal. In fact, the slope of the dashed vector only depends on n_a and n_e by

$$s = \frac{\Delta E}{\Delta p} = c\frac{n_a - n_e}{n_a + n_e}\,. \tag{2.10}$$

The relativistic energy momentum relation is taken as basis in the following considerations. It relates the kinetic energy E of an electron with restmass m and its momentum p_1 by the relation

$$E(p_1) = \sqrt{m^2c^4 + p_1^2c^2}\,. \tag{2.11}$$

The geometric argument works as follows:

1. Draw the relativistic energy momentum (2.11) relation in the electrons energy over time diagram, as it is done in figure 2.3.

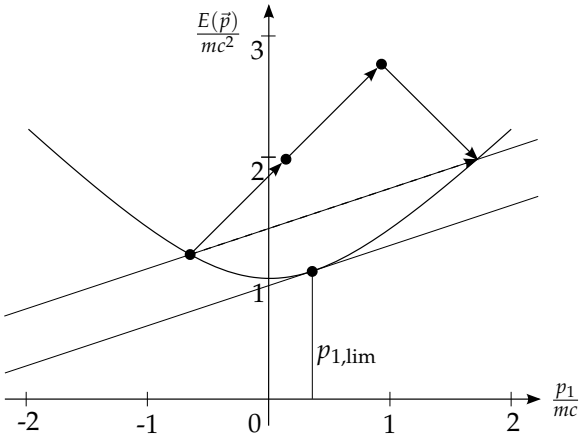

Figure 2.4: This figure shows the same energy over momentum diagram as in figure 2.3. The difference to figure 2.3 is, that n_a is 2 instead of 1. Therefore the dashed line of the total energy and momentum transfer has the slope $s = c/3$. The tangent line with slope $c/3$ at the dispersion relation consists of only one touching point with the initial and final electron momentum $p_{1,\mathrm{lim}}$.

2. Draw a line with slope s, which should intersect the relativistic energy momentum relation.

3. The intersection points of this secant are the initial and final momenta of the diffracted electron. The angular laser frequency can be obtained by dividing the transferred momentum by the number of photons

$$\omega = \frac{\Delta p c}{\hbar(n_a + n_e)} \,. \tag{2.12}$$

Figure 2.3 shows the geometric argument, in the case of the 2-photon Kapitza-Dirac effect, in which $n_a = 1$, $n_e = 1$ and $s = 0$. Another example of the geometric argument is shown in figure 2.4, in which the electron absorbs two photons $n_a = 2$ and emits one photon $n_e = 1$. Therefore, the slope is $c/3$ in this example.

It remains to tell the modification of the geometric argument from above in the case of non-vanishing electron momenta perpendicular to the laser propagation direction. This corresponds to $p_2 \neq 0$ or $p_3 \neq 0$ or both. In this case one may formally replace the electron rest mass m with the increased mass

$$m' = c^{-2}\sqrt{m^2c^4 + c^2p_2^2 + c^2p_3^2} \tag{2.13}$$

in equation (2.11). The modified energy momentum relation

$$E(p_1) = \sqrt{m'^2c^4 + c^2p_1^2} \tag{2.14}$$

is reparameterized but identical to that of figures 2.3 and 2.4, if one replaces $E/(mc^2)$ by $E/(m'c^2)$ and $p_1/(mc)$ by $p_1/(m'c)$. Therefore, the geometric argument can be traced back to the situation with vanishing p_2 and p_3. Note, that equation (2.14) is the same relativistic energy momentum relation as equation (3.22). This work will refer to the ladder equation from now on.

2.2.4 Analytic derivation

The condition, of the initial electron momentum $\vec{p}_{1,\mathrm{in}}$ and the laser frequency ω, for an n-photon Kapitza-Dirac effect need not to be determined graphically. One may also derive a formula for these parameters from energy and momentum conservation, which is done in the appendix C. Energy conservation implies, that the final electron energy has to be the initial electron energy plus the energy of

the absorbed photons, minus the energy of the emitted photons, yielding the equation

$$E(\vec{p}_{\text{out}}) = E(\vec{p}_{\text{in}}) + n_a\hbar\omega - n_e\hbar\omega\,. \tag{2.15}$$

Similarly, momentum conservation implies, that the final electron momentum is the initial electron momentum plus the momentum of the absorbed photons from the left laser beam plus the momentum of photons, which are emitted into the right laser beam.

$$c\vec{p}_{\text{out}} = c\vec{p}_{\text{in}} + n_a\hbar\omega\vec{e}_1 + n_e\hbar\omega\vec{e}_1 \tag{2.16}$$

If one inserts equation (2.16) into equation (2.15), one obtains an equation, which puts exactly one constraint on the four parameters $\hbar k_L$, $p_{1,\text{in}}$, $p_{2,\text{in}}$ and $p_{3,\text{in}}$ of classical particles. The property of this resonance condition is, that one may freely choose three of these parameters. The fourth parameter however, must fulfill the combined equations (2.15), (2.16), otherwise no n-photon Kaptiza-Dirac diffraction will occur. One may, for example, solve both equations for the initial electron momentum in laser propagation direction and obtains

$$\frac{p_{1,\text{in}}}{m'c} = -\frac{n_a+n_e}{2}\frac{\hbar\omega}{m'c^2} \pm \frac{|n_a-n_e|}{2}\sqrt{\frac{\hbar^2\omega^2}{m'^2c^4}+\frac{1}{n_an_e}}\,. \tag{2.17}$$

One may analogously solve for the laser frequency, resulting in the dimensionless energy

$$\frac{\hbar\omega}{m'c^2} = \left[-(n_a+n_e)\frac{p_{1,\text{in}}}{m'c} \pm |n_a-n_e|\frac{\sqrt{c^2p_{1,\text{in}}^2+m'^2c^4}}{m'c^2}\right]\frac{1}{2n_an_e}\,. \tag{2.18}$$

The computation for equation (2.17) and (2.18) is performed in appendix C.2.

It should be mentioned, that the two solutions (2.17) and (2.18) are resulting from the relativistic energy momentum relation (3.22). In the case of the non-relativistic energy momentum relation (3.4), the corresponding solution of the system of equations (2.15) and (2.16) results in

$$\frac{p_{1,\text{in}}}{mc} = -\frac{n_a+n_e}{2}\frac{\hbar\omega}{mc^2} + \frac{n_a-n_e}{n_a+n_e}\,, \tag{2.19}$$

and

$$\frac{\hbar\omega}{mc^2} = \left[-(n_a+n_e)\frac{p_{1,\text{in}}}{mc} + (n_a-n_e)\right]\frac{2}{(n_a+n_e)^2} \tag{2.20}$$

as it is also computed in appendix C.1.

Note, that the equations (2.17) and (2.19) as well as the equations (2.18) and (2.20) differ from each other for $n_a \neq n_e$, because they are based on a different energy-momentum relation $E(\vec{k})$. The relativistic resonance condition (2.17) or (2.18) is applied for relativistic quantum wave equations, whereas the non-relativistic resonance condition (2.19) or (2.20) is applied for non-relativistic quantum wave equations. The important consequence, which is drawn out of this property is, that the simulation parameters for the relativistic and the non-relativistic quantum wave equations can never be exactly the same. Either the laser frequency or the initial electron momentum *must* be slightly different, if one switches between relativistic and non-relativistic quantum wave equations, for Kaptiza-Dirac scattering with $n_a \neq n_e$.

2.2.5 The number of absorbed and emitted photons

The slope of the relativistic energy momentum dispersion relation is always in the interval $]-c, c[$, or in other words

$$-c < \frac{\partial E(\vec{p})}{\partial p_1} < c \qquad \forall p_1 \in \mathbb{R}\,. \tag{2.21}$$

Table 2.1: This table shows, for what values of n_a and n_e condition (2.22) is fulfilled. 'and' is a logical conjunction. All possible combinations of n_a and n_e are covered in this table.

$n_a > 0$	and	$n_e > 0$	$\Rightarrow$	condition (2.22) is fulfilled
$n_a < 0$	and	$n_e < 0$	$\Rightarrow$	condition (2.22) is fulfilled
$n_a > 0$	and	$n_e < 0$	$\Rightarrow$	condition (2.22) is not fulfilled
$n_a < 0$	and	$n_e > 0$	$\Rightarrow$	condition (2.22) is not fulfilled
$n_a = 0$	and	$n_e \in \mathbb{Z}$	$\Rightarrow$	condition (2.22) is not fulfilled
$n_a \in \mathbb{Z}$	and	$n_e = 0$	$\Rightarrow$	condition (2.22) is not fulfilled

Since the relativistic energy momentum dispersion relation is convex, only secants and tangents with a slope in this interval can be drawn at this dispersion relation. And since the slope is related to equation (2.10), n_a and n_e have to fulfill the condition

$$-1 < \frac{n_a - n_e}{n_a + n_e} < 1\,. \tag{2.22}$$

Table 2.1 shows for what values of n_a and n_e this condition is fulfilled and for what values it is not fulfilled. Note, that the cases with $n_a = 0$ and $n_e \neq 0$ or $n_a \neq 0$ and $n_e = 0$ contain the well known property, that an electron never scatters only at one photon, because of conservation of energy and momentum. One can further conclude that the Kapitza-Dirac effect only takes place, if photons are absorbed *and* emitted during the interaction process with the laser, which means, that both n_a and n_e must be positive or that both must be negative. Therefore, pure photon emission and pure photon absorption not allowed for Kapitza-Dirac scattering. Note, that the two allowed cases imply, that all photon momenta are transferred in one direction only. Either the electron only gathers photon momenta to the left (photon absorption from the left beam and photon emission into the right beam) or it only gathers photon momenta to the right (photon absorption from right beam and photon emission into the left beam). This is the reason, why the laser angular frequency in equation (2.12) can be obtained by dividing the transferred momentum by $n_a + n_e$.

2.2.6 The limit of small laser frequencies

Figure 2.4 shows one unique point with momentum $p_{1,\mathrm{lim}}$, which is the tangent point at the dispersion relation with slope s. Parallel translation of the secant changes the size (but not the angles) of the triangle, formed by the dashed and solid arrows in figure 2.3 and 2.4. This means, that parallel translation of the secant towards the tangent line of the tangent point at $p_{1,\mathrm{lim}}$ decreases the length of the dashed arrow. Decreasing the length of the dashed arrow implies in turn, that the momentum transfer Δp and the angular frequency ω of the external laser field decrease too. The touch point of the tangent with momentum $p_{1,\mathrm{lim}}$ at the energy-momentum relation marks therefore an unphysical transition, in which the laser frequency would be zero and the initial and final momentum would coincide.

One may derive $p_{1,\mathrm{lim}}$ by solving the condition

$$s \stackrel{!}{=} \frac{\partial E(p_1)}{\partial p_1} \tag{2.23}$$

for p_1. The reason is, that the derivative of $E(p_1)$ with respect to p_1 is the slope of the bended line at the momentum p_1 in figures 2.3 and 2.4. The condition (2.23) is therefore the analytical formulation of the question "At what momentum p_1 has the bended line in figures 2.3 and 2.4 the slope s?" The solution of (2.23) with respect to p_1 is

$$p_{1,\mathrm{lim}} = \frac{n_a - n_e}{\sqrt{4 n_a n_e}} m' c\,, \tag{2.24}$$

where p_1 is denoted as $p_{1,\mathrm{lim}}$. In the case of the two-photon Kapitza-Dirac effect [6], n_e and n_a are 1, yielding $p_{1,\mathrm{lim}} = 0$. The case $n_a = 2$, $n_e = 1$ of figure 2.4 yields $p_{1,\mathrm{lim}} = m'c/\sqrt{8}$. If the secant in figures 2.3 and 2.4 is parallel translated towards the tangent, initial and final electron momentum gets closer to $p_{1,\mathrm{lim}}$ and the laser frequency gets smaller. In the limiting case of an infinite small laser frequency, initial and final electron momenta will be infinitely close to $p_{1,\mathrm{lim}}$. This means, that the electron is nearly at rest, in the case of the 2-photon Kapitza-Dirac effect of figure 2.3.

Chapter 3

Theoretical framework: Quantum wave equations

Since the Kapitza-Dirac effect is a diffraction process, it requires a quantum mechanical description. Therefore, four different quantum wave equations are introduced in this chapter, which are the Schrödinger equation (section 3.1), the Pauli equation (section 3.2), the Klein-Gordon equation (section 3.3) and the Dirac equation (section 3.4). In the next chapter, all these quantum wave equations are transformed into momentum space. In the subsequent chapters, these transformed equations are applied for studying the quantum dynamics of the Kapitza-Dirac effect.

All quantum wave equations have in common, that they can be written in the form

$$\mathrm{i}\hbar\frac{\partial}{\partial t}\psi(\vec{x},t) = \hat{\boldsymbol{H}}\psi(\vec{x},t)\,, \tag{3.1}$$

where $\psi(\vec{x},t)$ is the quantum mechanical wave function, whose time evolution is determined by the Hamiltonian $\hat{\boldsymbol{H}}$. Note, that all symbols, which are set in bold in this thesis have the structure of a $n \times n$ matrix, where n ($n \in \mathbb{N}$) is the dimension of the wave function $\psi(\vec{x},t)$ in equation (3.1). The hat over a symbol means, that it contains spacial derivatives. Since the different quantum wave equations are determined by their Hamiltonians, it is sufficient to discuss these characteristic Hamiltonians in the following.

3.1 Schrödinger equation

The Hamiltonian of the Schrödinger equation is [44]

$$\hat{H} = \frac{1}{2m}\left(\hat{\vec{p}} - \frac{e}{c}\vec{A}\right)^2 + V\,. \tag{3.2}$$

The wave function of the Schrödinger equation has only one component. Therefore, the Hamiltonian $\hat{H}$ it is not set in bold font. One may insert the vector potential (2.1) as $\vec{A}$ or the ponderomotive potential (2.4) as external potential V of the standing light wave in the Schrödinger equation.

A plane wave with initial momentum $\vec{p}_{\mathrm{in}} = \hbar\vec{k}$ has the wave function

$$\psi_{\vec{k}}(\vec{x}) = e^{\mathrm{i}\vec{k}\cdot\vec{x}}\,. \tag{3.3}$$

The eigenvalue of the non-relativistic energy-momentum relation

$$E^{\mathrm{nr}}(\vec{k}) = \frac{\hbar^2\vec{k}^2}{2m} \tag{3.4}$$

results, if the wave function is applied to the Hamiltonian.

3.2 Pauli equation

The Hamiltonian of the Pauli equation is [44]

$$\hat{\boldsymbol{H}} = \frac{1}{2m}\left(\hat{\vec{p}} - \frac{e}{c}\vec{A}\right)^2 \mathbf{1} + V\mathbf{1} - \frac{e\hbar}{2mc}\vec{\boldsymbol{\sigma}}\cdot\vec{B}\,, \tag{3.5}$$

where $\vec{\boldsymbol{\sigma}}$ is the vector of the Pauli matrices

$$\boldsymbol{\sigma}_1 = \begin{pmatrix} 0 & 1 \\ 1 & 0 \end{pmatrix} \quad , \quad \boldsymbol{\sigma}_2 = \begin{pmatrix} 0 & -\mathrm{i} \\ \mathrm{i} & 0 \end{pmatrix} \quad , \quad \boldsymbol{\sigma}_3 = \begin{pmatrix} 1 & 0 \\ 0 & -1 \end{pmatrix}, \tag{3.6}$$

and $\mathbf{1}$ is the identity matrix in two dimensions. Therefore, the wave function of the Pauli equation has two components, which are coupled only by the Pauli term $\vec{\boldsymbol{\sigma}}\cdot\vec{B}$ at the right hand side of equation (3.5). The other part, which is proportional to the identity $\mathbf{1}$ is the same as the Schrödinger equation (3.2).

Spinors are used to encode the two components of the Pauli equation. Spinors consist of two components

$$u^{\mathrm{P},1} = \begin{pmatrix} 1 \\ 0 \end{pmatrix} \qquad \text{and} \qquad u^{\mathrm{P},2} = \begin{pmatrix} 0 \\ 1 \end{pmatrix}. \tag{3.7}$$

The plane wave function of the Pauli equation is similar to the wave function of the Schrödinger equation except the additional spin component $u^{\mathrm{P},\sigma}$.

$$\psi^{\mathrm{P},\sigma}_{\vec{k}}(\vec{x}) = u^{\mathrm{P},\sigma} e^{\mathrm{i}\vec{k}\cdot\vec{x}}\,,\ \sigma \in \{1,2\}\,. \tag{3.8}$$

These two wave functions are degenerate with respect to the free Pauli equation, which means, that both have the eigen energy

$$E^{\mathrm{nr}}(\vec{k}) = \frac{\hbar^2\vec{k}^2}{2m}\,. \tag{3.9}$$

In contrast to the eigen energy, the spinors (3.7) have different spin eigenvalues

$$S^\sigma = \begin{cases} +\hbar/2 & \text{, if } \sigma = 1 \\ -\hbar/2 & \text{, if } \sigma = 2 \end{cases} \tag{3.10}$$

with respect to the third component of the Pauli spin operator

$$\vec{S}^P = \frac{\hbar}{2}\vec{\boldsymbol{\sigma}}\,. \tag{3.11}$$

This thesis uses the additional index assignment

- $\sigma = 1$ corresponds to spin up $\uparrow$
- $\sigma = 2$ corresponds to spin down $\downarrow$.

3.3 Klein-Gordon equation

The Schrödinger and Pauli equations are non-relativistic quantum wave equations, which are invariant under Galilei transformations. Since this thesis focuses on relativistic phenomena in the Kapitza-Dirac effect, relativistic quantum wave equations which are invariant under Lorentz transformations are required. The simplest, manifest covariant object for a relativistic quantum wave equation is the Klein-Gordon equation in covariant form [45].

$$\left[\left(\mathrm{i}\hbar\frac{\partial}{\partial t} - e\Phi\right)^2 - c^2\left(\hat{\vec{p}} - \frac{e}{c}\vec{A}\right)^2 - m^2c^4\right]\mathrm{Y} = 0 \tag{3.12}$$

One may rewrite this equation, in order to fit it into the form of equation (3.1). According to [45], one introduces two variables ϕ and χ with the requirement

$$\Upsilon = \phi + \chi \qquad \text{and} \qquad \left(\mathrm{i}\hbar\frac{\partial}{\partial t} - e\Phi\right)\Upsilon = mc^2(\phi - \chi)\,. \tag{3.13}$$

From these two requirements it follows, that ϕ and χ are related to the function Υ by

$$\phi = \frac{1}{2mc^2}\left(mc^2 + \mathrm{i}\hbar\frac{\partial}{\partial t} - e\Phi\right)\Upsilon\,, \tag{3.14}$$

$$\chi = \frac{1}{2mc^2}\left(mc^2 - \mathrm{i}\hbar\frac{\partial}{\partial t} + e\Phi\right)\Upsilon\,. \tag{3.15}$$

Equation (3.12) can be rewritten by making use of the equations (3.13), (3.14) and (3.15). By defining the two component wave function

$$\psi = \begin{pmatrix}\phi\\ \chi\end{pmatrix}\,, \tag{3.16}$$

the Hamiltonian of equation (3.1) transforms to

$$\hat{\boldsymbol{H}} = \frac{\sigma_3 + \mathrm{i}\sigma_2}{2m}\left(\hat{\vec{p}} - \frac{e}{c}\vec{A}\right)^2 + \sigma_3 mc^2 + V\mathbf{1}\,, \tag{3.17}$$

where $e\Phi$ has been replaced by V. This equation is referred to as the Klein-Gordon equation of Hamiltonian form. Note, that the Hamiltonian (3.17) is non-Hermitian, because of the $\mathrm{i}\sigma_2$ term. The Hamiltonian is split into a free part

$$\hat{\boldsymbol{H}}_0 = (\sigma_3 + \mathrm{i}\sigma_2)\,\hat{\vec{p}}^2 + \sigma_3 mc^2 \tag{3.18}$$

and an interaction part

$$\hat{\boldsymbol{V}} = (\sigma_3 + \mathrm{i}\sigma_2)\left(-\frac{e\vec{A}\cdot\hat{\vec{p}}}{mc} + \frac{e^2\vec{A}^2}{2mc^2}\right) + \mathbf{1}V \tag{3.19}$$

for later convenience.

The eigenfunctions of the free Klein-Gordon equation are

$$\psi^{\mathrm{KG},\sigma}_{\vec{k}}(\vec{x}) = u^{\mathrm{KG},\sigma}(\vec{k})e^{\mathrm{i}\vec{k}\cdot\vec{x}}\,,\ \sigma \in \{1,2\}\,, \tag{3.20}$$

with the bi-scalars [45]

$$u^{\mathrm{KG},1}(\vec{k}) = \begin{pmatrix}mc^2 + E(\vec{k})\\ mc^2 - E(\vec{k})\end{pmatrix}\,, \qquad u^{\mathrm{KG},2}(\vec{k}) = \begin{pmatrix}mc^2 - E(\vec{k})\\ mc^2 + E(\vec{k})\end{pmatrix}\,, \tag{3.21}$$

where $E(\vec{k})$ is the relativistic energy-momentum relation

$$E(\vec{k}) = \sqrt{m^2c^4 + c^2\hbar^2\vec{k}^2}\,. \tag{3.22}$$

Since bi-scalars are no longer degenerate with respect to their eigen energy, they are functions of the wave vector $\vec{k}$. Their different energy eigen values are

$$E^\sigma(\vec{k}) = \begin{cases}+E(\vec{k}) & \text{, if } \sigma = 1\\ -E(\vec{k}) & \text{, if } \sigma = 2\,,\end{cases} \tag{3.23}$$

which is calculated in appendix A. This thesis uses the additional index assignment

- $\sigma = 1$ corresponds to positive eigen energy $+$

- $\sigma = 2$ corresponds to negative eigen energy $-$.

The bi-scalars may be written in a compact matrix notation, by employing the coefficients

$$d_+^{\mathrm{KG}}(\vec{k}) = \left(2\sqrt{E(\vec{k})mc^2}\right)^{-1}\left(mc^2 + E(\vec{k})\right) \quad \text{and} \quad d_-^{\mathrm{KG}}(\vec{k}) = \left(2\sqrt{E(\vec{k})mc^2}\right)^{-1}\left(mc^2 - E(\vec{k})\right) . \tag{3.24}$$

With these coefficients, the bi-scalars of the eigenfunctions of the free Klein-Gordon equation are the columns of the matrix

$$\boldsymbol{u}^{\mathrm{KG}}(\vec{k})^\dagger = d_+^{\mathrm{KG}}(\vec{k})\mathbf{1} + d_-^{\mathrm{KG}}(\vec{k})\boldsymbol{\sigma}_1 = \boldsymbol{u}^{\mathrm{KG}}(\vec{k}) . \tag{3.25}$$

It should be mentioned, that bi-scalars are not orthogonal to each other. One may need the pseudo orthogonal properties of bi-scalars [45] for later calculations.

$$u^{\mathrm{KG},\sigma}(\vec{k})\boldsymbol{\sigma}_3 u^{\mathrm{KG},\sigma'}(\vec{k}) = \mathrm{sign}(\sigma)\delta_{\sigma,\sigma'} \tag{3.26}$$

The sign function returns the sign of its index: $\mathrm{sign}(1) = +$, $\mathrm{sign}(2) = -$. In particular, the scalar product (4.5), which is introduced in section 4.1 needs to be exchanged by

$$\langle \psi_a \,|\, \psi_b \rangle = \int_{-\pi/k_L}^{\pi/k_L} \psi_a(\vec{x})^\dagger \boldsymbol{\sigma}_3 \psi_b(\vec{x}) \mathrm{d}x_k . \tag{3.27}$$

in the case of the Klein-Gordon equation.

3.4 Dirac equation

The Dirac equation is defined by using Dirac matrices, which have to fulfill the algebra

$$\boldsymbol{\alpha}_j\boldsymbol{\alpha}_k + \boldsymbol{\alpha}_k\boldsymbol{\alpha}_j = 2\delta_{jk}\mathbf{1} , \tag{3.28a}$$

$$\boldsymbol{\alpha}_j\boldsymbol{\beta} + \boldsymbol{\beta}\boldsymbol{\alpha}_j = \mathbf{0} , \tag{3.28b}$$

$$\boldsymbol{\beta}\boldsymbol{\beta} = \mathbf{1} . \tag{3.28c}$$

One realization of this algebra is the standard representation

$$\boldsymbol{\alpha}_1 = \begin{pmatrix} 0 & \boldsymbol{\sigma}_1 \\ \boldsymbol{\sigma}_1 & 0 \end{pmatrix} = \begin{pmatrix} 0 & 0 & 0 & 1 \\ 0 & 0 & 1 & 0 \\ 0 & 1 & 0 & 0 \\ 1 & 0 & 0 & 0 \end{pmatrix} , \qquad \boldsymbol{\alpha}_2 = \begin{pmatrix} 0 & \boldsymbol{\sigma}_2 \\ \boldsymbol{\sigma}_2 & 0 \end{pmatrix} = \begin{pmatrix} 0 & 0 & 0 & -\mathrm{i} \\ 0 & 0 & \mathrm{i} & 0 \\ 0 & -\mathrm{i} & 0 & 0 \\ \mathrm{i} & 0 & 0 & 0 \end{pmatrix} ,$$

$$\boldsymbol{\alpha}_3 = \begin{pmatrix} 0 & \boldsymbol{\sigma}_3 \\ \boldsymbol{\sigma}_3 & 0 \end{pmatrix} = \begin{pmatrix} 0 & 0 & 1 & 0 \\ 0 & 0 & 0 & -1 \\ 1 & 0 & 0 & 0 \\ 0 & -1 & 0 & 0 \end{pmatrix} , \qquad \boldsymbol{\beta} = \begin{pmatrix} \mathbf{1} & 0 \\ 0 & -\mathbf{1} \end{pmatrix} = \begin{pmatrix} 1 & 0 & 0 & 0 \\ 0 & 1 & 0 & 0 \\ 0 & 0 & -1 & 0 \\ 0 & 0 & 0 & -1 \end{pmatrix} , \tag{3.29}$$

which is employed in this thesis. In terms of these matrices, the Dirac Hamiltonian is [46]

$$\hat{\boldsymbol{H}} = c\left(\hat{\vec{p}} - \frac{e}{c}\vec{A}\right)\cdot\vec{\boldsymbol{\alpha}} + V\mathbf{1} + mc^2\boldsymbol{\beta} . \tag{3.30}$$

The Hamiltonian is split into a free part

$$\hat{\boldsymbol{H}}_0 = c\hat{\vec{p}}\cdot\vec{\boldsymbol{\alpha}} + mc^2\boldsymbol{\beta} \tag{3.31}$$

and an interaction part

$$\boldsymbol{V} = -e\vec{A}\cdot\vec{\boldsymbol{\alpha}} + V\mathbf{1} \tag{3.32}$$

for later convenience.

The eigenfunctions of the free Dirac equation can be denoted by

$$\psi_{\vec{k}}^{\sigma}(\vec{x}) = u^{\sigma}(\vec{k})e^{i\vec{k}\cdot\vec{x}}\,,\ \sigma \in \{1,2,3,4\}\,, \tag{3.33}$$

where the $u^{\sigma}(\vec{k})$ are bi-spinors. This thesis follows the convention of [46] for the introduction of bi-spinors. In a first step, the coefficients

$$d_+(\vec{k}) = \frac{1}{\sqrt{2}}\left(1+\frac{mc^2}{E(\vec{k})}\right)^{\frac{1}{2}} \qquad \text{and} \qquad d_-(\vec{k}) = \frac{\hbar c}{\sqrt{2}}\left(\frac{1}{E(\vec{k})(E(\vec{k})+mc^2)}\right)^{\frac{1}{2}} \tag{3.34}$$

are defined, where $E(\vec{k})$ is the relativistic energy-momentum relation (3.22). After that, these coefficients enter in the definition of the matrix

$$\begin{aligned}\boldsymbol{u}(\vec{k}) &:= d_+(\vec{k})\mathbf{1} + d_-(\vec{k})\boldsymbol{\beta}\vec{\boldsymbol{\alpha}}\cdot\vec{k} \\ &= \begin{pmatrix} d_+ & 0 & (+k_3)d_- & (+k_1-\mathrm{i}k_2)d_- \\ 0 & d_+ & (+k_1+\mathrm{i}k_2)d_- & (-k_3)d_- \\ (-k_3)d_- & (-k_1+\mathrm{i}k_2)d_- & d_+ & 0 \\ (-k_1-\mathrm{i}k_2)d_- & (+k_3)d_- & 0 & d_+ \end{pmatrix}\end{aligned} \tag{3.35}$$

and its adjoint matrix

$$\begin{aligned}\boldsymbol{u}(\vec{k})^{\dagger} &= d_+(\vec{k})\mathbf{1} + d_-(\vec{k})\vec{k}\cdot\vec{\boldsymbol{\alpha}}\boldsymbol{\beta} = d_+(\vec{k})\mathbf{1} - d_-(\vec{k})\boldsymbol{\beta}\vec{\boldsymbol{\alpha}}\cdot\vec{k} \\ &= \begin{pmatrix} d_+ & 0 & (-k_3)d_- & (-k_1+\mathrm{i}k_2)d_- \\ 0 & d_+ & (-k_1-\mathrm{i}k_2)d_- & (+k_3)d_- \\ (+k_3)d_- & (+k_1-\mathrm{i}k_2)d_- & d_+ & 0 \\ (+k_1+\mathrm{i}k_2)d_- & (-k_3)d_- & 0 & d_+ \end{pmatrix}.\end{aligned} \tag{3.36}$$

The bi-spinors $u^{\sigma}(\vec{k})$ are defined as the columns of this adjoint matrix.

$$\boldsymbol{u}(\vec{k})^{\dagger} = \left(u^1(\vec{k}), u^2(\vec{k}), u^3(\vec{k}), u^4(\vec{k})\right) \tag{3.37}$$

The energy eigen values of bi-spinors are

$$E^{\sigma}(\vec{k}) = \begin{cases} +E(\vec{k}) & \text{, if } \sigma = 1 \\ +E(\vec{k}) & \text{, if } \sigma = 2 \\ -E(\vec{k}) & \text{, if } \sigma = 3 \\ -E(\vec{k}) & \text{, if } \sigma = 4\,, \end{cases} \tag{3.38}$$

which is calculated in appendix (B.2). The spin eigen values of the bi-spinors are

$$S^{\sigma} = \begin{cases} +\hbar/2 & \text{, if } \sigma = 1 \\ -\hbar/2 & \text{, if } \sigma = 2 \\ +\hbar/2 & \text{, if } \sigma = 3 \\ -\hbar/2 & \text{, if } \sigma = 4\,, \end{cases} \tag{3.39}$$

with respect to the third component of the spin operator, which has been suggested by Foldy and Wouthuysen [47, 48, 49]

$$\vec{S}_{FW} = \boldsymbol{u}(\hat{\vec{p}})^{\dagger}\frac{\hbar}{2}\vec{\boldsymbol{\Sigma}}\,\boldsymbol{u}(\hat{\vec{p}})\,, \tag{3.40}$$

where, for dimensional reasons the factor $\hbar$ must be taken out of the relativistic energy-momentum relation (3.22) and the definition of the d_- coefficient (3.34) for the operator version $\boldsymbol{u}(\hat{\vec{p}})$. The definition of this relativistic spin operator (3.40) makes use of the non-relativistic spin operator $\vec{\boldsymbol{\Sigma}}$

$$\vec{\boldsymbol{\Sigma}} = \begin{pmatrix} \vec{\sigma} & \mathbf{0} \\ \mathbf{0} & \vec{\sigma} \end{pmatrix} = \begin{pmatrix} -\mathrm{i}\boldsymbol{\alpha_2\alpha_3} \\ -\mathrm{i}\boldsymbol{\alpha_3\alpha_1} \\ -\mathrm{i}\boldsymbol{\alpha_1\alpha_2} \end{pmatrix} . \tag{3.41}$$

This thesis uses the additional index assignment

- $\sigma = 1$ corresponds to positive eigen energy with spin up $+\uparrow$
- $\sigma = 2$ corresponds to positive eigen energy with spin down $+\downarrow$
- $\sigma = 3$ corresponds to negative eigen energy with spin up $-\uparrow$
- $\sigma = 4$ corresponds to negative eigen energy with spin down $-\downarrow$.

It should be mentioned that reference [46] uses the coefficient

$$\tilde{d}_-(\vec{k}) = \frac{1}{\sqrt{2}} \left(1 - \frac{mc^2}{E(\vec{k})} \right)^{\frac{1}{2}} \tag{3.42}$$

instead of $d_-(\vec{k})$ of equation (3.34). One may rewrite $\tilde{d}_-(\vec{k})$ by multiplying nominator and denominator with $(E(\vec{k}) + mc^2)^{1/2}$, yielding

$$\tilde{d}_-(\vec{k}) = \frac{1}{\sqrt{2}} \left(\frac{(E(\vec{k}))^2 - m^2c^4}{E(\vec{k})(E(\vec{k}) + mc^2)} \right)^{\frac{1}{2}} = |\vec{k}| d_-(\vec{k}) . \tag{3.43}$$

From this transformation one may conclude, that the matrix

$$\tilde{\boldsymbol{u}}(\vec{k}) = d_+(\vec{k})\mathbf{1} + \tilde{d}_-(\vec{k})\boldsymbol{\beta}\vec{\boldsymbol{\alpha}} \cdot \frac{\vec{k}}{|\vec{k}|} , \tag{3.44}$$

defined in [46] is equivalent to the matrix $\boldsymbol{u}(\vec{k})$ of equation (3.35). The usage of the $d_-(\vec{k})$ coefficients avoids the division by the factor $|\vec{k}|$ in the calculation of the matrix (3.44). Since the avoidance of singularities at $\vec{k} = 0$ appears to be more stable for numerical applications, the coefficients $d_-(\vec{k})$ and $\boldsymbol{u}(\vec{k})$ are favored over $\tilde{d}_-(\vec{k})$ and $\tilde{\boldsymbol{u}}(\vec{k})$.

Chapter 4

Quantum wave equations in momentum space

Even though the Kapitza-Dirac effect may be discussed by solving the quantum dynamics from first principles, i.e. by numerically implementing the equations of motion presented in section 3, one may solve these equations of motion with less effort, by rewriting them into a system of coupled ordinary differential equations in momentum space. The transformation of the quantum wave equations in chapter 3 from position into momentum space is performed in this chapter. Note, that the notion in momentum space is commonly used in literature of the Kapitza-Dirac effect.

The transformation into momentum space is performed in the same order, as in chapter 3, which means, that this chapter starts with the Schrödinger equation 4.1, then discusses the Pauli equation 4.2, then the Klein-Gordon equation 4.3 and finally treats the Dirac equation 4.4. The first section in this chapter also contains an introductory explanation, of how the quantum wave equations are transformed into momentum space.

The resulting, transformed equations are used for numerically replicating the 2-photon Kapitza-Dirac effect in chapter 5, for solving the Kapitza-Dirac effect with time-dependent perturbation theory in chapter 7 and for a numerical treatment of the 3-photon Kapitza-Dirac effect in chapter 8.

4.1 Exemplification by the Schrödinger equation

All quantum wave equations can be transformed into momentum space by inserting the plane wave expansion (Fourier transform) of the wave-function in the quantum wave equation and projecting it with solutions of the free Hamiltonian of the quantum wave equation. In order to perform the transformation into momentum space, one might start out with the general ansatz for the wave-function

$$\psi(\vec{x}) = \int_{-\infty}^{\infty} \mathrm{d}^3k\, \tilde{\psi}(\vec{k}) e^{\mathrm{i}\vec{k}\cdot\vec{x}} \tag{4.1}$$

and use the general scalar product

$$\langle \psi_a \,|\, \psi_b \rangle = \int_{-\infty}^{\infty} \mathrm{d}^3x\, \psi_a(\vec{x})^\dagger \psi_b(\vec{x})\,, \tag{4.2}$$

for the computation of the projection. However, since the external vector potential (2.1) as well as the external ponderomotive potential (2.4) contains multiples of plane waves $\mathrm{e}^{\mathrm{i}n\vec{k}_L\cdot\vec{x}}$ in every quantum wave equation, the generalized scalar product will result in delta spikes $\delta(\vec{k}, \vec{k} + n\vec{k}_L)$, $n \in \mathbb{Z}$. The momentum integral of equation (4.1) will turn these delta spikes into a system of coupled differential

equations of the subset $\tilde{\psi}(\vec{k}+n\vec{k}_L)$, $n \in \mathbb{Z}$. Therefore, the basis functions

$$\psi_n(\vec{x}) = \sqrt{\frac{k_L}{2\pi}} \mathrm{e}^{\mathrm{i}(\vec{k}+n\vec{k}_L)\cdot\vec{x}}, \tag{4.3}$$

with the plane wave ansatz

$$\psi(\vec{x}) = \sum_n c_n \psi_n(\vec{x}) = \sqrt{\frac{k_L}{2\pi}} \sum_n c_n \mathrm{e}^{\mathrm{i}(\vec{k}+n\vec{k}_L)\cdot\vec{x}} \tag{4.4}$$

and the scalar product

$$\langle \psi_a \,|\, \psi_b \rangle = \int_{-\pi/k_L}^{\pi/k_L} \mathrm{d}x_k \psi_a(\vec{x})^\dagger \psi_b(\vec{x}) \tag{4.5}$$

are sufficient for rewriting the quantum wave equations into momentum space. The integration element $\mathrm{d}x_k$ in equation (4.5) denotes, that the integration is performed in the $\vec{k}_L$ direction.

In the case of the Schrödinger equation (3.2) with the ponderomotive potential (2.4)

$$\mathrm{i}\hbar\dot{\psi} = \frac{\hat{\vec{p}}^2}{2m}\psi + V_0 \cos^2\left(\vec{k}_L \cdot \vec{x}\right)\psi, \tag{4.6}$$

the projection with basis element ψ_n from the left would read

$$\langle \psi_n \,|\, \mathrm{i}\hbar \,|\, \dot{\psi} \rangle = \left\langle \psi_n \middle| \frac{\hat{\vec{p}}^2}{2m} \middle| \psi \right\rangle + \left\langle \psi_n \middle| V_0 \cos^2\left(\vec{k}_L \cdot \vec{x}\right) \middle| \psi \right\rangle. \tag{4.7}$$

Each of the three terms can be computed separately. The time derivative term at the left-hand side results in

$$\langle \psi_n \,|\, \mathrm{i}\hbar \,|\, \dot{\psi} \rangle = \mathrm{i}\hbar \int_{-\pi/k_L}^{\pi/k_L} \frac{k_L}{2\pi} \mathrm{e}^{-\mathrm{i}(\vec{k}+n\vec{k}_L)\cdot\vec{x}} \sum_a \dot{c}_a \mathrm{e}^{\mathrm{i}(\vec{k}+a\vec{k}_L)\cdot\vec{x}} \mathrm{d}x_k = \mathrm{i}\hbar \frac{k_L}{2\pi}\frac{2\pi}{k_L} \sum_a \delta_{n,a}\dot{c}_a = \mathrm{i}\hbar\dot{c}_n. \tag{4.8}$$

The kinetic term at the right-hand side of equation (4.7) is rewritten into

$$\begin{aligned}\left\langle \psi_n \middle| \frac{\hat{\vec{p}}^2}{2m} \middle| \psi \right\rangle &= \int_{-\pi/k_L}^{\pi/k_L} \frac{k_L}{2\pi} \mathrm{e}^{-\mathrm{i}(\vec{k}+n\vec{k}_L)\cdot\vec{x}} \frac{\hat{\vec{p}}^2}{2m} \sum_a c_a \mathrm{e}^{\mathrm{i}(\vec{k}+a\vec{k}_L)\cdot\vec{x}} \mathrm{d}x_k \\ &= \sum_a \frac{\hbar^2(\vec{k}+a\,\vec{k}_L)^2}{2m}\delta_{n,a}c_a = \frac{\hbar^2(\vec{k}+n\vec{k}_L)^2}{2m}c_n. \end{aligned} \tag{4.9}$$

The ponderomotive coupling term at the right-hand side of equation (4.7) transforms into

$$\begin{aligned}\left\langle \psi_n \middle| V_0 \cos^2\left(\vec{k}_L \cdot \vec{x}\right) \middle| \psi \right\rangle &= \int_{-\pi/k_L}^{\pi/k_L} \frac{k_L}{2\pi} \mathrm{e}^{-\mathrm{i}(\vec{k}+n\vec{k}_L)\cdot\vec{x}} \frac{V_0}{4}\left(\mathrm{e}^{\mathrm{i}2\vec{k}_L\cdot\vec{x}} + 2 + \mathrm{e}^{-\mathrm{i}2\vec{k}_L\cdot\vec{x}}\right) \sum_a c_a \mathrm{e}^{\mathrm{i}(\vec{k}+a\vec{k}_L)\cdot\vec{x}} \mathrm{d}x_k \\ &= \frac{V_0}{4}\sum_a \left(\delta_{n,a+2} + 2\delta_{n,a} + \delta_{n,a-2}\right) c_a = \frac{V_0}{4}\left(c_{n-2} + 2c_n + c_{n+2}\right). \end{aligned} \tag{4.10}$$

Plugging back the projections (4.8), (4.9) and (4.10) into equation (4.7) yields

The Schrödinger equation with ponderomotive potential in momentum space

$$\mathrm{i}\hbar\dot{c}_n = \frac{\hbar^2(\vec{k}+n\vec{k}_L)^2}{2m}c_n + \frac{V_0}{2}c_n + \frac{V_0}{4}(c_{n-2} + c_{n+2}), \tag{4.11}$$

which is very similar to what Batelaan found in 2000 [27].

The numerical implementation of equation (4.11) requires a matrix notation of the Hamiltonian of equation (4.11), which is

$$H_{a,b} = \frac{\hbar^2(\vec{k}+a\vec{k}_L)^2}{2m}\delta_{a,b} + \frac{V_0}{2}\delta_{a,b} + \frac{V_0}{4}(\delta_{a,b+2}+\delta_{a,b-2})\,. \tag{4.12}$$

This can be checked by calculating

$$\sum_b H_{a,b}\,c_b\,. \tag{4.13}$$

The result is identical with the right-hand side of equation (4.11).

Tedious arrays of equations are resulting, if one expands the projection in equation (4.7) in every detail. Those arrays of equations have always the same structure and provide almost no insight about important physics to the reader. Therefore, the always reoccurring calculation steps are discussed here and are not shown later.

Assume an operator diagonal in position space which, by the above considerations, is of the form $V(\vec{x}) = \sum_a V_a \mathrm{e}^{\mathrm{i}a\vec{k}_L\cdot\vec{x}}$. Since the scalar product is linear, one may write it as the sum of all plane wave terms

$$\langle\psi_n \mid V(\vec{x}) \mid \psi\rangle = \sum_a \left\langle \psi_n \,\middle|\, V_a \mathrm{e}^{\mathrm{i}a\vec{k}_L\cdot\vec{x}} \,\middle|\, \psi \right\rangle\,. \tag{4.14}$$

The calculation of each term can be carried out separately. The expanded scalar product reads

$$\left\langle \psi_n \,\middle|\, V_a \mathrm{e}^{\mathrm{i}a\vec{k}_L\cdot\vec{x}} \,\middle|\, \psi \right\rangle = \int_{-\pi/k_L}^{\pi/k_L} \psi_n(\vec{x})^\dagger V_a \mathrm{e}^{\mathrm{i}a\vec{k}_L\cdot\vec{x}}\psi(\vec{x})\mathrm{d}x_k \tag{4.15a}$$

$$= \int_{-\pi/k_L}^{\pi/k_L} \sqrt{\frac{k_L}{2\pi}}\mathrm{e}^{-\mathrm{i}(\vec{k}+n\vec{k}_L)\cdot\vec{x}} V_a \mathrm{e}^{\mathrm{i}a\vec{k}_L\cdot\vec{x}} \sqrt{\frac{k_L}{2\pi}} \sum_b c_b \mathrm{e}^{\mathrm{i}(\vec{k}+b\vec{k}_L)\cdot\vec{x}}\mathrm{d}x_k\,. \tag{4.15b}$$

This can be rearranged and constants can be pulled out of the integral, where the integral reduces to a delta function.

$$\left\langle \psi_n \,\middle|\, V_a \mathrm{e}^{\mathrm{i}a\vec{k}_L\cdot\vec{x}} \,\middle|\, \psi \right\rangle = V_a \sum_b c_b \frac{k_L}{2\pi} \int_{-\pi/k_L}^{\pi/k_L} \mathrm{e}^{\mathrm{i}(a+b-n)\vec{k}_L\cdot\vec{x}}\mathrm{d}x_k = V_a \sum_b c_b \delta_{b,n-a} \tag{4.16}$$

The sum over b results in

$$\left\langle \psi_n \,\middle|\, V_a \mathrm{e}^{\mathrm{i}a\vec{k}_L\cdot\vec{x}} \,\middle|\, \psi \right\rangle = V_a c_{n-a}\,. \tag{4.17}$$

Resubstituting this into the expansion (4.14) yields

$$\langle\psi_n \mid V(\vec{x}) \mid \psi\rangle = \sum_a V_a c_{n-a}\,. \tag{4.18}$$

In summary, one may perform the projection (4.14) by expanding the operator diagonal in position space into plane waves and replace each plane wave $\mathrm{e}^{\mathrm{i}a\vec{k}_L\cdot\vec{x}}$ by c_{n-a}.

On the other hand, operators occur which are diagonal in momentum space. Assume a function $\hat{V}(\hat{\vec{p}})$ of the momentum operator $\hat{\vec{p}} = -\mathrm{i}\hbar\vec{\nabla}$. This momentum operator acts on the plane wave $\mathrm{e}^{\mathrm{i}(\vec{k}+b\vec{k}_L)\cdot\vec{x}}$, which by derivation turns into the number $V(\hbar(\vec{k}+b\vec{k}_L))$ in equation (4.15b).

$$\left\langle \psi_n \,\middle|\, \hat{V}(\hat{\vec{p}}) \,\middle|\, \psi \right\rangle = \int_{-\pi/k_L}^{\pi/k_L} \sqrt{\frac{k_L}{2\pi}}\mathrm{e}^{-\mathrm{i}(\vec{k}+n\vec{k}_L)\cdot\vec{x}} V(\hbar(\vec{k}+b\vec{k}_L)) \sqrt{\frac{k_L}{2\pi}} \sum_b c_b \mathrm{e}^{\mathrm{i}(\vec{k}+b\vec{k}_L)\cdot\vec{x}}\mathrm{d}x_k \tag{4.19}$$

The integral along $\mathrm{d}x_k$ yields a delta function again, which in turn fixes the summation index b of the sum.

$$\left\langle \psi_n \,\middle|\, \hat{V}(\hat{\vec{p}}) \,\middle|\, \psi \right\rangle = \sum_b V(\hbar(\vec{k}+b\vec{k}_L))c_b\delta_{b,n} = V(\hbar(\vec{k}+n\vec{k}_L))c_n \tag{4.20}$$

In summary, one may compute the projection with an operator diagonal in momentum space, by replacing the vector of derivatives $\vec{\nabla}$ of the momentum operator with the wave vector $\mathrm{i}(\vec{k}+n\vec{k}_L)$, where n and $\vec{k}$ are properties of the projecting basis element ψ_n. An expansion coefficient c_n has to be multiplied at the converted operator.

Operators, which are neither diagonal in position space, nor diagonal in momentum space may also occur. In all cases of this work those operators will appear as a product of position space operators and momentum space operators. Furthermore, all operators and basis elements in this work occur in a configuration, which allows to treat position and momentum space operators independently of each other according to the rules (4.18) and (4.20). For example, the scalar product of the operator $\vec{A}_0(\mathrm{e}^{\mathrm{i}\vec{k}_L\cdot\vec{x}}+\mathrm{e}^{-\mathrm{i}\vec{k}_L\cdot\vec{x}})\cdot\hat{\vec{p}}$ turns into

$$\left\langle \psi_n \left| \vec{A}_0(\mathrm{e}^{\mathrm{i}\vec{k}_L\cdot\vec{x}}+\mathrm{e}^{-\mathrm{i}\vec{k}_L\cdot\vec{x}})\cdot\hat{\vec{p}} \right| \psi \right\rangle = \vec{A}_0(c_{n-1}+c_{n+1})\cdot\hbar(\vec{k}+n\vec{k}_L) = \vec{A}_0\cdot\hbar\vec{k}(c_{n-1}+c_{n+1})\,. \tag{4.21}$$

4.2 Pauli equation

The spinor eigenfunctions (3.8) are employed as basis elements, for rewriting the Pauli equation with Hamiltonian (3.5) into momentum space. Since the Pauli equation is a partial differential equation with two components, the basis elements consist of two components

$$\psi_n^{\mathrm{P},\sigma}(\vec{x}) = \sqrt{\frac{k_L}{2\pi}}u^{\mathrm{P},\sigma}\mathrm{e}^{\mathrm{i}(\vec{k}+n\vec{k}_L)\cdot\vec{x}} \tag{4.22}$$

with the two spinors $u^{\mathrm{P},\sigma}$ of equation (3.7). The expansion (4.4) of the wave function is extended by including an additional spinor index to the expansion coefficients.

$$\psi(\vec{x}) = \sum_{n,\sigma} c_n^\sigma \psi_n^{\mathrm{P},\sigma}(\vec{x}) = \sqrt{\frac{k_L}{2\pi}}\sum_{n,\sigma} c_n^\sigma u^{\mathrm{P},\sigma}\mathrm{e}^{\mathrm{i}(\vec{k}+n\vec{k}_L)\cdot\vec{x}} \tag{4.23}$$

The transformation of the Pauli equation into momentum space makes use of the linear property of the scalar product (4.5). This means, that each term of the Hamiltonian (3.5) and the wave equation (3.1) may be contracted separately with the projecting basis elements (4.22) and the wave function (4.23). The first term of interest is the time derivative of the wave function

$$\left\langle \psi_n^{\mathrm{P},\sigma} \left| \mathrm{i}\hbar\frac{\partial}{\partial t} \right| \psi \right\rangle = \mathrm{i}\hbar\frac{\partial}{\partial t}\sum_{\sigma'} u^{\mathrm{P},\sigma\,\dagger}u^{\mathrm{P},\sigma'}c_n^{\sigma'} = \mathrm{i}\hbar\frac{\partial}{\partial t}\sum_{\sigma'}\delta_{\sigma,\sigma'}c_n^{\sigma'} = \mathrm{i}\hbar\dot{c}_n^\sigma\,, \tag{4.24}$$

where the spinor $u^{\sigma'}$ originates from the wave function $|\psi\rangle$ of equation (4.23) and the adjungated spinor $u^{\sigma\,\dagger}$ originates from the projecting basis element $\langle\psi_n^{\mathrm{P},\sigma}|$ of equation (4.22). The next term is the gauge invariant derivative $(\hat{\vec{p}}-\mathrm{e}\vec{A}/c)^2\mathbf{1}/(2m)$ of the Pauli Hamiltonian (3.5), which can be expanded into

$$\begin{aligned}\frac{1}{2m}\left(\hat{\vec{p}}-\frac{e}{c}\vec{A}\right)^2\mathbf{1} &= \left(\frac{\hat{\vec{p}}^2}{2m}-\frac{e\hat{\vec{p}}\cdot\vec{A}}{2mc}-\frac{e\vec{A}\cdot\hat{\vec{p}}}{2mc}+\frac{e^2\vec{A}^2}{2mc^2}\right)\mathbf{1}\\ &= \left(\frac{\hat{\vec{p}}^2}{2m}-\frac{e(\hat{\vec{p}}\cdot\vec{A})}{2mc}-\frac{e\vec{A}\cdot\hat{\vec{p}}}{mc}+\frac{e^2\vec{A}^2}{2mc^2}\right)\mathbf{1}\,.\end{aligned} \tag{4.25}$$

The term proportional to $\hat{\vec{p}}\cdot\vec{A}$ vanishes, because the divergence of the vector potential (2.1b) is zero. The mode expansion of the kinetic term proportional to $\hat{\vec{p}}^2$ results in

$$\left\langle \psi_n^{\mathrm{P},\sigma} \left| \frac{\hat{\vec{p}}^2}{2m}\mathbf{1} \right| \psi \right\rangle = \frac{\hbar^2(\vec{k}+n\vec{k}_L)^2}{2m}\sum_{\sigma'} u^{\mathrm{P},\sigma\,\dagger}\mathbf{1}u^{\mathrm{P},\sigma'}c_n^{\sigma'} = \frac{\hbar^2(\vec{k}+n\vec{k}_L)^2}{2m}\sum_{\sigma'} u^{\mathrm{P},\sigma\,\dagger}u^{\mathrm{P},\sigma'}c_n^{\sigma'} = \frac{\hbar^2(\vec{k}+n\vec{k}_L)^2}{2m}c_n^\sigma\,. \tag{4.26}$$

The mode expansion of the term proportional to $\vec{A} \cdot \hat{\vec{p}}$ is similar to the example in equation (4.21), because the plane wave expansion of the vector potential (2.1b) is

$$\vec{A}(\vec{x},t) = \frac{\vec{A}_0}{2}\left(\mathrm{e}^{\mathrm{i}\vec{k}_L\cdot\vec{x}} + \mathrm{e}^{\mathrm{i}\vec{k}_L\cdot\vec{x}}\right)\sin(\omega t)\,. \tag{4.27}$$

Therefore, one may write in analogy to equation (4.21)

$$\left\langle \psi_n^{\mathrm{P},\sigma} \middle| \left(-\frac{e\vec{A}\cdot\hat{\vec{p}}}{mc}\right)\mathbf{1} \middle| \psi \right\rangle = -\frac{e\vec{A}_0\cdot\hbar\vec{k}\sin(\omega t)}{2mc}\left(c_{n-1}^{\sigma} + c_{n+1}^{\sigma}\right)\,. \tag{4.28}$$

The last term of equation (4.25) contains the squared vector potential, which by expansion into plane waves reads as

$$\vec{A}(\vec{x},t)^2 = \frac{\vec{A}_0^2}{4}\left(\mathrm{e}^{\mathrm{i}2\vec{k}_L\cdot\vec{x}} + 2 + \mathrm{e}^{-\mathrm{i}2\vec{k}_L\cdot\vec{x}}\right)\sin^2(\omega t)\,. \tag{4.29}$$

The mode expansion of this term yields

$$\left\langle \psi_n^{\mathrm{P},\sigma} \middle| \frac{e^2\vec{A}^2}{2mc^2}\mathbf{1} \middle| \psi \right\rangle = \frac{e^2\vec{A}_0^2\sin^2(\omega t)}{8mc^2}\left(c_{n-2}^{\sigma} + 2c_n^{\sigma} + c_{n+2}^{\sigma}\right)\,. \tag{4.30}$$

Since the scalar potential $\phi(\vec{x},t)$ is zero, the external potential $V = e\phi$ is zero too. It remains the Pauli term, which is proportional to $\vec{\sigma}\cdot\vec{B}$ and is the last term in the Pauli Hamiltonian (3.5). The plane wave expansion of the magnetic field (2.2b) is

$$\vec{B}(\vec{x},t) = \frac{\mathrm{i}}{2}\vec{k}_L \times \vec{A}_0\left(\mathrm{e}^{\mathrm{i}\vec{k}_L\cdot\vec{x}} - \mathrm{e}^{-\mathrm{i}\vec{k}_L\cdot\vec{x}}\right)\sin(\omega t)\,. \tag{4.31}$$

Therefore, the free state mode expansion of the Pauli term reads

$$\left\langle \psi_n^{\mathrm{P},\sigma} \middle| \left(-\frac{e\hbar}{2mc}\vec{\sigma}\cdot\vec{B}\right) \middle| \psi \right\rangle = -\mathrm{i}\frac{e\hbar\sin(\omega t)}{4mc}\sum_{\sigma'}\left(\vec{k}_L\times\vec{A}_0\right)\cdot\left[u^{\mathrm{P},\sigma\,\dagger}\vec{\sigma}u^{\mathrm{P},\sigma'}\right]\left(c_{n-1}^{\sigma'} - c_{n+1}^{\sigma'}\right)\,. \tag{4.32}$$

Since the spinors $u^{\mathrm{P},\sigma}$ are the canonical unit vectors, the contraction $u^{\mathrm{P},\sigma\,\dagger}\vec{\sigma}u^{\mathrm{P},\sigma'}$ of the Pauli matrices with the spinors is the σ^{th} row and the $\sigma'^{\,\mathrm{th}}$ column of the Pauli matrices $\vec{\sigma}$. Together with the sum over σ', one may write this as a matrix product of $\vec{\sigma}$ with the vector

$$c_n = \begin{pmatrix} c_n^{\uparrow} \\ c_n^{\downarrow} \end{pmatrix}\,. \tag{4.33}$$

This means the equality

$$\sum_{\sigma'}\left[u^{\mathrm{P},\sigma\,\dagger}\vec{\sigma}u^{\mathrm{P},\sigma'}\right]c_n^{\sigma'} = \sum_{\sigma'}\left[\vec{\sigma}\right]^{\sigma,\sigma'}c_n^{\sigma'} = \left[\vec{\sigma}c_n\right]^{\sigma} \tag{4.34}$$

holds. Note, that the right-hand side of equation (4.34) makes use of the component vector (4.33), which is multiplied at $\vec{\sigma}$. With this identity, equation (4.32) can be written as

$$\left\langle \psi_n^{\mathrm{P},\sigma} \middle| \left(-\frac{e\hbar}{2mc}\vec{\sigma}\cdot\vec{B}\right) \middle| \psi \right\rangle = -\mathrm{i}\frac{e\hbar\sin(\omega t)}{4mc}\left(\vec{k}_L\times\vec{A}_0\right)\cdot\vec{\sigma}\left(c_{n-1} - c_{n+1}\right)\,. \tag{4.35}$$

Adding up all terms of the Pauli equation (4.24), (4.26), (4.28), (4.30) and (4.35) yields

The Pauli equation in momentum space

$$\begin{aligned} \mathrm{i}\hbar\dot{c}_n = &\left[\frac{\hbar^2(\vec{k}+n\vec{k}_L)^2}{2m} + \frac{e^2\vec{A}_0^2}{4mc^2}\sin^2(\omega t)\right] c_n + \frac{e^2\vec{A}_0^2}{8mc^2}\sin^2(\omega t)\,(c_{n-2}+c_{n+2}) \\ &- \frac{e\hbar\sin(\omega t)}{4mc}\left[\left(2\vec{A}_0\cdot\vec{k}\,\mathbf{1}+\vec{k}_L\times\vec{A}_0\cdot(\mathrm{i}\vec{\sigma})\right)c_{n-1} + \left(2\vec{A}_0\cdot\vec{k}\,\mathbf{1}-\vec{k}_L\times\vec{A}_0\cdot(\mathrm{i}\vec{\sigma})\right)c_{n+1}\right], \end{aligned} \tag{4.36}$$

which is expressed completely in terms of the two component vector (4.33) of the expansion coefficients c_n^σ. The corresponding Hamiltonian matrix of this system of differential equations is

$$\boldsymbol{H}_{0;a,b} = \frac{\hbar^2(\vec{k}+n\vec{k}_L)^2}{2m}\mathbf{1}\delta_{a,b} \tag{4.37}$$

for the free Hamiltonian and

$$\begin{aligned} \boldsymbol{V}_{a,b} = &\frac{e^2\vec{A}_0^2}{4mc^2}\sin^2(\omega t)\mathbf{1}\delta_{a,b} + \frac{e^2\vec{A}_0^2}{8mc^2}\sin^2(\omega t)\mathbf{1}\,(\delta_{a,b+2}+\delta_{a,b-2}) \\ &- \frac{e\hbar\sin(\omega t)}{4mc}\left[\left(2\vec{A}_0\cdot\vec{k}\,\mathbf{1}+\vec{k}_L\times\vec{A}_0\cdot(\mathrm{i}\vec{\sigma})\right)\delta_{a,b+1} + \left(2\vec{A}_0\cdot\vec{k}\,\mathbf{1}-\vec{k}_L\times\vec{A}_0\cdot(\mathrm{i}\vec{\sigma})\right)\delta_{a,b-1}\right] \end{aligned} \tag{4.38}$$

for the interaction Hamiltonian.

4.3 Klein-Gordon equation

Since the Klein-Gordon equation consists of two coupled partial differential equations, its basis elements include the two component bi-scalars (3.21), analogously to the Pauli equation.

$$\psi_n^{\mathrm{KG},\sigma}(\vec{x}) = \sqrt{\frac{k_L}{2\pi}}u^{\mathrm{KG},\sigma}(\vec{k}+n\vec{k}_L)\mathrm{e}^{\mathrm{i}(\vec{k}+n\vec{k}_L)\cdot\vec{x}}. \tag{4.39}$$

However, the difference between bi-scalars and spinors is that bi-scalars are not canonical basis vectors and that bi-scalars depend on the wave vector $\vec{k}+n\vec{k}_L$. The expansion of the wave function includes bi-scalars and a corresponding bi-scalar index of the expansion coefficients.

$$\psi(\vec{x}) = \sum_{n,\sigma} c_n^\sigma \psi_n^{\mathrm{KG},\sigma}(\vec{x}) = \sqrt{\frac{k_L}{2\pi}}\sum_{n,\sigma} c_n^\sigma u^{\mathrm{KG},\sigma}(\vec{k}+n\vec{k}_L)\mathrm{e}^{\mathrm{i}(\vec{k}+n\vec{k}_L)\cdot\vec{x}} \tag{4.40}$$

The $\vec{k}+n\vec{k}_L$ dependence of the basis elements (4.39) must be considered by performing the free state mode expansion. If one starts out with the mode expanded operator $\boldsymbol{V}_a\mathrm{e}^{\mathrm{i}a\vec{k}_L\cdot\vec{x}}$ of equation (4.15), which has a matrix structure in the case of the Klein-Gordon equation and follows the steps of calculation in section 4.1, one recognizes that the step (4.16) is not affected by the bi-scalar components. However, in equation (4.17) the sum over the index b fixes the index of the wave vector argument $\vec{k}+b\vec{k}_L$ of the bi-scalar.

$$\begin{aligned} \left\langle \psi_n^{\mathrm{KG},\sigma}\,\middle|\,\boldsymbol{V}_a\mathrm{e}^{\mathrm{i}a\vec{k}_L\cdot\vec{x}}\,\middle|\,\psi\right\rangle &= \sum_{b,\sigma'}\left[u^{\mathrm{KG},\sigma}(\vec{k}+n\vec{k}_L)\boldsymbol{V}_a u^{\mathrm{KG},\sigma'}(\vec{k}+b\vec{k}_L)\right]\,c_b\,\delta_{b,n-a} \\ &= \sum_{\sigma'}\left[u^{\mathrm{KG},\sigma}(\vec{k}+n\vec{k}_L)^\dagger\boldsymbol{V}_a u^{\mathrm{KG},\sigma'}(\vec{k}+(n-a)\vec{k}_L)\right]\,c_{n-a} \end{aligned} \tag{4.41}$$

Since bi-scalars $u^{\mathrm{KG},\sigma'}$ and $u^{\mathrm{KG},\sigma\,\dagger}$ are the $\sigma'^{\,\mathrm{th}}$ column and the σ^{th} row of the $\boldsymbol{u}^{\mathrm{KG}\,\dagger}$ and $\boldsymbol{u}^{\mathrm{KG}}$ matrices of equation (3.25), the contraction of the matrix $\boldsymbol{V}_a$ with the two bi-spinors corresponds to the matrix

element at the σ'^{th} column and the σ^{th} row of the matrix product $\boldsymbol{u}^{\mathrm{KG}}\boldsymbol{V}_a\boldsymbol{u}^{\mathrm{KG}\,\dagger}$. This means, that the equality

$$u^{\mathrm{KG},\sigma}(\vec{k})^\dagger \boldsymbol{V}_a u^{\mathrm{KG},\sigma'}(\vec{k}') = \left[\boldsymbol{u}^{\mathrm{KG}}(\vec{k})\boldsymbol{V}_a\boldsymbol{u}^{\mathrm{KG}}(\vec{k}')^\dagger\right]^{\sigma,\sigma'} \tag{4.42}$$

holds, where $[\boldsymbol{M}]^{\sigma,\sigma'}$ is the σ'^{th} column and the σ^{th} row of a matrix $\boldsymbol{M}$. The following results of the transformation into momentum space are expressed in terms of matrix entries of the matrix $\boldsymbol{u}^{\mathrm{KG}}\boldsymbol{V}_a\boldsymbol{u}^{\mathrm{KG}\,\dagger}$. For a compact, analytic expression one may define the functions

$$t^{\mathrm{KG}}(\vec{k},\vec{k}') = d_+^{\mathrm{KG}}(\vec{k})d_+^{\mathrm{KG}}(\vec{k}') + d_-^{\mathrm{KG}}(\vec{k})d_-^{\mathrm{KG}}(\vec{k}')\,, \tag{4.43a}$$

$$s^{\mathrm{KG}}(\vec{k},\vec{k}') = d_+^{\mathrm{KG}}(\vec{k})d_-^{\mathrm{KG}}(\vec{k}') + d_-^{\mathrm{KG}}(\vec{k})d_+^{\mathrm{KG}}(\vec{k}')\,, \tag{4.43b}$$

$$f^{\mathrm{KG}}(\vec{k},\vec{k}') = d_+^{\mathrm{KG}}(\vec{k})d_+^{\mathrm{KG}}(\vec{k}') - d_-^{\mathrm{KG}}(\vec{k})d_-^{\mathrm{KG}}(\vec{k}')\,, \tag{4.43c}$$

$$r^{\mathrm{KG}}(\vec{k},\vec{k}') = d_+^{\mathrm{KG}}(\vec{k})d_-^{\mathrm{KG}}(\vec{k}') - d_-^{\mathrm{KG}}(\vec{k})d_+^{\mathrm{KG}}(\vec{k}')\,. \tag{4.43d}$$

Matrix products, involving $\mathbf{1}$, $\boldsymbol{\sigma}_1$ and $\boldsymbol{\sigma}_3$ can be written as bi-scalar contractions

$$\boldsymbol{u}^{\mathrm{KG}}(\vec{k})\boldsymbol{u}^{\mathrm{KG}}(\vec{k}')^\dagger = t^{\mathrm{KG}}(\vec{k},\vec{k}')\mathbf{1} + s^{\mathrm{KG}}(\vec{k},\vec{k}')\boldsymbol{\sigma}_1\,, \tag{4.44a}$$

$$\boldsymbol{u}^{\mathrm{KG}}(\vec{k})\boldsymbol{\sigma}_1\boldsymbol{u}^{\mathrm{KG}}(\vec{k}')^\dagger = s^{\mathrm{KG}}(\vec{k},\vec{k}')\mathbf{1} + t^{\mathrm{KG}}(\vec{k},\vec{k}')\boldsymbol{\sigma}_1\,, \tag{4.44b}$$

$$\boldsymbol{u}^{\mathrm{KG}}(\vec{k})\boldsymbol{\sigma}_3\boldsymbol{u}^{\mathrm{KG}}(\vec{k}')^\dagger = f^{\mathrm{KG}}(\vec{k},\vec{k}')\boldsymbol{\sigma}_3 + r^{\mathrm{KG}}(\vec{k},\vec{k}')\mathrm{i}\boldsymbol{\sigma}_2 \tag{4.44c}$$

and are derived in appendix A. The property, that bi-scalars are pseudo orthonormal (see the end of section 3.3) must be accounted for. The pseudo scalar product (3.27), of the basis elements (4.39) results in

$$\begin{aligned}\left\langle \psi_a^{\mathrm{KG},\sigma} \,\middle|\, \boldsymbol{\sigma}_3 \,\middle|\, \psi_b^{\mathrm{KG},\sigma'} \right\rangle &= \left[\boldsymbol{u}^{\mathrm{KG}}(\vec{k}+a\vec{k}_L)\boldsymbol{\sigma}_3\boldsymbol{u}^{\mathrm{KG}}(\vec{k}+b\vec{k}_L)^\dagger\right]^{\sigma,\sigma'}\delta_{a,b} \\ &= \left[\boldsymbol{u}^{\mathrm{KG}}(\vec{k}+a\vec{k}_L)\boldsymbol{\sigma}_3\boldsymbol{u}^{\mathrm{KG}}(\vec{k}+a\vec{k}_L)^\dagger\right]^{\sigma,\sigma'}\delta_{a,b} = [\boldsymbol{\sigma}_3]^{\sigma,\sigma'}\delta_{a,b}\,.\end{aligned} \tag{4.45}$$

The last equality makes use of equation (A.5). Therefore, each projection of the Klein-Gordon equation with the basis elements (4.39) must include a $\boldsymbol{\sigma}_3$ at the left-hand side, which turns the object $\langle\psi_n^\sigma|\,\boldsymbol{\sigma}_3|$ into the dual basis element of $|\psi_n^\sigma\rangle$. The computation of the mode expansion can be divided in projections of each term of equation (3.1) and (3.17), similar to the procedure of the Pauli equation. The time-derivative term in equation (3.1) can be transformed into

$$\left\langle \psi_n^{\mathrm{KG},\sigma} \,\middle|\, \boldsymbol{\sigma}_3\,\mathrm{i}\hbar\frac{\partial}{\partial t} \,\middle|\, \psi \right\rangle = \mathrm{i}\hbar\sum_{\sigma'}\left[\boldsymbol{u}^{\mathrm{KG}}(\vec{k}+n\vec{k}_L)\boldsymbol{\sigma}_3\boldsymbol{u}^{\mathrm{KG}}(\vec{k}+n\vec{k}_L)^\dagger\right]^{\sigma,\sigma'}\dot{c}_n^{\sigma'} = \mathrm{i}\hbar\sum_{\sigma'}[\boldsymbol{\sigma}_3]^{\sigma\sigma'}\dot{c}_n^{\sigma'}\,. \tag{4.46}$$

The next term is the free Hamiltonian (3.18) of the Klein-Gordon Hamiltonian (3.17), which turns into the relativistic energy momentum relation.

$$\left\langle \psi_n^{\mathrm{KG},\sigma} \,\middle|\, \boldsymbol{\sigma}_3\hat{\boldsymbol{H}}_0 \,\middle|\, \psi \right\rangle = \sum_{\sigma'}\left[\boldsymbol{u}^{\mathrm{KG}}(\vec{k}+n\vec{k}_L)\boldsymbol{\sigma}_3\boldsymbol{H}_0(\vec{k}+n\vec{k}_L)\boldsymbol{u}^{\mathrm{KG}}(\vec{k}+n\vec{k}_L)^\dagger\right]^{\sigma,\sigma'}c_n^{\sigma'} = E(\vec{k}+n\vec{k}_L)c_n^\sigma \tag{4.47}$$

The last equality made use of equation (A.9). The relativistic energy momentum relation $E(\vec{k}+n\vec{k}_L)$ may be abbreviated by

$$E_n = E(\vec{k}+n\vec{k}_L)\,. \tag{4.48}$$

The mode expansion of the interaction Hamiltonian (3.19) is similar to the mode expansion of the Pauli equation and results in

$$\begin{aligned}\left\langle \psi_n^{\mathrm{KG},\sigma} \,\middle|\, \hat{\boldsymbol{V}} \,\middle|\, \psi \right\rangle = \sum_{b,\sigma'}&\left[\boldsymbol{u}^{\mathrm{KG}}(\vec{k}+n\vec{k}_L)\,(\mathbf{1}+\boldsymbol{\sigma}_1)\,\boldsymbol{u}^{\mathrm{KG}}(\vec{k}+b\vec{k}_L)^\dagger\right]^{\sigma,\sigma'} \\ &\cdot\left(-\frac{e\vec{A}_0\cdot\hbar\vec{k}\sin(\omega t)}{2mc}\left(\delta_{b,n-1}+\delta_{b,n+1}\right) + \frac{e^2\vec{A}_0^2\sin^2(\omega t)}{8mc}\left(\delta_{b,n-2}+2\delta_{b,n}+\delta_{b,n+2}\right)\right)c_b^{\sigma'}\,,\end{aligned} \tag{4.49}$$

where a vanishing scalar potential ϕ is assumed and the mode expansion of the vector potential (4.27) and the squared vector potential (4.29) are used. The matrix $\boldsymbol{u}^{\mathrm{KG}}(\vec{k}+n\vec{k}_L)\,(\mathbf{1}+\boldsymbol{\sigma}_1)\,\boldsymbol{u}^{\mathrm{KG}}(\vec{k}+b\vec{k}_L)^\dagger$ may be simplified to

$$\boldsymbol{u}^{\mathrm{KG}}(\vec{k}+n\vec{k}_L)\,(\mathbf{1}+\boldsymbol{\sigma}_1)\,\boldsymbol{u}^{\mathrm{KG}}(\vec{k}+b\vec{k}_L)^\dagger = \Big(t(\vec{k},\vec{k}')+s(\vec{k},\vec{k}')\Big)\,(\mathbf{1}+\boldsymbol{\sigma}_1)\ . \tag{4.50}$$

The sum $t(\vec{k},\vec{k}')+s(\vec{k},\vec{k}')$ simplifies to

$$t(\vec{k},\vec{k}')+s(\vec{k},\vec{k}') = \Big(d_+(\vec{k})+d_-(\vec{k})\Big)\Big(d_+(\vec{k}')+d_-(\vec{k}')\Big) = \frac{mc^2}{\sqrt{E(\vec{k})E(\vec{k}')}}\,. \tag{4.51}$$

Therefore, one may write

$$\boldsymbol{u}^{\mathrm{KG}}(\vec{k}+n\vec{k}_L)\,(\mathbf{1}+\boldsymbol{\sigma}_1)\,\boldsymbol{u}^{\mathrm{KG}}(\vec{k}+b\vec{k}_L)^\dagger = \frac{mc^2}{\sqrt{E_nE_b}}\,[\mathbf{1}+\boldsymbol{\sigma}_1]\ . \tag{4.52}$$

The transformation of the Klein-Gordon equation into momentum space is the sum of the equations (4.46), (4.47) and (4.49). But the time-derivative of the expansion coefficients with a negative index c_n^- will be negative compared to the time-derivative of the expansion coefficients with positive index c_n^+. It makes sense to demand, that the time-derivatives all have the same sign. Therefore, the equations (4.46), (4.47) and (4.49) are multiplied by $\boldsymbol{\sigma}_3$ with respect to the index σ. The resulting system of coupled ordinary differential equations is

The Klein-Gordon equation in momentum space

$$\begin{aligned}\mathrm{i}\hbar\dot{c}_n = E_n\boldsymbol{\sigma}_3c_n &- \frac{e\vec{A}_0\cdot c\hbar\vec{k}\sin(\omega t)}{2}\left(\frac{[\mathrm{i}\boldsymbol{\sigma}_2+\boldsymbol{\sigma}_3]c_{n-1}}{\sqrt{E_nE_{n-1}}}+\frac{[\mathrm{i}\boldsymbol{\sigma}_2+\boldsymbol{\sigma}_3]c_{n+1}}{\sqrt{E_nE_{n+1}}}\right)\\ &+\frac{e^2\vec{A}_0^2\sin^2(\omega t)}{8}\left(\frac{[\mathrm{i}\boldsymbol{\sigma}_2+\boldsymbol{\sigma}_3]c_{n-2}}{\sqrt{E_nE_{n-2}}}+\frac{2[\mathrm{i}\boldsymbol{\sigma}_2+\boldsymbol{\sigma}_3]c_n}{E_n}+\frac{[\mathrm{i}\boldsymbol{\sigma}_2+\boldsymbol{\sigma}_3]c_{n+2}}{\sqrt{E_nE_{n+2}}}\right),\end{aligned} \tag{4.53}$$

if the two component vector

$$c_n = \begin{pmatrix} c_n^+ \\ c_n^- \end{pmatrix} \tag{4.54}$$

of the expansion coefficients is used. The matrix structure of the $[\mathrm{i}\boldsymbol{\sigma}_2+\boldsymbol{\sigma}_3]$ matrix is

$$[\mathrm{i}\boldsymbol{\sigma}_2+\boldsymbol{\sigma}_3]^{\sigma,\sigma'} = \begin{array}{c} \\ \sigma \\ \downarrow \end{array}\begin{array}{c} \sigma' \ \rightarrow \\ \begin{pmatrix} 1 & 1 \\ -1 & -1 \end{pmatrix} \end{array}. \tag{4.55}$$

The matrix entries of the Hamiltonian of the Klein-Gordon equation (4.53) are

$$\begin{aligned}\boldsymbol{H}_{a,b} = E_a\boldsymbol{\sigma}_3\delta_{a,b} &- \frac{e\vec{A}_0\cdot c\hbar\vec{k}\sin(\omega t)}{2}\left(\frac{[\mathrm{i}\boldsymbol{\sigma}_2+\boldsymbol{\sigma}_3]}{\sqrt{E_aE_{a-1}}}\delta_{a,b+1}+\frac{[\mathrm{i}\boldsymbol{\sigma}_2+\boldsymbol{\sigma}_3]}{\sqrt{E_aE_{a+1}}}\delta_{a,b-1}\right)\\ &+\frac{e^2\vec{A}_0^2\sin^2(\omega t)}{8}\left(\frac{[\mathrm{i}\boldsymbol{\sigma}_2+\boldsymbol{\sigma}_3]}{\sqrt{E_aE_{a-2}}}\delta_{a,b+2}+\frac{2[\mathrm{i}\boldsymbol{\sigma}_2+\boldsymbol{\sigma}_3]}{E_a}\delta_{a,b}+\frac{[\mathrm{i}\boldsymbol{\sigma}_2+\boldsymbol{\sigma}_3]}{\sqrt{E_aE_{a+2}}}\delta_{a,b-2}\right).\end{aligned} \tag{4.56}$$

4.4 Dirac equation

The free state mode expansion of the Dirac equation is analogous to that of the Klein-Gordon equation. The functions (3.33) serve as basis elements

$$\psi_n^\sigma(\vec{x}) = \sqrt{\frac{k_L}{2\pi}} u^\sigma(\vec{k} + n\vec{k}_L) \mathrm{e}^{\mathrm{i}(\vec{k}+n\vec{k}_L)\cdot\vec{x}} \tag{4.57}$$

with the four bi-spinors (3.37). The advantage of bi-spinors in contrast to bi-scalars is, that bi-spinors are orthonormal and not pseudo orthonormal. The expansion of the wave function with respect to these basis elements is

$$\psi(\vec{x}) = \sum_{n,\sigma} c_n^\sigma \psi_n^\sigma(\vec{x}) = \sqrt{\frac{k_L}{2\pi}} \sum_{n,\sigma} c_n^\sigma u^\sigma(\vec{k} + n\vec{k}_L) \mathrm{e}^{\mathrm{i}(\vec{k}+n\vec{k}_L)\cdot\vec{x}} \,. \tag{4.58}$$

Similar to equations (4.41) and (4.42) the transformation into momentum space of the Dirac equation can be written in terms of matrix products, for which the following functions are defined.

$$t(\vec{k},\vec{k}') = d_+(\vec{k}) d_+(\vec{k}') + \vec{k}\cdot\vec{k}'\, d_-(\vec{k}) d_-(\vec{k}') \,, \tag{4.59a}$$
$$s^l(\vec{k},\vec{k}') = k_l d_-(\vec{k}) d_+(\vec{k}') + k'_l d_+(\vec{k}) d_-(\vec{k}') \,, \tag{4.59b}$$
$$r^l(\vec{k},\vec{k}') = k_l d_-(\vec{k}) d_+(\vec{k}') - k'_l d_+(\vec{k}) d_-(\vec{k}') \,, \tag{4.59c}$$
$$w^{lq}(\vec{k},\vec{k}') = k_l k'_q d_-(\vec{k}) d_-(\vec{k}') + k_q k'_l d_-(\vec{k}) d_-(\vec{k}') \,, \tag{4.59d}$$
$$g^{lq}(\vec{k},\vec{k}') = k_l k'_q d_-(\vec{k}) d_-(\vec{k}') - k_q k'_l d_-(\vec{k}) d_-(\vec{k}') \,, \tag{4.59e}$$
$$h^l(\vec{k},\vec{k}') = \vec{e}_l \cdot \left(\vec{k}\times\vec{k}'\right) d_-(\vec{k}) d_-(\vec{k}') \tag{4.59f}$$

These functions enter in the bi-spinor contractions

$$\boldsymbol{u}(\vec{k})\boldsymbol{u}(\vec{k}')^\dagger = t(\vec{k},\vec{k}')\mathbf{1} + \sum_l r^l(\vec{k},\vec{k}')\boldsymbol{\beta}\boldsymbol{\alpha}_l + \sum_{\substack{1\le l<q \\ l<q\le 3}} g^{lq}(\vec{k},\vec{k}')\boldsymbol{\alpha}_l\boldsymbol{\alpha}_q \,, \tag{4.60a}$$

$$\boldsymbol{u}(\vec{k})\boldsymbol{\beta}\boldsymbol{u}(\vec{k})^\dagger = \frac{mc^2}{E(\vec{k})}\boldsymbol{\beta} - \frac{c\hbar k_l}{E(\vec{k})}\boldsymbol{\alpha}_l \,, \tag{4.60b}$$

$$\begin{aligned}\boldsymbol{u}(\vec{k})\boldsymbol{\alpha}_l\boldsymbol{u}(\vec{k}')^\dagger = {} & t(\vec{k},\vec{k}')\boldsymbol{\alpha}_l - \sum_q w^{lq}(\vec{k},\vec{k}')\boldsymbol{\alpha}_q + s^l(\vec{k},\vec{k}')\boldsymbol{\beta} \\ & + \sum_{q\neq l} r^q(\vec{k},\vec{k}')\boldsymbol{\beta}\boldsymbol{\alpha}_q\boldsymbol{\alpha}_l + h^l(\vec{k},\vec{k}')\boldsymbol{\alpha}_1\boldsymbol{\alpha}_2\boldsymbol{\alpha}_3 \,,\end{aligned} \tag{4.60c}$$

which are derived in the appendix B.1. The time projection turns into

$$\left\langle \psi_n^\sigma \middle| \mathrm{i}\hbar\frac{\partial}{\partial t} \middle| \psi \right\rangle = \mathrm{i}\hbar \sum_{\sigma'} \left[\boldsymbol{u}(\vec{k}+n\vec{k}_L)\boldsymbol{u}(\vec{k}+n\vec{k}_L)^\dagger\right]^{\sigma,\sigma'} \dot{c}_n^{\sigma'} = \mathrm{i}\hbar\dot{c}_n^\sigma \,, \tag{4.61}$$

by using the orthonormality relation (B.16). The free Hamiltonian of the Dirac equation (3.31) results in the relativistic energy momentum relation

$$\left\langle \psi_n^\sigma \,\middle|\, \hat{\boldsymbol{H}}_0 \,\middle|\, \psi \right\rangle = \sum_{\sigma'} \left[\boldsymbol{u}(\vec{k}+n\vec{k}_L)\boldsymbol{H}_0(\vec{k}+n\vec{k}_L)\boldsymbol{u}(\vec{k}+n\vec{k}_L)^\dagger\right]^{\sigma,\sigma'} c_n^{\sigma'} = E(\vec{k}+n\vec{k}_L) \sum_{\sigma'} [\boldsymbol{\beta}]^{\sigma,\sigma'} c_n^{\sigma'} \,, \tag{4.62}$$

according to equation (B.18). The interaction Hamiltonian (3.32) with the vector potential (2.1b), in the form (4.27) and vanishing scalar potential Φ results in

$$\left\langle \psi_n^\sigma \,\middle|\, \boldsymbol{V} \,\middle|\, \psi \right\rangle = -\frac{e\sin(\omega t)}{2} \sum_{b,\sigma'} \left[\boldsymbol{u}(\vec{k}+n\vec{k}_L)^\dagger \left(\vec{A}_0\cdot\vec{\boldsymbol{\alpha}}\right) \boldsymbol{u}(\vec{k}+b\vec{k}_L)\right]^{\sigma,\sigma'} \left(\delta_{n,b-1} + \delta_{n,b+1}\right) c_b^{\sigma'} \,. \tag{4.63}$$

Adding up (4.61), (4.62) and (4.63) yields

The Dirac equation in momentum space

$$\begin{aligned} \mathrm{i}\hbar\dot{c}_n = E_n\boldsymbol{\beta}c_n &- \frac{e\sin(\omega t)}{2}\boldsymbol{u}(\vec{k}+n\vec{k}_L)^\dagger\left(\vec{A}_0\cdot\vec{\boldsymbol{\alpha}}\right)\boldsymbol{u}(\vec{k}+(n-1)\vec{k}_L)c_{n-1} \\ &- \frac{e\sin(\omega t)}{2}\boldsymbol{u}(\vec{k}+n\vec{k}_L)^\dagger\left(\vec{A}_0\cdot\vec{\boldsymbol{\alpha}}\right)\boldsymbol{u}(\vec{k}+(n+1)\vec{k}_L)c_{n+1}\,, \end{aligned} \tag{4.64}$$

with the four component vector of expansion coefficients

$$c_n = \left(c_n^{+\uparrow}, c_n^{+\downarrow}, c_n^{-\uparrow}, c_n^{-\downarrow}\right)^T . \tag{4.65}$$

The corresponding Hamiltonian matrix of this system of differential equations is

$$\boldsymbol{H}_{0;a,b} = E_a\boldsymbol{\beta}\delta_{a,b} \tag{4.66}$$

for the free Hamiltonian and

$$\begin{aligned} \boldsymbol{V}_{a,b} = &- \frac{e\sin(\omega t)}{2}\boldsymbol{u}(\vec{k}+a\vec{k}_L)^\dagger\left(\vec{A}_0\cdot\vec{\boldsymbol{\alpha}}\right)\boldsymbol{u}(\vec{k}+b\vec{k}_L)\delta_{a,b+1} \\ &- \frac{e\sin(\omega t)}{2}\boldsymbol{u}(\vec{k}+a\vec{k}_L)^\dagger\left(\vec{A}_0\cdot\vec{\boldsymbol{\alpha}}\right)\boldsymbol{u}(\vec{k}+b\vec{k}_L)\delta_{a,b-1} \end{aligned} \tag{4.67}$$

for the interaction Hamiltonian.

Chapter 5

Properties of the 2-photon Kapitza-Dirac effect

In this chapter, the quantum dynamics of the 2-photon Kapitza-Dirac effect is solved by numerical application of the quantum wave equations in chapter 4. The chapters 6, 7 and 8 introduce and consider properties of the 3-photon Kapitza-Dirac effect and are based on the contents of this chapter.

There are two simulation scenarios in this chapter: One scenario applies the Pauli equation 4.2 and reproduces the experiment, which has been carried out by Batelaan [50]. In the second scenario, the laser frequency and the laser intensity are substantially higher than in [50]. As a result, the quantum dynamics is faster in the second scenario and can be simulated by numerically solving the Klein-Gordon equation and the Dirac equation. The last section of this chapter discusses the influence of long turn on and long turn off times of the external laser field on the diffraction process.

5.1 Setup

The simplest application of the derived wave equations in momentum space of chapter 4 is the 2-photon Kapitza-Dirac effect for the parameters of its first experimental verification in the Bragg regime [50]. The optical wavelength of 532 nm translates in the wave number $k_L = 4.6 \cdot 10^{-6}\, mc/\hbar$ for the laser and the kinetic energy of 380 eV translates in the momentum of about $0.039\, mc$ for the electron. From the intensity of $3 \cdot 10^8 \mathrm{W/cm^2}$ one computes a ponderomotive amplitude (see equation (2.5)) of $7.5 \cdot 10^{-12} mc^2$. Since the electron inclines almost perpendicularly at the laser beam, one can use a geometry, in which the wave vector of the laser is $\vec{k}_L = 4.6 \cdot 10^{-6}\, mc/\hbar\, \vec{e}_1$ and the electron momentum component perpendicular to the laser beam is $\hbar\vec{k} = 0.039\, mc\, \vec{e}_3$. It remains to determine the small electron momentum in laser propagation direction from energy and momentum conservation, as it is discussed in section 2.2. According to the considerations in this section, the 2-photon Kapitza-Dirac effect should occur, if one photon is absorbed from the left laser beam and one photon is emitted into the right laser beam. Equation (2.19) tells, that the initial electron momentum must be minus one photon momentum. Therefore, the initial momentum vector of the incoming electron is $\vec{p}_{\mathrm{in}} = \hbar(\vec{k} - \vec{k}_L)$ and the final momentum of the outgoing electron is $\vec{p}_{\mathrm{out}} = \hbar(\vec{k} + \vec{k}_L)$. The initial momentum corresponds to the initial quantum state, in which the expansion coefficient $c^{\uparrow}_{-1}(0)$ is 1.0 and all other expansion coefficients are zero at time 0. The choice of setting the $c^{\uparrow}_{-1}(0)$ coefficient to one and the $c^{\downarrow}_{-1}(0)$ coefficient to zero implies that the electron spin points in the x_3-direction, initially.

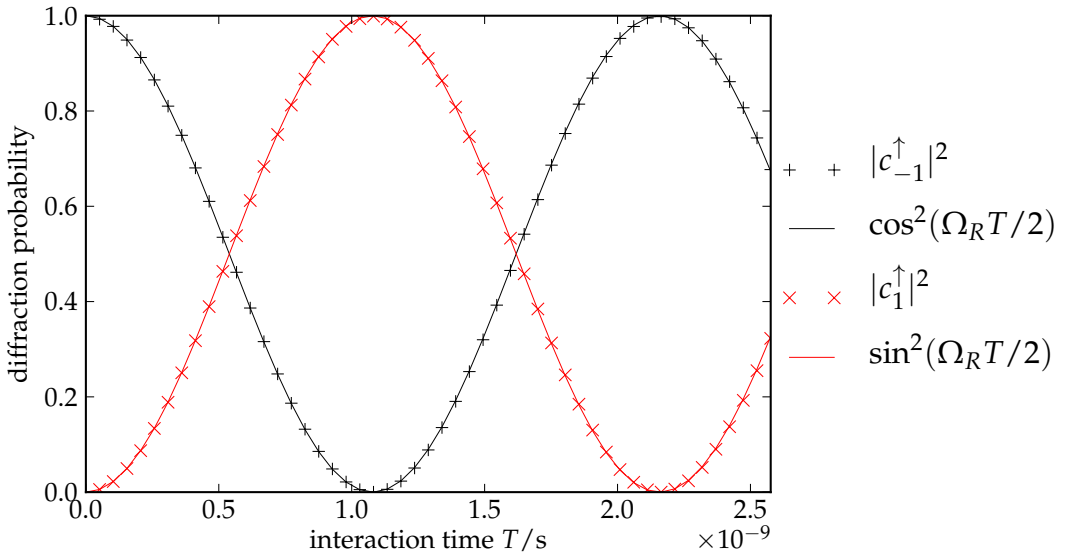

Figure 5.1: This figure shows the quantum mechanical time-evolution of the Kapitza-Dirac effect by integrating the Pauli equation (4.36). The result is directly compared with the analytical result (5.1) from Batelaan [50]. The simulation parameters are consistent with the first experimental demonstration of the Kapitza-Dirac effect by Freimund and Batelaan [50]. The parameters in [50] are a laser intensity of $3.0 \cdot 10^8\,\mathrm{W/cm^2}$, a laser wave length of 532 nm, an electron momentum of $19.7\,\mathrm{keV}/c$ and an interaction time in the range of nanoseconds, whereas the amplitude of the external laser field is turned on and turned off in ten laser cycles in the simulation.

5.2 Rabi oscillations

The time evolution of the discussed initial quantum state is shown in figure 5.1, where the absolute square of the coefficients $c_{-1}^{\uparrow}$ and $c_1^{\uparrow}$ is plotted. Note, that the amplitude of the external vector potential is turned on and turned off by a sine shaped envelope of ten laser cycles for each data point in figure 5.1, according to equation (5.4). The turn on and turn off of the external field is discussed in detail in section 5.3.

The absolute squares of all other coefficients than $c_{-1}^{\uparrow}$ and $c_1^{\uparrow}$ are negligibly small. This is consistent with the property, that the sum of $|c_{-1}^{\uparrow}|^2$ and $|c_1^{\uparrow}|^2$ is one, because the time-evolution is unitary. Figure 5.1 also shows, that the diffraction probability oscillates in Rabi cycles according to

$$|c_{-1}^{\uparrow}|^2 = \cos^2\left(\frac{\Omega_R T}{2}\right) \tag{5.1a}$$

$$|c_1^{\uparrow}|^2 = \sin^2\left(\frac{\Omega_R T}{2}\right) . \tag{5.1b}$$

This property has been clearly pointed out in 1971 by Gush and Gush [31]. The Rabi frequency

$$\Omega_R = \frac{V_0}{2\hbar} \tag{5.2}$$

is proportional to the ponderomotive amplitude, according to Batelaan [27]. Equation (5.2) yields the frequency $\Omega_R = 3.75 \cdot 10^{-12}\, mc^2/\hbar$ for the ponderomotive amplitude $V_0 = 7.50 \cdot 10^{-12}\, mc^2$. The corresponding Rabi period of 2.16 ns is consistent with the simulation in figure 5.1. The experiment [50] also agrees with the numerical solution of the Pauli equation in figure 5.1. Note, that the negligibly small spin-flip probability $|c_1^{\downarrow}|^2$ implies, that the quantum dynamics of the 2-photon Kapitza-Dirac effect does not affect the electron spin.

Even though, the interaction time of one nanosecond appears short compared to the speed of human response, it is a long time compared to one laser period and an even longer time compared to the oscillation period of the electron phase in the relativistic quantum wave equations. In the example of figure 5.1, one Rabi cycle consists of $1.2 \cdot 10^6$ laser cycles and $2.7 \cdot 10^{11}$ periods of the electron phase in the complex plane. A quantum dynamical simulation should resolve these oscillations appropriately, which means, that a simulation of the Pauli equation (4.36) requires at least one million time steps and a simulation with the Klein-Gordon or Dirac equation (4.53),(4.64) requires at least one trillion time steps. It seems that the Klein-Gordon and Dirac equation in the form (4.53),(4.64) are not suited for simulation parameters with optical light and low intensities. Therefore, the main part of this work will consider standing light waves of high frequencies in the X-ray regime with much higher intensities than used in the experiment [50].

The resonance conditions (2.17) and (2.19) of energy and momentum conservation imply, that the electron is always diffracted from momentum $-k_L$ (or k_L) to k_L (or $-k_L$ respectively) in laser propagation direction in the case of the 2-photon Kapitza-Dirac effect. This means, the 2-photon Kapitza-Dirac effect would occur for every laser photon momentum $\hbar k_L$, if the initial electron momentum was $\vec{p}_{\text{in}} = \hbar(\vec{k}_0 \pm \vec{k}_L)$. This means in turn, that the electron must approach the laser beam at the Bragg angle. The laser photon momentum $k_L = 0.05\, mc/\hbar$ with a corresponding photon energy of 25.55 keV seems to fit well for a high but still non-relativistic photon energy.

The ponderomotive amplitude of the external potential needs to be adjusted to the laser frequency. The amplitude should be as high as possible, such that one Rabi period is short and the number of time steps for simulations with relativistic quantum wave equations is short. On the other hand, the uncertainty in transition energy of the 2-photon Kapitza-Dirac effect should be larger than the energy spacing of different energy eigen values of the free Hamiltonian. This requirement led Batelaan to the condition

$$\Delta E\, T \gg \frac{\hbar}{2} \tag{5.3}$$

for the so-called "Bragg regime" [27], where ΔE is the recoil shift $\hbar^2 k_L^2/(2m)$ and T is one Rabi period. The opposite case would be the so-called "Diffraction regime". If one chooses a ponderomotive amplitude of $V_0 = 2.0 \cdot 10^{-5} mc^2$, the inequality of condition (5.3) turns into $157.1 \gg 1$ and the quantum dynamics corresponds to the Bragg regime. The duration of one Rabi cycle reduces to 0.77 fs due to the higher amplitude of the ponderomotive potential. Figure 5.2 shows a simulation of the 2-photon Kapitza-Dirac effect with the new parameters. Like in figure 5.1, the data points from the simulation with the Pauli equation fit to the analytical solution (5.1). The same holds for the simulation data of the Klein-Gordon and Dirac equation. The spin-flip probability is negligibly small again.

5.3 Realistic pulse shape

The turn on and turn off time of the external vector potential is only 10 laser cycles for the quantum dynamics in the sections 5.1 and 5.2. This is a very short time compared to the full interaction time T. The advantage of this short turn on and short turn off time is, that the time evolution is numerically easier to compute and that the quantum dynamics evolves in a more systematic behavior, which makes it easier to investigate it. One may ask, whether the Kapitza-Dirac effect takes place for a longer turn on, a longer turn off and a shorter plateau phase of the external potential, given by the envelope function

$$A_3(t) = A_{3,\max} \cdot \begin{cases} \sin^2\left(\frac{\pi}{2}\frac{t}{\Delta T}\right) & \text{, if } 0 \le t \le \Delta T \\ 1 & \text{, if } \Delta T < t < T - \Delta T \\ \sin^2\left(\frac{\pi}{2}\frac{(T-t)}{\Delta T}\right) & \text{, if } T - \Delta T \le t \le T \\ 0 & \text{else.} \end{cases} \tag{5.4}$$

The turn on and turn off duration $\Delta T = fT/2$ is the fraction f of the full interaction time T. The fraction f may vary between 0 and 1, where $f = 0$ corresponds to an instantaneous turn on and turn off and $f = 1$ corresponds to a vanishing plateau phase.

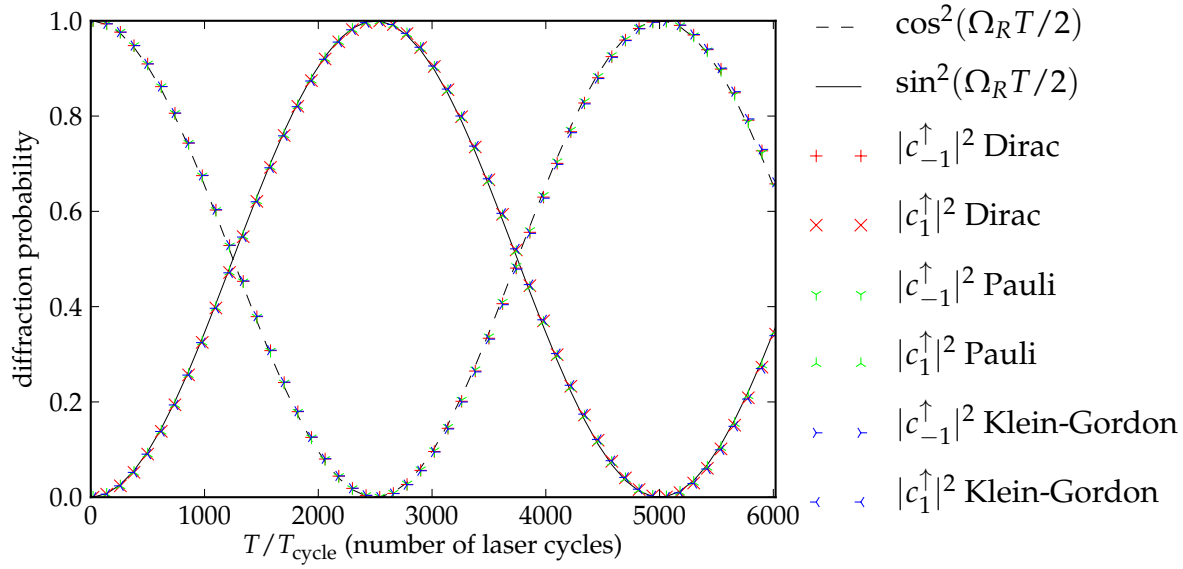

Figure 5.2: This figure shows the same time evolution, as in figure 5.1, but with other laser parameters and for a different initial electron momentum. The result of simulations with relativistic quantum wave equations (Klein-Gordon and Dirac equation equation) is shown in addition to the results of the Pauli equation. The laser intensity of this simulation corresponds to $2.32 \cdot 10^{22}\,\mathrm{W/cm^2}$, with a laser wave length of 48.5 nm. The electron momentum perpendicular to the laser propagation direction is $0.05mc = 25.55\,\mathrm{keV}/c$.

If the external potential is turned on and off more slowly, the Rabi cycle will be delayed, which has to be accounted for in the analytic solution (5.1) of the Kapitza-Dirac effect. The solution (5.1) originates from the truncated Schrödinger equation with a ponderomotive potential (4.11)

$$\mathrm{i}\hbar\dot{c}_{-1} = \frac{V_0(t)}{4} c_1 \tag{5.5a}$$

$$\mathrm{i}\hbar\dot{c}_{1} = \frac{V_0(t)}{4} c_{-1}\,, \tag{5.5b}$$

which in this case has been shifted in energy by $-\hbar^2(\vec{k} + n\vec{k}_L)^2/2m - V_0/2$, resulting in a time-dependent, dispensable change of the global phase of the solution. A solution of equation (5.5), whose time-dependent ponderomotive coupling is related via equation (2.5) to the amplitude (5.4) is given by

$$c_{-1}(t) = \quad \cos(t') \tag{5.6a}$$

$$c_{1}(t) = -\mathrm{i}\sin(t')\,, \tag{5.6b}$$

with the warped time parameter

$$t'(t) = \int_0^t \frac{V_0(\tau)}{4\hbar} d\tau\,. \tag{5.7}$$

If one performs the integral (5.7) and requires, that $t'(T) \stackrel{!}{=} \pi/2$ and solves for T, one obtains

$$T = \frac{\pi}{2} \frac{16mc^2\hbar}{e^2 A_{3,\max}^2} \frac{8}{8-5f} = \frac{\pi}{\Omega_R} \frac{8}{8-5f}\,, \tag{5.8}$$

where the ponderomotive amplitude (2.5) is reidentified in equation (5.8) and also the Rabi frequency (5.2) is resubstituted. Equation (5.8) tells, that one half Rabi cycle π/Ω_R needs to be extended by the

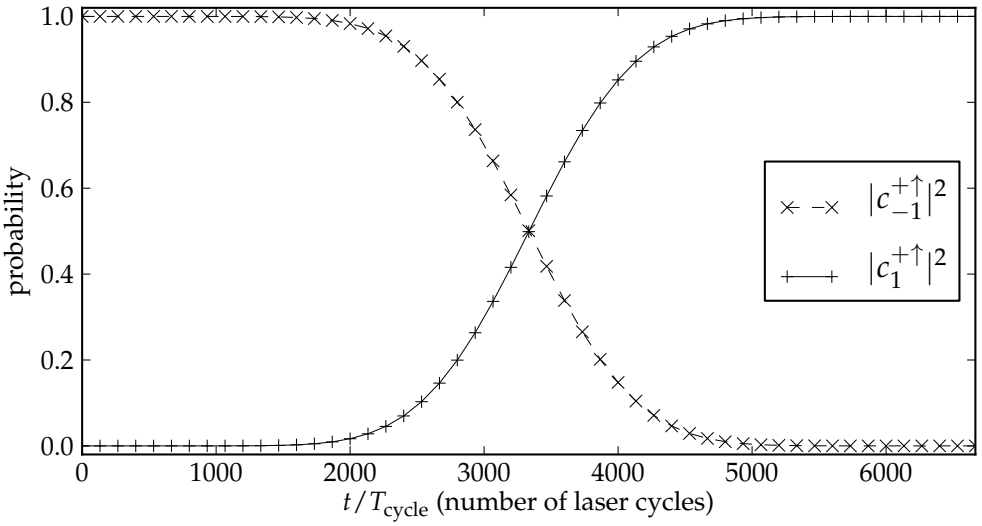

Figure 5.3: This figure shows the same Kapitza-Dirac effect as in figure 5.2, simulated by using the Dirac equation. In contrast to figure 5.2, the turn on and turn off time ΔT is the half of the interaction time T, which corresponds to $f = 1$. Note, that in contrast to the figures 5.1 and 5.2, the in-field quantum dynamics is shown, in which the external field is not smoothly turned off. If, according to (5.8) the full interaction time T is stretched by the factor $8/3$, a full quantum transition from mode -1 to mode 1 appears for an interaction time T, which is larger than in figure 5.2.

factor $8/(8-5f)$, if the fraction fT of the interaction time elapses for the turn on and turn off of the external laser field. The extension by this factor compensates the turn on and turn off phase of the interaction such, that the occupation probability fully evolves from c_{-1} to c_1 after the interaction.

Figure 5.3 shows the stretched quantum dynamics by an explicit example, in which f equals 1. The property, that the electron beam is always diffracted by 100%, if one accounts for the envelope form (5.4) and stretches the interaction time according to equation (5.8), is demonstrated in figure 5.4.

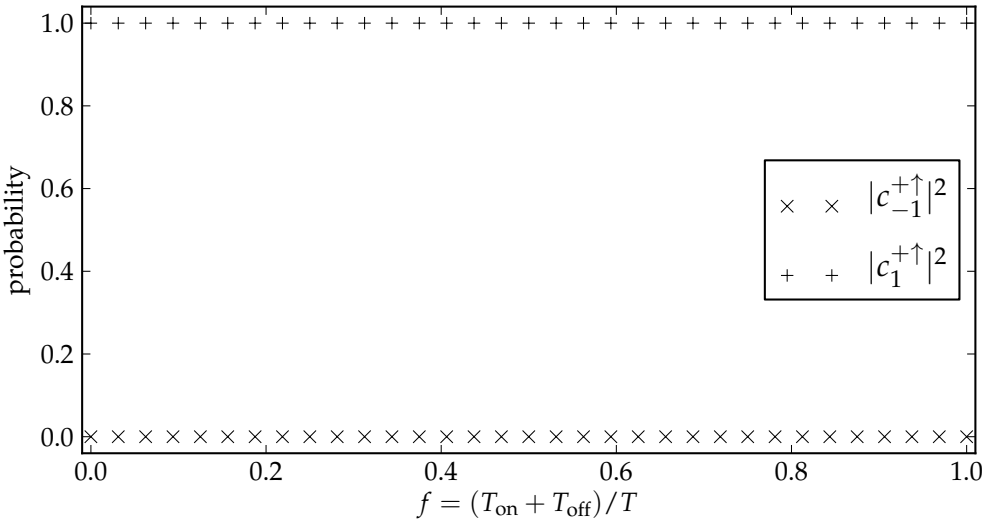

Figure 5.4: This figure shows the final diffraction probability of the Kapitza-Dirac effect, for a variation of the fraction f in the time-dependent envelope function (5.4) of the potential amplitude of the external laser field. For each f, the interaction time T has been chosen according to (5.8). The simulations are identical to the simulations in figure 5.3, except the different potential envelope. One can see, that the electron is always diffracted by 100%, if one accounts for the extension factor $8/(8-5f)$ for the interaction time T. The figures 5.2 and 5.3 show the time-evolution of the extreme cases, in which f almost vanishes or equals 1, respectively.

Chapter 6

Electron spin dynamics: Conceptual considerations

No spin effects appeared in the quantum dynamics of the 2-photon Kapitza-Dirac effect in chapter 5. This is expected from the Schrödinger equation (4.11). Even in the case of the Pauli equation (4.36), it seems, that the spin-dependent coupling term $\vec{\sigma} \cdot \vec{B}$ plays a minor role in the quantum dynamics of the 2-photon Kapitza-Dirac effect. This is different for the case of the 3-photon Kapitza-Dirac effect, which is discussed analytically in chapter 7 and numerically in chapter 8.

Whereas the 2-photon Kapitza-Dirac effect is not relying on a distinction of the spin-up and spin-down components of the wave function, the 3-photon Kapitza-Dirac effect connects both components with each other. The general diffraction properties and an interpretation of the quantum dynamics of the 3-photon Kapitza-Dirac effect are discussed in this chapter. In order to do so, the propagator of the wave function is introduced. The propagator contains not only information about the time-evolution of *one* quantum state but it contains information about the time-evolution of *any* quantum state. Therefore, the information, which can be extracted from properties of the propagator is comprehensive.

A subsequent consideration discusses, whether the configuration of the initial electron spin affects the diffraction pattern. By anticipation of the results from perturbation theory in chapter 7 and the numerical investigation in chapter 8 it is concluded, that the diffraction probability does not depend on the initial electron spin. This implies, that the spin-dependent part of the propagator can be parameterized by a $\mathcal{SU}(2)$ representation. A further analysis of the properties of the $\mathcal{SU}(2)$ representation illustrates, that the electron spin is rotated, when it is diffracted.

6.1 The propagator

The quantum state of the wave functions' expansion coefficients c_a^σ may be mapped from the initial time t_0 to the final time t by the propagator $\boldsymbol{U}_{a,b}^{\sigma,\sigma'}(t,t_0)$ according to

$$c_a^\sigma(t) = \sum_{b,\sigma'} \boldsymbol{U}_{a,b}^{\sigma,\sigma'}(t,t_0) c_b^{\sigma'}(t_0)\,. \tag{6.1}$$

The propagation from time t_0 to t_0 is the quantum state itself. Therefore, the propagator has the property

$$\boldsymbol{U}_{a,b}^{\sigma,\sigma'}(t_0,t_0) = \delta_{a,b}\delta_{\sigma,\sigma'}\,. \tag{6.2}$$

This means, that the propagator is related to a solution of the fundamental system of the differential equation

$$\mathrm{i}\hbar \dot{c}_a^\sigma = \sum_{b,\sigma'} \hat{\boldsymbol{H}}_{a,b}^{\sigma,\sigma'} c_b^{\sigma'}\,, \tag{6.3}$$

which is the general quantum wave equation (3.1) in momentum space. The propagator entries with an identical mode index $\boldsymbol{U}_{a,a}^{\sigma,\sigma'}(t,t_0)$ correspond to the probability, that the electron does not change its momentum after Kapitza-Dirac scattering. All other propagator entries $\boldsymbol{U}_{a,b}^{\sigma,\sigma'}(t,t_0)$ with $a \neq b$ correspond to a transition matrix element, which describes the change of the electron momentum from $\hbar(\vec{k}+b\vec{k}_L)$ to momentum $\hbar(\vec{k}+a\vec{k}_L)$ after Kapitza-Dirac scattering. In the case of the 3-photon Kapitza-Dirac effect, the electron starts in mode 0, with momentum $\hbar\vec{k}$ and is diffracted to mode 3 with momentum $\hbar(\vec{k}+3\vec{k}_L)$. Therefore, the propagator subentry $\boldsymbol{U}_{3,0}(t,t_0)$ is of interest in the following.

In the case of the Pauli equation, the propagator $\boldsymbol{U}_{3,0}(t,t_0)$ is a 2×2 matrix. However, in the case of the Dirac equation, $\boldsymbol{U}_{3,0}(t,t_0)$ is a 4×4 matrix. But the propagator entries, which relate the negative energy eigenstates to the positive energy eigenstates are negligibly small and are not of interest here. The propagator entries of interest for the Kapitza-Dirac effect, are those, which relate the positive energy eigenstates $\sigma' \in \{+\uparrow,+\downarrow\}$ to the positive energy eigenstates $\sigma \in \{+\uparrow,+\downarrow\}$. The corresponding subentry of $\boldsymbol{U}_{3,0}(t,t_0)$ of the propagator of the Dirac equation is a 2×2 matrix, too. The following considerations only refer to these 2×2 subentries of the propagator in the case of the Dirac equation.

The propagator is denoted by

$$\boldsymbol{U}_{3,0}(t,t_0) = \sqrt{P(t,t_0)}\mathrm{e}^{\mathrm{i}\phi(t,t_0)}\boldsymbol{S}(t,t_0)\,, \tag{6.4}$$

where $\sqrt{P(t,t_0)}$ is some amplitude, $\mathrm{e}^{\mathrm{i}\phi(t,t_0)}$ is some phase and $\boldsymbol{S}(t,t_0)$ is a spin-dependent part. $\boldsymbol{S}(t,t_0)$ is denoted by

$$\boldsymbol{S}(t,t_0) = \left[\cos\left(\frac{\alpha(t,t_0)}{2}\right)\mathbf{1} - \mathrm{i}\,\sin\left(\frac{\alpha(t,t_0)}{2}\right)\vec{n}(t,t_0)\cdot\vec{\boldsymbol{\sigma}}\right]\,, \tag{6.5}$$

with some angle α and some vector $\vec{n}$. If one requires, that $P,\phi,\alpha \in \mathbb{R}$, $\vec{n}\in\mathbb{C}^3$ and $|\vec{n}|^2 = 1$, the representation (6.4) has the 8 degrees of freedom, corresponding to the 8 degrees of freedom of a complex 2×2 matrix.

6.2 Spin dependence of the diffraction pattern

With the two component vector (4.33) of the Pauli equation or the corresponding two component vector of positive eigen energies of the Dirac equation

$$c_n^+ = \begin{pmatrix} c_n^{+\uparrow} \\ c_n^{+\downarrow} \end{pmatrix} \tag{6.6}$$

the quantum state propagation (6.1) from mode 0 to mode 3 can be noted by

$$c_3(t) = \boldsymbol{U}_{3,0}(t,t_0)c_0(t_0) \text{ for the Pauli equation} \tag{6.7a}$$

$$\text{and } c_3^+(t) = \boldsymbol{U}_{3,0}(t,t_0)c_0^+(t_0) \text{ for the Dirac equation.} \tag{6.7b}$$

The vector of positive eigen energy coefficients (6.6) of the Dirac equation should not be confused with the positive eigen energy coefficient of the Klein-Gordon equation in section 4.3. The diffraction probability to mode 3 may therefore be expressed in terms of the initial quantum state of mode 0 by

$$|c_3^{\uparrow}(t)|^2 + |c_3^{\downarrow}(t)|^2 = ||c_3(t)||_2 = c_3(t)^\dagger c_3(t) = c_0(t_0)^\dagger \boldsymbol{U}_{3,0}(t,t_0)^\dagger \boldsymbol{U}_{3,0}(t,t_0)c_0(t_0)\,. \tag{6.8}$$

In the case of the Dirac equation an index $+$ needs to be added at each expansion coefficient to denote the positive eigen energy expansion coefficients only. The product of the adjoint propagator with itself in equation (6.8) can be expanded to

$$\boldsymbol{U}_{3,0}^\dagger \boldsymbol{U}_{3,0} = P\boldsymbol{S}^\dagger\boldsymbol{S} = P\left[\left(\cos^2\left(\frac{\alpha}{2}\right) + |\vec{n}|^2\sin^2\left(\frac{\alpha}{2}\right)\right)\mathbf{1} + 2\cos\left(\frac{\alpha}{2}\right)\sin\left(\frac{\alpha}{2}\right) Im(\vec{n})\cdot\vec{\boldsymbol{\sigma}}\right] = \tag{6.9a}$$

$$= P\left[\mathbf{1} + \sin(\alpha)\, Im(\vec{n})\cdot\vec{\boldsymbol{\sigma}}\right]\,, \tag{6.9b}$$

where the time-dependence (t, t_0) is omitted in this notion. The identity term in (6.9b), would yield

$$P_{3,0}(t,t_0)c_0(t_0)^\dagger c_0(t_0) = P_{3,0}(t,t_0)||c_0(t_0)||_2 = P_{3,0}(t,t_0)\left(|c_0^\uparrow(t_0)|^2 + |c_0^\downarrow(t_0)|^2\right) \tag{6.10}$$

in equation (6.8). Since probability $|c_3^\uparrow(t)|^2 + |c_3^\downarrow(t)|^2$ and the probability $|c_0^\uparrow(t_0)|^2 + |c_0^\downarrow(t_0)|^2$ are completely spin independent, the identity term in equation (6.9b) does not induce any spin dependence in the diffraction pattern. In contrast, the term, which is proportional to the imaginary part of $\vec{n}$ in equation (6.9b) results in

$$P_{3,0}(t,t_0)\sin\left(\alpha_{3,0}(t,t_0)\right) Im(\vec{n}_{3,0}(t,t_0)) \cdot \left(c_0(t_0)^\dagger \vec{\sigma} c_0(t_0)\right) . \tag{6.11}$$

This diffraction probability is spin dependent. If, for example, the parameters in equation (6.10) and (6.11) were $P = 1/\sqrt{2}$, $\phi = 0$, $\alpha = \pi/2$ and $\vec{n} = \mathrm{i}\vec{e}_3$, then the initial quantum state $c_0^\uparrow = 1$, $c_0^\downarrow = 0$ is diffracted with probability 1, if one sums up the equations (6.10) and (6.11). On the other hand, if the initial quantum state was a spin down state $c_0^\uparrow = 0$, $c_0^\downarrow = 1$, the sum of the diffraction probabilities (6.10) and (6.11) yields 0.

The results from perturbation theory (7.39) and (7.83) contain no imaginary part of the vector $\vec{n}$. And also the numerical results in chapter 8 fit to a propagator, in which the imaginary part of $\vec{n}$ is negligible. Since the imaginary part of $\vec{n}$ is vanishingly small, the diffraction probability in the case of the 3-photon Kapitza-Dirac effect is independent of the incoming electron spin. A spin independence of the diffraction pattern still allows for a rotation of the electron spin, which is described in the next section. Due to the vanishing imaginary part of $\vec{n}$ the electron cannot be sorted out by its initial spin configuration, as it has been suggested by Batelaan [38].

6.3 Spin rotation in Pauli theory

Since the imaginary part of $\vec{n}$ vanishes, the spin-dependent part (6.5) of the propagator (6.4) looses 3 of its 6 degrees of freedom and therewith fulfills the properties of an $\mathcal{SU}(2)$ representation of rotations. In fact, the expectation value of the spin operator (3.11) is rotated by the $\mathcal{SU}(2)$ representation of the propagator.

In order to explain this property, the initial quantum state of the electron is written in terms of the Bloch state

$$c_0^\uparrow = \mathrm{e}^{\phi_0}\cos\left(\frac{\theta}{2}\right) , \qquad c_b^\downarrow = \mathrm{e}^{\phi_0}\mathrm{e}^{\mathrm{i}\varphi}\sin\left(\frac{\theta}{2}\right) . \tag{6.12}$$

The spin expectation value of the operator (3.11) with respect to this quantum state results in the vector $\hbar\vec{n}_0^s/2$

$$\left\langle c_0 \middle| \vec{S}^P \middle| c_0 \right\rangle = \frac{\hbar}{2}\begin{pmatrix} c_0^\dagger\sigma_1 c_0 \\ c_0^\dagger\sigma_2 c_0 \\ c_0^\dagger\sigma_3 c_0 \end{pmatrix} = \begin{pmatrix} \sin(\theta)\cos(\varphi) \\ \sin(\theta)\sin(\varphi) \\ \cos(\theta) \end{pmatrix} = \frac{\hbar}{2}\vec{n}_0^s , \tag{6.13}$$

whose direction is parameterized by the angles θ and ϕ of spherical coordinates. The spin expectation value of the quantum state c_3 in equation (6.7) evaluates to

$$\left\langle c_3 \middle| S_i^P \middle| c_3 \right\rangle = P_{3,0}\frac{\hbar}{2}c_0^\dagger S_{3,0}^\dagger \sigma_i S_{3,0} c_0 = P_{3,0}\frac{\hbar}{2}\sum_j R_{ij}c_0^\dagger\sigma_j c_0 = P_{3,0}\frac{\hbar}{2}\sum_j R_{ij}n_{0,j}^s = P_{3,0}\frac{\hbar}{2}n_{3,i}^s , \tag{6.14}$$

where the left lower index of the vector $\vec{n}^s$ denotes the mode index and the right lower index denotes the three spacial components of the vector. The matrix R_{ij} is the $\mathcal{SO}(3)$ rotation matrix $R = \exp(-\alpha_{3,0}\vec{n}_{3,0}\vec{D})$ with the generating Lie algebra $D_1 = \delta_{3,2} - \delta_{2,3}$, $D_2 = \delta_{1,3} - \delta_{3,1}$ and $D_3 = \delta_{2,1} - \delta_{1,2}$. The matrix R_{ij} acts as right-handed rotation around the axis $\vec{n}_{3,0}$ with the rotation angle α on vectors in $\mathbb{R}^3$. In particular, the direction $\vec{n}_0^S$ is right-handed rotated by the angle $\alpha_{3,0}$ around axis $\vec{n}_{3,0}$ to the angle $\vec{n}_3^S$, if the $\mathcal{SU}(2)$ representation $S_{3,0}$ acts at the quantum state c_0 in mode 0. This is illustrated in figure 6.1.

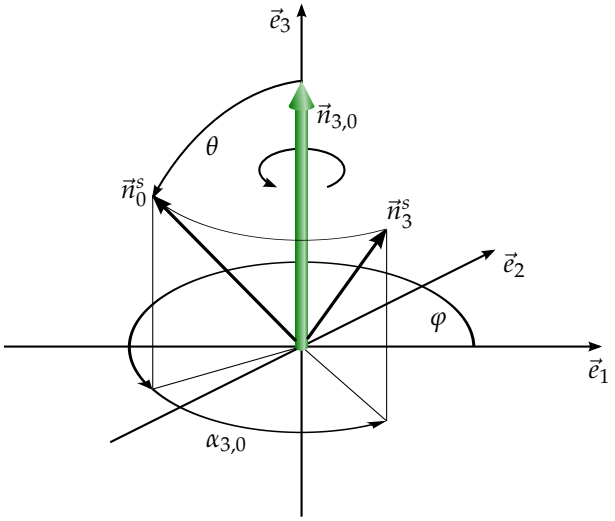

Figure 6.1: The direction of the spin $\vec{n}_0^s$ of the quantum state c_0 is rotated by the $\mathcal{SU}(2)$ representation $S_{3,0}$ to the direction $\vec{n}_3^s$ of the quantum state c_3 around the axis $\vec{n}_{3,0}$ by the angle $\alpha_{3,0}$. In this illustrative sketch, the rotation axis coincides with the 3-axis, such that the azimuthal angle θ of the spherical coordinates is not changed, but the polar angle φ of the polar coordinates is increased by $\alpha_{a,b}$ modulo 2π. This implies, that the spin is conserved in $\vec{n}_{3,0}$ direction but changes in all directions perpendicular to $\vec{n}_{3,0}$. The statement of this figure also applies for Dirac theory, if the electron spin of the incoming and outgoing electron is considered in its rest frame of reference.

6.4 Spin rotation in Dirac theory

The objects of interest in Dirac theory are the spin expectation value of the Foldy-Wouthuysen spin operator (3.40) with the basis functions (3.33). Since $\boldsymbol{u}(\vec{k})$ of equation (3.35) is a unitary matrix and the bi-spinors $u^\sigma(\vec{k})$ are columns of $\boldsymbol{u}^\dagger(\vec{k})$, the $u^\sigma(\vec{k})$ are mapped at the unit vectors $\vec{e}^\sigma$ of $\mathbb{R}^4$, by $\boldsymbol{u}(\vec{k})$.

Therefore, the matrix entries of the spin operator (3.40) with respect to the basis elements (4.57) at mode n

$$\langle \psi_n^\sigma | \boldsymbol{S}_{FW} | \psi_n^{\sigma'} \rangle = u^\sigma(\vec{k}+n\vec{k}_L)^\dagger \boldsymbol{u}(\vec{k}+n\vec{k}_L)^\dagger \frac{\hbar}{2}\vec{\boldsymbol{\Sigma}}\, \boldsymbol{u}(\vec{k}+n\vec{k}_L) u^{\sigma'}(\vec{k}+n\vec{k}_L) = \vec{e}^{\sigma\dagger}\frac{\hbar}{2}\vec{\boldsymbol{\Sigma}}\vec{e}^{\sigma'} = \frac{\hbar}{2}\vec{\boldsymbol{\Sigma}}^{(\sigma,\sigma')} \tag{6.15}$$

is equivalent to the matrix entries of the non-relativistic spin operator (3.41).

Similar to section 6.3, the positive eigen energy quantum state of mode 0 can be expressed in terms of the Bloch state

$$c_0^{+\uparrow} = \mathrm{e}^{\phi_0}\cos\left(\frac{\theta}{2}\right), \qquad c_0^{+\downarrow} = \mathrm{e}^{\phi_0}\mathrm{e}^{\mathrm{i}\varphi}\sin\left(\frac{\theta}{2}\right), \qquad c_0^{-\uparrow} = 0\,, \qquad c_0^{-\downarrow} = 0\,. \tag{6.16}$$

The occupation probability of all other modes is 0. Therefore, the expectation value of the wave function (4.58) reduces to

$$\langle \psi | \boldsymbol{S}_{FW} | \psi \rangle = c_0^\dagger \frac{\hbar}{2}\vec{\boldsymbol{\Sigma}} c_0 = c_0^{+\dagger}\frac{\hbar}{2}\vec{\boldsymbol{\sigma}} c_0^+ = \frac{\hbar}{2}\vec{n}_0^s\,. \tag{6.17}$$

The quantum state of the diffracted mode is given by equation (6.7b). If one assumes a 100% diffraction probability $P_{3,0} = 1$, the occupation probability of mode 0 is 0. Hence, the spin expectation value after the diffraction results in

$$\langle \psi_{\text{out}} | \boldsymbol{S}_{FW,i} | \psi_{\text{out}} \rangle = c_0^{+\dagger}\frac{\hbar}{2}\boldsymbol{U}_{3,0}^\dagger \boldsymbol{\sigma}_i \boldsymbol{U}_{3,0} c_0^+ = \frac{\hbar}{2}\sum_j R_{ij} n_{0,j}^s = \frac{\hbar}{2} n_{3,i}^s\,. \tag{6.18}$$

Therefore, the spin rotation described by Pauli theory also applies to quantum dynamics with the Dirac equation, if the spin was measured with the Foldy-Wouthuysen spin operator. Since the bi-spinors $u^\sigma(\vec{k})$ at rest are just the unit vectors of $\mathbb{R}^4$, the Foldy-Wouthuysen spin operator measures

the spin in the rest-frame of the electron. Therefore, the statement in the case of the Pauli equation, that electron spin $\vec{n}_0^s$ is right-handed rotated around the axis $\vec{n}_{3,0}$ with the angle $\alpha_{3,0}$ also applies to Dirac theory. The difference to Pauli theory is, that this statement applies to the electron spin in the rest-frame of the electron, in the case of Dirac theory.

Chapter 7

Electron spin dynamics: Analytical small-time behavior

This chapter solves the quantum dynamics of the 3-photon Kapitza-Dirac effect, by utilizing time-dependent perturbation theory with the quantum wave equations in momentum space of chapter 4. The result of the calculation is identified with the $\mathcal{SU}(2)$-representation (6.4) in chapter 6. Diffraction properties, like the Rabi frequency and the rotation angle, with which the spin is rotated are concluded from the perturbative result. These results are checked numerically in chapter 8.

This chapter starts with a general summary of time-dependent perturbation theory in section 7.1. The lowest order contributions of time-dependent perturbation theory are computed for the 3-photon Kaptiza-Dirac effect for the case of the Pauli equation (section 7.2) and for the case of the Dirac equation (section 7.3). The resonance condition resulting from considerations of energy and momentum conservation of chapter 2.2 is explicitly used in the calculations and plays an important role in the derivation of the perturbative result. Only terms, with a divergent time dependence are dominant over all other terms and are accounted in the calculation.

7.1 General procedure

This summary of time-dependent perturbation theory is based on the lecture notes of Christof Wetterich from the year 2009 [51]. Time dependent perturbation theory relies on the identity

$$\boldsymbol{U}(t,t_0) = \boldsymbol{U}_0(t,t_0) + \frac{1}{\mathrm{i}\hbar}\int_{t_0}^{t} dt_1 \boldsymbol{U}_0(t,t_1)\hat{\boldsymbol{V}}(t_1)\boldsymbol{U}(t_1,t_0)\,, \tag{7.1}$$

which satisfies

$$\frac{\partial}{\partial t}\boldsymbol{U}(t,t_0) = \frac{1}{\mathrm{i}\hbar}(\hat{\boldsymbol{H}}_0 + \hat{\boldsymbol{V}}(t))\boldsymbol{U}(t,t_0) \tag{7.2}$$

with the free propagator

$$\boldsymbol{U}_0(t,t_0) = \mathrm{e}^{-\frac{\mathrm{i}}{\hbar}(t-t_0)\hat{\boldsymbol{H}}_0}\,. \tag{7.3}$$

and the interaction Hamiltonian $\hat{\boldsymbol{V}}$. Since equation (7.2) is equivalent to equation (3.1), the solution (7.1) contains the time evolution of the wave function. Inserting eq. (7.1) recursively into itself yields a series, which is assumed to converge on the interval $[t_0, t]$. The first four terms of this series are

$$\boldsymbol{U}(t,t_0) = \boldsymbol{U}_0(t,t_0) + \boldsymbol{U}_{\mathrm{st}}(t,t_0) + \boldsymbol{U}_{\mathrm{nd}}(t,t_0) + \boldsymbol{U}_{\mathrm{rd}}(t,t_0) + \text{higher terms}\,, \tag{7.4}$$

where $\boldsymbol{U}_0(t,t_0)$ is the interaction-less time propagation,

$$\boldsymbol{U}_{\mathrm{st}}(t,t_0) = \frac{1}{\mathrm{i}\hbar}\int_{t_0}^{t} dt_1 \boldsymbol{U}_0(t,t_1)\hat{\boldsymbol{V}}(t_1)\boldsymbol{U}_0(t_1,t_0) \tag{7.5}$$

is the first order perturbation,

$$\boldsymbol{U}_{\mathrm{nd}}(t,t_0) = \frac{1}{(\mathrm{i}\hbar)^2}\int_{t_0}^{t} dt_2 \int_{t_0}^{t_2} dt_1 \boldsymbol{U}_0(t,t_2)\hat{\boldsymbol{V}}(t_2)\boldsymbol{U}_0(t_2,t_1)\hat{\boldsymbol{V}}(t_1)\boldsymbol{U}_0(t_1,t_0) \tag{7.6}$$

is the second order perturbation and

$$\boldsymbol{U}_{\mathrm{rd}}(t,t_0) = \frac{1}{(\mathrm{i}\hbar)^3}\int_{t_0}^{t} dt_3 \int_{t_0}^{t_3} dt_2 \int_{t_0}^{t_2} dt_1 \boldsymbol{U}_0(t,t_3)\hat{\boldsymbol{V}}(t_3)\boldsymbol{U}_0(t_3,t_2)\hat{\boldsymbol{V}}(t_2)\boldsymbol{U}_0(t_2,t_1)\hat{\boldsymbol{V}}(t_1)\boldsymbol{U}_0(t_1,t_0) \tag{7.7}$$

is the third order perturbation in time-dependent perturbation theory.

7.2 Perturbation Theory for the Pauli equation

This section considers time-dependent perturbation theory of the Pauli equation. The time-dependent perturbation theory of the Dirac equation of section 7.3 is based on the concepts of this section.

7.2.1 Derivation

Since the Pauli equation contains coupling terms to its neighboring and second next neighboring modes, the lowest order non-vanishing contribution of time-dependent perturbation theory of the 3-photon Kapitza-Dirac effect is of second order. The second order term (7.6) of time-dependent perturbation theory can be written as

$$\begin{aligned}&\boldsymbol{U}_{\mathrm{nd};3,0}(t,t_0) = \\ &\sum_{n_i, i\in\{1,2,3,4\}} \frac{1}{(\mathrm{i}\hbar)^2}\int_{t_0}^{t} dt_2 \int_{t_0}^{t_2} dt_1 \boldsymbol{U}_{0;3,n_1}(t,t_2)\boldsymbol{V}_{n_1,n_2}(t_2)\boldsymbol{U}_{0;n_2,n_3}(t_2,t_1)\boldsymbol{V}_{n_3,n_4}(t_1)\boldsymbol{U}_{0;n_4,0}(t_1,t_0)\,,\end{aligned} \tag{7.8}$$

with the free propagator

$$\boldsymbol{U}_{0;a,b}(t,t_0) = \mathrm{e}^{-\frac{\mathrm{i}}{\hbar}E_a^{\mathrm{nr}}(t-t_0)}\delta_{a,b}\mathbf{1} \tag{7.9}$$

from equation (4.37) and the abbreviation of the energy

$$E_n^{\mathrm{nr}} = \frac{(\vec{k}+n\vec{k}_L)^2}{2m}\,. \tag{7.10}$$

Since the quantum mechanical operators $\boldsymbol{U}_0$ and $\hat{\boldsymbol{V}}$ change into the matrices (7.9) and (4.38), the second order perturbation contribution (7.6) is converted in a matrix product of five matrices in equation (7.8). The matrices (7.9) and (4.38) are indexed with the mode index a and b, whereas the spin-dependent part ($\mathbf{1}$ and $\vec{\sigma}$) is still kept as 2×2 matrix and is not indexed. Accordingly the matrix products in equation (7.8) are sums over the mode indices n_1, n_2, n_3 and n_4 and matrix products in 2×2 spinor space. The 2×2 matrix products in spinor space are denoted by the bold symbols $\boldsymbol{U}_{0;a,b}$ and $\boldsymbol{V}_{a,b}$. The result of equation (7.8) is a matrix with mode indices a and b and a matrix structure in 2×2 spinor space, denoted by the bold symbol $\boldsymbol{U}_{\mathrm{nd};3,0}$.

The free propagator (7.9) does not change the mode index, because it only contains a Kronecker delta $\delta_{a,b}$. This property results in the conditions $3 = n_1$, $n_2 = n_3$ and $n_4 = 0$ in the sum of equation (7.8). The interaction Hamiltonian (4.38) contains the Kronecker deltas $\delta_{a,b-2}$, $\delta_{a,b-1}$, $\delta_{a,b}$, $\delta_{a,b+1}$ and $\delta_{a,b+2}$. Therefore, there are two combinations of interaction Hamiltonian terms, which contribute in the propagator for the desired initial mode index 0 and final mode index 3, which are the terms

$$-\frac{e^2\vec{A}_0^2}{8mc^2}\sin^2(\omega t_2)\mathbf{1}\frac{e\sin(\omega t_1)}{4mc}\left(2\vec{A}_0\cdot\hbar\vec{k}\,\mathbf{1} + \hbar\vec{k}_L\times\vec{A}_0\cdot(\mathrm{i}\vec{\sigma})\right) \tag{7.11}$$

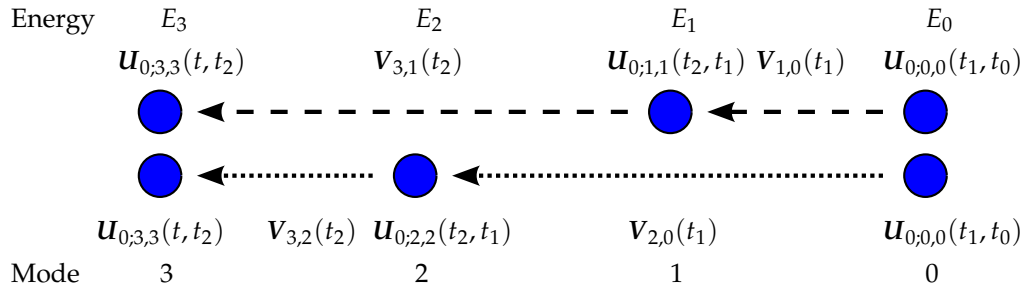

Figure 7.1: This picture illustrates the two contributions (7.13) (dashed arrows) and (7.14) (dotted arrows) of second order time dependent perturbation theory of the Pauli equation for the 3-photon Kapitza-Dirac effect. In the dashed arrows, the electron starts in mode 0, is scattered to mode 1 at time t_1 and is again scattered to mode 3 at time t_2. The roles of 2-photon and 1-photon scattering are interchanged in the case of the dotted line. In the dotted arrows, the electron starts in mode 0, is scattered to mode 2 at time t_1 and is again scattered to mode 3 at time t_2. Note, that the 2-photon scattering is caused by the ponderomotive term of the Pauli equation, which does not influence the electron spin. In contrast, to the 1-photon scattering term of the Pauli equation influences the electron spin.

for the product $\boldsymbol{V}_{3,1}(t_2)\boldsymbol{V}_{1,0}(t_1)$ and

$$-\frac{e\sin(\omega t_2)}{4mc}\left(2\vec{A}_0\cdot\hbar\vec{k}\,\mathbf{1}+\hbar\vec{k}_L\times\vec{A}_0\cdot(\mathrm{i}\vec{\sigma})\right)\frac{e^2\vec{A}_0^2}{8mc^2}\sin^2(\omega t_1)\mathbf{1} \tag{7.12}$$

for the product $\boldsymbol{V}_{3,2}(t_2)\boldsymbol{V}_{2,0}(t_1)$. Consequently, second order time-dependent perturbation theory (7.8) consists of the two contributions

$$\begin{aligned}\boldsymbol{U}_{\mathrm{nd};3,0}(t,t_0) = &-\frac{1}{(\mathrm{i}\hbar)^2}\frac{e^2\vec{A}_0^2}{8mc^2}\frac{e}{4mc}\left(2\vec{A}_0\cdot\hbar\vec{k}\,\mathbf{1}+\hbar\vec{k}_L\times\vec{A}_0\cdot(\mathrm{i}\vec{\sigma})\right) \\ &\cdot\int_{t_0}^{t}dt_2\int_{t_0}^{t_2}dt_1\exp\left[-\frac{\mathrm{i}}{\hbar}\left(E_3^{\mathrm{nr}}(t-t_2)+E_1^{\mathrm{nr}}(t_2-t_1)+E_0^{\mathrm{nr}}(t_1-t_0)\right)\right]\sin^2(\omega t_2)\sin(\omega t_1)\end{aligned} \tag{7.13}$$

and

$$\begin{aligned}\boldsymbol{U}_{\mathrm{nd};3,0}(t,t_0) = &-\frac{1}{(\mathrm{i}\hbar)^2}\frac{e}{4mc}\left(2\vec{A}_0\cdot\hbar\vec{k}\,\mathbf{1}+\hbar\vec{k}_L\times\vec{A}_0\cdot(\mathrm{i}\vec{\sigma})\right)\frac{e^2\vec{A}_0^2}{8mc^2} \\ &\cdot\int_{t_0}^{t}dt_2\int_{t_0}^{t_2}dt_1\exp\left[-\frac{\mathrm{i}}{\hbar}\left(E_3^{\mathrm{nr}}(t-t_2)+E_2^{\mathrm{nr}}(t_2-t_1)+E_0^{\mathrm{nr}}(t_1-t_0)\right)\right]\sin(\omega t_2)\sin^2(\omega t_1)\,.\end{aligned} \tag{7.14}$$

These two contributions are sketched in figure (7.1). All four sums in equation (7.8) are collapsed according to the considerations above. The 2×2 identity of the ponderomotive 2-photon coupling term of the interaction Hamiltonian (4.38) is multiplied at the other 1-photon interaction term and vanishes thereby.

It remains to compute the time integrals over t_1 and t_2 of equation (7.13) and (7.14). The integration can be performed by expanding the sine functions into exponentials. If the phase is constant with respect to the integration variables t_1 and t_2, the integrals will diverge for infinite long times. This means, that parts of the integral with a constant phase will dominate over all other terms for long times $t-t_0$. The following considerations focus on the identification of these divergent, constant phase terms, in order to neglect all other terms with a fast oscillating phase.

The resonance condition from energy and momentum conservation (C.3) may cause a constant phase in the time integral of (7.13) and (7.14). In the case of the 3-photon Kapitza-Dirac effect, with $n_a=2$ and $n_e=1$, equation (C.3) reduces to

$$E_3^{\mathrm{nr}} = E_0^{\mathrm{nr}} + \hbar\omega\,. \tag{7.15}$$

If one solves this equation for $\hbar\omega$, one will know, that the energy difference has the property

$$\Delta E^{\mathrm{nr}}_{a,b} = E^{\mathrm{nr}}_a - E^{\mathrm{nr}}_b \stackrel{!}{=} \hbar\omega\,, \tag{7.16}$$

if either condition (2.19) or condition (2.20) was fulfilled. The factor $\hbar\omega$ times an integration variable t_1 or t_2 in the exponent appears from the expansion of the sine functions in the time integral of (7.13) and (7.14). Therefore, one has to search for the energy difference $\Delta E^{\mathrm{nr}}_{3,0}$ or $\Delta E^{\mathrm{nr}}_{0,3}$ times the time integration variable t_1 or t_2 in the exponential of the time integral of (7.13) and (7.14), because this energy difference plus $\hbar\omega$ yields a constant phase, which in turn yields a diverging and dominating integral. The exponent resulting from the free electron propagation (7.9)

$$-\frac{\mathrm{i}}{\hbar}\left(E^{\mathrm{nr}}_3(t-t_2)+E^{\mathrm{nr}}_1(t_2-t_1)+E^{\mathrm{nr}}_0(t_1-t_0)\right) = -\frac{\mathrm{i}}{\hbar}\left(E^{\mathrm{nr}}_3 t - E^{\mathrm{nr}}_0 t_0 + \Delta E^{\mathrm{nr}}_{1,3} t_2 + \Delta E^{\mathrm{nr}}_{0,1} t_1\right) \tag{7.17}$$

of equation (7.13) or

$$-\frac{\mathrm{i}}{\hbar}\left(E^{\mathrm{nr}}_3(t-t_2)+E^{\mathrm{nr}}_2(t_2-t_1)+E^{\mathrm{nr}}_0(t_1-t_0)\right) = -\frac{\mathrm{i}}{\hbar}\left(E^{\mathrm{nr}}_3 t - E^{\mathrm{nr}}_0 t_0 + \Delta E^{\mathrm{nr}}_{2,3} t_2 + \Delta E^{\mathrm{nr}}_{0,2} t_1\right) \tag{7.18}$$

of equation (7.14) neither contains an energy difference $\Delta E^{\mathrm{nr}}_{3,0}$ times t_1 or t_2, nor $\Delta E^{\mathrm{nr}}_{0,3}$ times t_1 or t_2. However, the upper limit of the integral over t_1 in (7.13) and (7.14) changes t_1 into t_2, resulting in

$$-\frac{\mathrm{i}}{\hbar}\left(E^{\mathrm{nr}}_3 t - E^{\mathrm{nr}}_0 t_0 + \Delta E^{\mathrm{nr}}_{1,3} t_2 + \Delta E^{\mathrm{nr}}_{0,1} t_1\right) \underset{t_1\to t_2}{\to} -\frac{\mathrm{i}}{\hbar}\left(E^{\mathrm{nr}}_3 t - E^{\mathrm{nr}}_0 t_0 + \Delta E^{\mathrm{nr}}_{0,3} t_2\right) \tag{7.19}$$

for the term (7.17) and

$$-\frac{\mathrm{i}}{\hbar}\left(E^{\mathrm{nr}}_3 t - E^{\mathrm{nr}}_0 t_0 + \Delta E^{\mathrm{nr}}_{2,3} t_2 + \Delta E^{\mathrm{nr}}_{0,2} t_1\right) \underset{t_1\to t_2}{\to} -\frac{\mathrm{i}}{\hbar}\left(E^{\mathrm{nr}}_3 t - E^{\mathrm{nr}}_0 t_0 + \Delta E^{\mathrm{nr}}_{0,3} t_2\right) \tag{7.20}$$

for the term (7.18). According to the considerations above, the term $-\mathrm{i}\Delta E^{\mathrm{nr}}_{0,3} t_2/\hbar$ should be compensated by a term $-\mathrm{i}\omega t_2$ from the expansion of the sine functions in equations (7.13) and (7.14), which has to be seeked for. The $\sin^2(\omega t_2)\sin(\omega t_1)$ of equation (7.13) results in

$$\sin^2(\omega t_2)\sin(\omega t_1) = \frac{\mathrm{i}}{8}\left(e^{2\mathrm{i}\omega t_2+\mathrm{i}\omega t_1} - e^{2\mathrm{i}\omega t_2-\mathrm{i}\omega t_1} - 2\left(e^{\mathrm{i}\omega t_1} - e^{-\mathrm{i}\omega t_1}\right) + e^{-2\mathrm{i}\omega t_2+\mathrm{i}\omega t_1} - e^{-2\mathrm{i}\omega t_2-\mathrm{i}\omega t_1}\right). \tag{7.21}$$

The terms

$$\frac{\mathrm{i}}{8}e^{-2\mathrm{i}\omega t_2+\mathrm{i}\omega t_1} = \frac{\mathrm{i}}{8}\exp\left[-\frac{\mathrm{i}}{\hbar}\left(2\hbar\omega t_2 - \hbar\omega t_1\right)\right] \qquad \text{and} \qquad \frac{\mathrm{i}}{4}e^{-\mathrm{i}\omega t_1} = \frac{\mathrm{i}}{4}\exp\left[-\frac{\mathrm{i}}{\hbar}\left(\hbar\omega t_1\right)\right] \tag{7.22}$$

in equation (7.21) will change into an exponential of $-\mathrm{i}\omega t_2$, by focusing again only on the upper limit of the first integral over t_1. Similarly, the $\sin(\omega t_2)\sin^2(\omega t_1)$ term in equation (7.14) may be expanded into

$$\sin(\omega t_2)\sin^2(\omega t_1) = \frac{\mathrm{i}}{8}\left(e^{2\mathrm{i}\omega t_1+\mathrm{i}\omega t_2} - e^{2\mathrm{i}\omega t_1-\mathrm{i}\omega t_2} - 2\left(e^{\mathrm{i}\omega t_2} - e^{-\mathrm{i}\omega t_2}\right) + e^{-2\mathrm{i}\omega t_1+\mathrm{i}\omega t_2} - e^{-2\mathrm{i}\omega t_1-\mathrm{i}\omega t_2}\right). \tag{7.23}$$

One identifies the terms

$$\frac{\mathrm{i}}{8}e^{-2\mathrm{i}\omega t_1+\mathrm{i}\omega t_2} = \frac{\mathrm{i}}{8}\exp\left[-\frac{\mathrm{i}}{\hbar}\left(2\hbar\omega t_1 - \hbar\omega t_2\right)\right] \qquad \text{and} \qquad \frac{\mathrm{i}}{4}e^{-\mathrm{i}\omega t_2} = \frac{\mathrm{i}}{4}\exp\left[-\frac{\mathrm{i}}{\hbar}\left(\hbar\omega t_2\right)\right], \tag{7.24}$$

which contain an exponential of $-\mathrm{i}\omega t_2$ after the integration over t_1 by taking only the upper limit. One concludes, that the integrals of (7.17) times the terms (7.22) of equation (7.13) and the integrals of (7.18) times the terms (7.24) of equation (7.14) are the only diverging contributions and are therefore computed in the following. As discussed above, only the upper limit of the integral over t_1 contributes

to the diverging terms. Therefore, the lower limit of the integral over t_1 is neglected in the following calculations.

The integral over t_1 of the exponential of (7.17) times the exponential of the left term of (7.22) of equation (7.13) results in

$$\frac{\mathrm{i}}{8}\int_{t_0}^{t} dt_2 \int^{t_2} dt_1 \exp\left[-\frac{\mathrm{i}}{\hbar}\left(E_3^{\mathrm{nr}}t - E_0^{\mathrm{nr}}t_0 + (\Delta E_{1,3}^{\mathrm{nr}} + 2\hbar\omega)t_2 + (\Delta E_{0,1}^{\mathrm{nr}} - \hbar\omega)t_1\right)\right] = -\frac{1}{\Delta E_{0,1}^{\mathrm{nr}} - \hbar\omega}\frac{\hbar}{8}\int_{t_0}^{t} dt_2 \exp\left[-\frac{\mathrm{i}}{\hbar}\left(E_3^{\mathrm{nr}}t - E_0^{\mathrm{nr}}t_0 + (\Delta E_{0,3}^{\mathrm{nr}} + \hbar\omega)t_2\right)\right]. \quad (7.25)$$

The integral over t_1 of the exponential of (7.17) times the exponential of the right term of (7.22) of equation (7.13) results in

$$\frac{\mathrm{i}}{4}\int_{t_0}^{t} dt_2 \int^{t_2} dt_1 \exp\left[-\frac{\mathrm{i}}{\hbar}\left(E_3^{\mathrm{nr}}t - E_0^{\mathrm{nr}}t_0 + \Delta E_{1,3}^{\mathrm{nr}}t_2 + (\Delta E_{0,1}^{\mathrm{nr}} + \hbar\omega)t_1\right)\right] = -\frac{1}{\Delta E_{0,1}^{\mathrm{nr}} + \hbar\omega}\frac{\hbar}{4}\int_{t_0}^{t} dt_2 \exp\left[-\frac{\mathrm{i}}{\hbar}\left(E_3^{\mathrm{nr}}t - E_0^{\mathrm{nr}}t_0 + (\Delta E_{0,3}^{\mathrm{nr}} + \hbar\omega)t_2\right)\right]. \quad (7.26)$$

The integral over t_1 of the exponential of (7.18) times the exponential of the left term of (7.24) of equation (7.14) results in

$$\frac{\mathrm{i}}{8}\int_{t_0}^{t} dt_2 \int^{t_2} dt_1 \exp\left[-\frac{\mathrm{i}}{\hbar}\left(E_3^{\mathrm{nr}}t - E_0^{\mathrm{nr}}t_0 + (\Delta E_{2,3}^{\mathrm{nr}} - \hbar\omega)t_2 + (\Delta E_{0,2}^{\mathrm{nr}} + 2\hbar\omega)t_1\right)\right] = -\frac{1}{\Delta E_{0,2}^{\mathrm{nr}} + 2\hbar\omega}\frac{\hbar}{8}\int_{t_0}^{t} dt_2 \exp\left[-\frac{\mathrm{i}}{\hbar}\left(E_3^{\mathrm{nr}}t - E_0^{\mathrm{nr}}t_0 + (\Delta E_{0,3}^{\mathrm{nr}} + \hbar\omega)t_2\right)\right]. \quad (7.27)$$

The integral over t_1 of the exponential of (7.18) times the exponential of the right term of (7.24) of equation (7.14) results in

$$\frac{\mathrm{i}}{4}\int_{t_0}^{t} dt_2 \int^{t_2} dt_1 \exp\left[-\frac{\mathrm{i}}{\hbar}\left(E_3^{\mathrm{nr}}t - E_0^{\mathrm{nr}}t_0 + (\Delta E_{2,3}^{\mathrm{nr}} + \hbar\omega)t_2 + \Delta E_{0,2}^{\mathrm{nr}}t_1\right)\right] = -\frac{1}{\Delta E_{0,2}^{\mathrm{nr}}}\frac{\hbar}{4}\int_{t_0}^{t} dt_2 \exp\left[-\frac{\mathrm{i}}{\hbar}\left(E_3^{\mathrm{nr}}t - E_0^{\mathrm{nr}}t_0 + (\Delta E_{0,3}^{\mathrm{nr}} + \hbar\omega)t_2\right)\right]. \quad (7.28)$$

The time integration over t_2 is identical for all four terms (7.25 - 7.28) and may therefore be discussed once by ignoring the prefactors of the integration of t_1. The integral over t_2 evaluates to

$$\int_{t_0}^{t} dt_2 \exp\left[-\frac{\mathrm{i}}{\hbar}\left(E_3^{\mathrm{nr}}t - E_0^{\mathrm{nr}}t_0 + (\Delta E_{0,3}^{\mathrm{nr}} + \hbar\omega)t_2\right)\right] = \mathrm{i}\left(e^{-\mathrm{i}\Delta\omega t} - e^{-\mathrm{i}\Delta\omega t_0}\right)\frac{1}{\Delta\omega}e^{-\mathrm{i}\left(E_3^{\mathrm{nr}}t - E_0^{\mathrm{nr}}t_0\right)/\hbar}, \quad (7.29)$$

with the laser detuning

$$\Delta\omega = \omega - \Delta E_{3,0}^{\mathrm{nr}}/\hbar\,. \quad (7.30)$$

This integral is undefined for zero detuning $\Delta\omega = 0$, which is the case, if the resonance condition (2.15) is fulfilled. If one considers the first order Taylor expansion of

$$\mathrm{i}\left(e^{-\mathrm{i}\Delta\omega t} - e^{-\mathrm{i}\Delta\omega t_0}\right) = \Delta\omega(t - t_0) + \mathcal{O}(\Delta\omega^2) \quad (7.31)$$

with respect to $\Delta\omega$, one recognizes, that the nominator vanishes as fast as the denominator in equation (7.29) such that the integral is well-defined. Furthermore, one may compute the integral (7.29) for the case of zero detuning $\Delta\omega = 0$, resulting in

$$\int_{t_0}^{t} dt_2 \exp\left[-\frac{\mathrm{i}}{\hbar}\left(E_3^{\mathrm{nr}}t - E_0^{\mathrm{nr}}t_0\right)\right] = (t - t_0)e^{-\mathrm{i}(E_3^{\mathrm{nr}}t - E_0^{\mathrm{nr}}t_0)/\hbar}\,. \quad (7.32)$$

One would obtain the same result, if one substituted the first order Taylor expansion (7.31) in the result of the integral (7.29).

Summing up the double integral of all divergent contributions of the second order perturbation theory (7.8) yields

$$\boldsymbol{U}_{\mathrm{nd};3,0}(t,t_0) = -\frac{1}{64\hbar} PF \frac{e}{mc} \left(2\vec{A}_0 \cdot \hbar\vec{k}\,\mathbf{1} + \hbar\vec{k}_L \times \vec{A}_0 \cdot (\mathrm{i}\vec{\boldsymbol{\sigma}})\right) \frac{e^2\vec{A}_0^2}{4mc^2} \cdot e^{-\mathrm{i}(E_3^{\mathrm{nr}} t - E_0^{\mathrm{nr}} t_0)/\hbar} \begin{cases} t - t_0 & \text{on resonance} \\ \frac{\mathrm{i}}{\Delta\omega}\left(e^{-\mathrm{i}\Delta\omega t} - e^{-\mathrm{i}\Delta\omega t_0}\right) & \text{off resonance}\,, \end{cases} \tag{7.33}$$

with the prefactor

$$PF = \frac{1}{\Delta E_{0,1}^{\mathrm{nr}} - \hbar\omega} + \frac{2}{\Delta E_{0,1}^{\mathrm{nr}} + \hbar\omega} + \frac{1}{\Delta E_{0,2}^{\mathrm{nr}} + 2\hbar\omega} + \frac{2}{\Delta E_{0,2}^{\mathrm{nr}}} \tag{7.34}$$

of the integrals (7.25 - 7.28). The propagator can either be noted with an off-resonant term, from the time integral (7.29), or with a resonant term, which originates from the resonant integral (7.32).

It is difficult to read of a frequency dependent scaling law from equation (7.33), because of the prefactor (7.34). A simpler value of this prefactor in the resonant case $\Delta\omega = 0$ and small laser frequencies $\hbar c k_L \ll mc^2$ would be useful and is derived in the following. First, $\hbar\omega$ in the prefactor PF may be replaced with $\Delta E_{3,0}^{\mathrm{nr}}$ as it is implied by the resonance condition (7.16), yielding

$$\begin{aligned} PF &= \frac{1}{\Delta E_{0,1}^{\mathrm{nr}} - \Delta E_{3,0}^{\mathrm{nr}}} + \frac{2}{\Delta E_{0,1}^{\mathrm{nr}} + \Delta E_{3,0}^{\mathrm{nr}}} + \frac{1}{\Delta E_{0,2}^{\mathrm{nr}} + 2\Delta E_{3,0}^{\mathrm{nr}}} + \frac{2}{\Delta E_{0,2}^{\mathrm{nr}}} \\ &= \frac{2}{\Delta E_{0,2}^{\mathrm{nr}}} + \frac{2}{\Delta E_{3,1}^{\mathrm{nr}}} + \frac{1}{\Delta E_{0,1}^{\mathrm{nr}} + \Delta E_{0,3}^{\mathrm{nr}}} + \frac{1}{\Delta E_{3,2}^{\mathrm{nr}} + \Delta E_{3,0}^{\mathrm{nr}}}\,. \end{aligned} \tag{7.35}$$

If one inserts the definition of the energy difference (7.16) and the energy (7.10) into equation (7.35), one obtains

$$PF = -\frac{\hbar^2\vec{k}_L^2 m}{\hbar^4(\vec{k}_L\cdot\vec{k} + \vec{k}_L^2)(\vec{k}_L\cdot\vec{k} + 2\vec{k}_L^2)} - \frac{2\hbar^2\vec{k}_L^2 m}{\hbar^4(4\vec{k}_L\cdot\vec{k} + 5\vec{k}_L^2)(4\vec{k}_L\cdot\vec{k} + 7\vec{k}_L^2)}\,. \tag{7.36}$$

This term may be simplified by imposing the limit $\hbar c k_L \ll mc^2$ of small laser frequencies. In the case of the 3-photon Kapitza-Dirac effect, the initial electron momentum in laser propagation direction (2.19) changes into

$$\lim_{k_L\to 0} \hbar k_1(k_L) = \frac{n_a - n_e}{n_a + n_e} mc = \frac{1}{3} mc \tag{7.37}$$

for small laser frequencies. Note, that this limit corresponds to the momentum $p_{1,\mathrm{lim}}$ of subsection 2.2.6, but for the case of the non-relativistic energy momentum relation (3.4). This implies $k_L \ll k_1$ and therefore $\vec{k}_L^2 \ll \vec{k}_L\cdot\vec{k}$. Using this property simplifies the prefactor in equation (7.36) to

$$\tilde{P}F \approx -\frac{\hbar^2\vec{k}_L^2 m}{\hbar^4(\vec{k}_L\cdot\vec{k})^2} - \frac{\hbar^2\vec{k}_L^2 m}{8\hbar^4(\vec{k}_L\cdot\vec{k})^2} = -\frac{9m}{8\hbar^2 k_1^2} = -\frac{81}{8mc^2}\,, \tag{7.38}$$

where the momentum k_1 for small k_L in equation (7.37) is inserted in the last equality. The perturbation theory propagator (7.33) results in the simpler form

$$\boldsymbol{U}_{\mathrm{nd};3,0}(t,t_0) = \frac{81}{512\hbar} \frac{e}{m^2c^3} \left(2\vec{A}_0 \cdot \hbar\vec{k}\,\mathbf{1} + \hbar\vec{k}_L \times \vec{A}_0 \cdot (\mathrm{i}\vec{\boldsymbol{\sigma}})\right) \frac{e^2\vec{A}_0^2}{4mc^2} \cdot e^{-\mathrm{i}(E_3 t - E_0 t_0)/\hbar} \begin{cases} t - t_0 & \text{on resonance} \\ \frac{\mathrm{i}}{\Delta\omega}\left(e^{-\mathrm{i}\Delta\omega t} - e^{-\mathrm{i}\Delta\omega t_0}\right) & \text{off resonance} \end{cases} \tag{7.39}$$

in the case of the simplified prefactor (7.38).

7.2.2 Interpretation

Electron spin rotation

Equation (7.39) has the same form as the propagator (6.4), with a vanishing imaginary part of the unit vector $\vec{n}$. As it is discussed in section (6.2), the vanishing imaginary part of $\vec{n}$ implies, that the diffraction probability of the 3-photon Kapitza-Dirac effect does not depend on the initial electron spin and the spin part (6.5) of the propagator turns into a $\mathcal{SU}(2)$-representation of a rotation of the electron spin. The parameters for the ansatz (6.2) in the resonant case of equation (7.39) assume the values

$$P_{3,0}(t,t_0) = \frac{81}{512\hbar}\frac{e}{m^2c^3}\frac{e^2\vec{A}_0^2}{4mc^2}\left[\left(2\vec{A}_0\cdot\hbar\vec{k}\right)^2 + \left(\hbar\vec{k}_L\times\vec{A}_0\right)^2\right]^{\frac{1}{2}}(t-t_0)\,, \tag{7.40a}$$

$$\phi_{3,0}(t,t_0) = -\mathrm{i}\frac{E_3 t - E_0 t}{\hbar}\,, \tag{7.40b}$$

$$\cos\left(\frac{\alpha_{3,0}(t,t_0)}{2}\right) = 2\vec{A}_0\cdot\hbar\vec{k}\left[\left(2\vec{A}_0\cdot\hbar\vec{k}\right)^2 + \left(\hbar\vec{k}_L\times\vec{A}_0\right)^2\right]^{-\frac{1}{2}}\,, \tag{7.40c}$$

$$\vec{n}_{3,0}(t,t_0)\sin\left(\frac{\alpha_{3,0}(t,t_0)}{2}\right) = -\hbar\vec{k}_L\times\vec{A}_0\left[\left(2\vec{A}_0\cdot\hbar\vec{k}\right)^2 + \left(\hbar\vec{k}_L\times\vec{A}_0\right)^2\right]^{-\frac{1}{2}}\,. \tag{7.40d}$$

Note, that the four equations are unique. In particular, the division by the square root in the last two equations in (7.40) is necessary, because the unity of the determinant of the $\mathcal{SU}(2)$ representation (6.5) requires, that

$$\cos^2\left(\frac{\alpha_{3,0}(t,t_0)}{2}\right) + \sin^2\left(\frac{\alpha_{3,0}(t,t_0)}{2}\right)\vec{n}_{3,0}^2(t,t_0) \stackrel{!}{=} 1\,. \tag{7.41}$$

This unitarity constraint is only valid, if one substitutes the left-hand side of the equations (7.40c) and (7.40d) by their right-hand side in equation (7.41).

Furthermore, the angle $\alpha_{3,0}(t,t_0)$ is constant in time, because the right-hand side of equation (7.40c) is constant in time. For similar reasons $\vec{n}_{3,0}(t,t_0)$ is constant in time, because $\alpha_{3,0}$ and the right-hand side of equation (7.40d) are constant in time. Since $\vec{n}_{3,0}$ is a unit vector in the $\mathcal{SU}(2)$ representation, (7.40d) also implies, that

$$\vec{n}_{3,0} = -\frac{\vec{k}_L\times\vec{A}_0}{|\vec{k}_L\times\vec{A}_0|} = \frac{\vec{B}_0}{|\vec{B}_0|}\,. \tag{7.42}$$

This means, that the rotation axis of the $\mathcal{SU}(2)$ representation points in the direction of the magnetic field $\vec{B}_0$ of the laser beam and therewith the electron spin is rotated around this axis.

The rotation angle $\alpha_{3,0}$ can be resolved by multiplying equation (7.40d) with equation (7.42) and dividing it by equation (7.40c), resulting in

$$\tan\left(\frac{\alpha_{3,0}}{2}\right) = \frac{|\vec{k}_L\times\vec{A}_0|}{2\vec{A}_0\cdot\vec{k}}\,. \tag{7.43}$$

The tangent needs to be inverted on the interval $[-\pi/2,\pi/2]$ in order to solve for the rotation angle $\alpha_{3,0}$.

Rabi frequency

Section 8 suggests, that the diffraction probability of the 3-photon Kapitza-Dirac effect depends on the interaction time T with the probability

$$P_{3,0}(T,0) = \sin^2\left(\frac{\Omega_R T}{2}\right)\,, \tag{7.44}$$

if the turn on and turn off time of the interaction was infinitely short. If one uses this diffraction probability in the propagator ansatz (6.4) and accounts for the vanishing imaginary part of $\vec{n}$ one can compute

$$\boldsymbol{U}_{\mathrm{nd};3,0}(T,0)\boldsymbol{U}^{\dagger}_{\mathrm{nd};3,0}(T,0) = \sin^2\left(\frac{\Omega_R T}{2}\right)\mathbf{1}\,. \tag{7.45}$$

All parameters of the $\mathcal{SU}(2)$ representation and the complex phase $\phi_{3,0}(T,0)$ drop out in equation (7.45). The only quantity, which remains is the diffraction probability (7.44) times the 2×2 identity $\mathbf{1}$. A second order Taylor expansion with respect to T of the right-hand side of equation (7.45) results in

$$\boldsymbol{U}_{\mathrm{nd};3,0}(T,0)\boldsymbol{U}^{\dagger}_{\mathrm{nd};3,0}(T,0) = \left(\frac{\Omega_R T}{2}\right)^2\mathbf{1} + \mathcal{O}(T^3)\,. \tag{7.46}$$

On the other hand, one may compute the same quantity for the derived, resonant propagator (7.39), resulting in

$$\boldsymbol{U}_{\mathrm{nd};3,0}(T,0)\boldsymbol{U}^{\dagger}_{\mathrm{nd};3,0}(T,0) = \left(\frac{81}{512\hbar}\right)^2\left(\frac{e}{m^2c^3}\right)^2\left[\left(2\vec{A}_0\cdot\hbar\vec{k}\right)^2 + \left(\hbar\vec{k}_L\times\vec{A}_0\right)^2\right]\left(\frac{e^2\vec{A}_0^2}{4mc^2}\right)^2 T^2\mathbf{1}\,. \tag{7.47}$$

This short-time result is of the same structural form as the second order Taylor term in equation (7.46) and one may extract the Rabi frequency Ω_R from it by requiring equality between the second order Taylor term and the right-hand side of equation (7.47), yielding

$$\Omega_R = \left(\frac{81}{256\hbar}\right)^2\frac{e}{m^2c^3}\frac{e^2\vec{A}_0^2}{4mc^2}\sqrt{\left(2\vec{A}_0\cdot\hbar\vec{k}\right)^2 + \left(\hbar\vec{k}_L\times\vec{A}_0\right)^2}\,. \tag{7.48}$$

Note, that the Rabi frequency also appears in the diffraction probability (7.40a), such that one may write

$$P_{3,0}(t,t_0) = \frac{\Omega_R}{2}(t-t_0) \tag{7.49}$$

in equation (7.40a).

The property, that second order time-dependent perturbation theory (7.39) is the first term of a power series of a sine function suggests, that higher order perturbation theory results in higher order terms of the sine function. In fact, a publication of Gush and Gush in 1971 [31] computes all higher order terms of time-dependent perturbation theory of the Schödinger equation with an external vector potential for the 2-photon Kapitza-Dirac effect. The authors show, that the sum over all terms, up to infinite order perturbation theory results in a sine time-dependence of the diffraction probability. In the case of the discussed 3-photon Kapitza-Dirac effect, which is solved by using time-dependent perturbation theory of the Dirac equation, the next order term of the sine series is expected to originate from 9$^{\text{th}}$ order time-dependent perturbation theory[1].

Spin-flip probability

The time evolution of the expansion coefficients c_n^σ is given by equation (6.1). If one assumes an initial configuration, in which only the 0 mode with spin up is occupied, one may compute

$$c_3^{\uparrow}(t) = (\boldsymbol{U}_{\mathrm{nd};3,0})^{\uparrow,\uparrow}(t,t_0)c_0^{\uparrow}(t_0) = \frac{81}{512\hbar}\frac{2e\vec{A}_0\cdot\hbar\vec{k}}{m^2c^3}\frac{e^2\vec{A}_0^2}{4mc^2}e^{-\mathrm{i}(E_3^{\mathrm{nr}}t - E_0^{\mathrm{nr}}t_0)/\hbar}(t-t_0)c_0^{\uparrow}(t_0)\,, \tag{7.50a}$$

$$c_3^{\downarrow}(t) = (\boldsymbol{U}_{\mathrm{nd};3,0})^{\downarrow,\uparrow}(t,t_0)c_0^{\uparrow}(T) = \frac{81}{512\hbar}\frac{e\hbar\vec{k}_L\times\vec{A}_0}{m^2c^3}\frac{e^2\vec{A}_0^2}{4mc^2}e^{-\mathrm{i}(E_3^{\mathrm{nr}}t - E_0^{\mathrm{nr}}t_0)/\hbar}(t-t_0)c_0^{\downarrow}(t_0)\,. \tag{7.50b}$$

[1]The 9$^{\text{th}}$ order perturbation theory corresponds to the coupling from mode 0 to mode 3, back to mode 0 and back to mode 3.

With the more specific initial condition $c_0^{+\uparrow}(0) = 1$ one obtains

$$|c_3^{\uparrow}(T)|^2 = \left(\frac{81}{512\hbar}\right)^2 \left(\frac{2e\vec{A}_0 \cdot \hbar\vec{k}}{m^2c^3}\right)^2 \left(\frac{e^2\vec{A}_0^2}{4mc^2}\right)^2 T^2 \quad \text{and} \tag{7.51a}$$

$$|c_3^{\downarrow}(T)|^2 = \left(\frac{81}{512\hbar}\right)^2 \left(\frac{e\hbar\vec{k}_L \times \vec{A}_0}{m^2c^3}\right)^2 \left(\frac{e^2\vec{A}_0^2}{4mc^2}\right)^2 T^2 . \tag{7.51b}$$

after time T. One may define the non-spin-flip probability

$$P_{\text{noflip}} = \frac{|c_3^{\uparrow}(T)|^2}{|c_3^{\uparrow}(T)|^2 + |c_3^{\downarrow}(T)|^2} \tag{7.52}$$

and the spin-flip probability

$$P_{\text{flip}} = \frac{|c_3^{\downarrow}(T)|^2}{|c_3^{\uparrow}(T)|^2 + |c_3^{\downarrow}(T)|^2} \tag{7.53}$$

of the diffracted beam. If the wave vector component parallel to the laser polarization $k_{\parallel} = \vec{A}_0 \cdot \vec{k}/|\vec{A}_0|$ is introduced and one considers, that $\vec{k}_L \times \vec{A}_0 = k_L|\vec{A}_0|$ for the vacuum Maxwell equations, one can compute

$$P_{\text{noflip}} = \frac{(2e\vec{A}_0 \cdot \hbar\vec{k})^2}{(2e\vec{A}_0 \cdot \hbar\vec{k})^2 + (e\hbar\vec{k}_L \times \vec{A}_0)^2} = \frac{(2k_{\parallel})^2}{(2k_{\parallel})^2 + (k_L)^2} = \frac{1}{1 + k_L^2/(4k_{\parallel}^2)} \quad \text{and} \tag{7.54a}$$

$$P_{\text{flip}} = \frac{(e\hbar\vec{k}_L \times \vec{A}_0)^2}{(2e\vec{A}_0 \cdot \hbar\vec{k})^2 + (e\hbar\vec{k}_L \times \vec{A}_0)^2} = \frac{(k_L)^2}{(2k_{\parallel})^2 + (k_L)^2} = \frac{1}{4k_{\parallel}^2/k_L^2 + 1} . \tag{7.54b}$$

7.3 Perturbation Theory for the Dirac equation

The derivation and the results of time-dependent perturbation theory of the Dirac equation is often similar to the derivation and the results from time-dependent perturbation theory of the Pauli equation of section 7.2. Therefore, the concepts of section 7.2 are adopted and analogous explanations are referred to section 7.2.

7.3.1 Derivation

Since the interaction Hamiltonian (4.67) of the Dirac equation contains only next neighbor coupling terms, the lowest non-vanishing contribution in time-dependent perturbation theory is of third order. The term (7.7) of third order time-dependent perturbation theory can be written as

$$\begin{aligned} \boldsymbol{U}_{\text{rd};3,0}(t,t_0) = \sum_{n_i, i\in\{1,2,3,4,5,6\}} \frac{1}{(\mathrm{i}\hbar)^3} \int_{t_0}^{t} dt_3 \int_{t_0}^{t_3} dt_2 \int_{t_0}^{t_2} dt_1 \boldsymbol{U}_{0;3,n_1}(t,t_3)\boldsymbol{V}_{n_1,n_2}(t_3) \\ \cdot \boldsymbol{U}_{0;n_2,n_3}(t_3,t_2)\boldsymbol{V}_{n_3,n_4}(t_2)\boldsymbol{U}_{0;n_4,n_5}(t_2,t_1)\boldsymbol{V}_{n_5,n_6}(t_1)\boldsymbol{U}_{0;n_6,0}(t_1,t_0) . \end{aligned} \tag{7.55}$$

with the free propagator

$$\boldsymbol{U}_{0;a,b}(t,t_0) = \mathrm{e}^{-\frac{\mathrm{i}}{\hbar}E_a\boldsymbol{\beta}(t-t_0)}\delta_{a,b} = \begin{pmatrix} \exp\left(-\mathrm{i}E_a(t-t_0)/\hbar\right)\mathbf{1} & \mathbf{0} \\ \mathbf{0} & \exp\left(\mathrm{i}E_a(t-t_0)/\hbar\right)\mathbf{1} \end{pmatrix} \delta_{a,b} \tag{7.56}$$

from equation (4.66) and the abbreviation for the energy

$$E_n = \sqrt{m^2c^4 + c^2\hbar^2(\vec{k} + nk_L)^2} . \tag{7.57}$$

The matrix $\boldsymbol{V}_{a,b}$ is the interaction Hamiltonian (4.67). Note, that the free propagator (7.56) has a 4×4 bi-spinor matrix form, which is denoted by four 2×2 matrices on the right-hand side of equation (7.56). The free propagator (7.9) does not change the mode index, because it only contains a Kronecker delta $\delta_{a,b}$. This property results in the conditions $3 = n_1$, $n_2 = n_3$, $n_4 = n_5$ and $n_6 = 0$ in the sum in (7.55). Since the interaction Hamiltonian (4.67) contains the Kronecker deltas $\delta_{a,b-1}$ and $\delta_{a,b+1}$, only one combination of interaction Hamiltonian terms contribute to the propagator. Therefore equation (7.55) reduces to

$$\begin{aligned}
\boldsymbol{U}_{\mathrm{rd};3,0}(t,t_0) &= \frac{1}{(\mathrm{i}\hbar)^3}\int_{t_0}^{t} dt_3 \int_{t_0}^{t_3} dt_2 \int_{t_0}^{t_2} dt_1 \boldsymbol{U}_{0;3,3}(t,t_3)\boldsymbol{V}_{3,2}(t_3) \\
&\quad \cdot \boldsymbol{U}_{0;2,2}(t_3,t_2)\boldsymbol{V}_{2,1}(t_2)\boldsymbol{U}_{0;1,1}(t_2,t_1)\boldsymbol{V}_{1,0}(t_1)\boldsymbol{U}_{0;0,0}(t_1,t_0) \\
&= \frac{1}{(\mathrm{i}\hbar)^3}\int_{t_0}^{t} dt_3 \int_{t_0}^{t_3} dt_2 \int_{t_0}^{t_2} dt_1 \boldsymbol{U}_{0;3,3}(t,t_3) \\
&\quad \cdot -\frac{e\sin(\omega t_3)}{2}\boldsymbol{u}(\vec{k}+3\vec{k}_L)^\dagger \left(\vec{A}_0\cdot\vec{\boldsymbol{\alpha}}\right)\boldsymbol{u}(\vec{k}+2\vec{k}_L)\boldsymbol{U}_{0;2,2}(t_3,t_2) \\
&\quad \cdot -\frac{e\sin(\omega t_2)}{2}\boldsymbol{u}(\vec{k}+2\vec{k}_L)^\dagger \left(\vec{A}_0\cdot\vec{\boldsymbol{\alpha}}\right)\boldsymbol{u}(\vec{k}+1\vec{k}_L)\boldsymbol{U}_{0;1,1}(t_2,t_1) \\
&\quad \cdot -\frac{e\sin(\omega t_1)}{2}\boldsymbol{u}(\vec{k}+1\vec{k}_L)^\dagger \left(\vec{A}_0\cdot\vec{\boldsymbol{\alpha}}\right)\boldsymbol{u}(\vec{k}+0\vec{k}_L)\boldsymbol{U}_{0;0,0}(t_1,t_0)\,.
\end{aligned} \tag{7.58}$$

In contrast to the computation of time-dependent perturbation theory with the Pauli equation, the free propagators $\boldsymbol{U}_{0;a,b}$ do not commute with the interaction Hamiltonian, because of the $\boldsymbol{\beta}$ in the exponential of (7.56). It is necessary to expand the matrix product further, because the time-dependence of all four propagators enters in the time integration over the variables t_1, t_2 and t_3. Therefore the matrix part of the interaction Hamiltonian is broken up into four 2×2 matrices

$$\begin{aligned}
\boldsymbol{u}^{\sigma}(\vec{k}+n\vec{k}_L)^\dagger \left(\vec{A}_0\cdot\vec{\boldsymbol{\alpha}}\right)\boldsymbol{u}^{\sigma'}(\vec{k}+(n-1)\vec{k}_L) &= t\vec{A}_0\cdot\vec{\boldsymbol{\alpha}} - \vec{A}_0^T\underline{\underline{w}}\,\vec{\boldsymbol{\alpha}} + \vec{A}_0\cdot\vec{s}\,\boldsymbol{\beta} + \mathrm{i}\boldsymbol{\beta}\vec{\boldsymbol{\Sigma}}\cdot\left(\vec{r}\times\vec{A}_0\right) + \vec{A}_0\cdot\vec{h}\,\boldsymbol{\alpha}_1\boldsymbol{\alpha}_2\boldsymbol{\alpha}_3 \\
&= \begin{pmatrix} \vec{A}_0\cdot\vec{s}\,\mathbf{1} + \mathrm{i}\left(\vec{r}\times\vec{A}_0\right)\cdot\vec{\boldsymbol{\sigma}} & t\vec{A}_0\cdot\vec{\boldsymbol{\sigma}} - \vec{A}_0^T\underline{\underline{w}}\,\vec{\boldsymbol{\sigma}} + \mathrm{i}\vec{A}_0\cdot\vec{h}\,\mathbf{1} \\ t\vec{A}_0\cdot\vec{\boldsymbol{\sigma}} - \vec{A}_0^T\underline{\underline{w}}\,\vec{\boldsymbol{\sigma}} + \mathrm{i}\vec{A}_0\cdot\vec{h}\,\mathbf{1} & -\left(\vec{A}_0\cdot\vec{s}\,\mathbf{1} + \mathrm{i}\left(\vec{r}\times\vec{A}_0\right)\cdot\vec{\boldsymbol{\sigma}}\right) \end{pmatrix} = \begin{pmatrix} \boldsymbol{M}^{uu} & \boldsymbol{M}^{ud} \\ \boldsymbol{M}^{du} & \boldsymbol{M}^{dd} \end{pmatrix},
\end{aligned} \tag{7.59}$$

where $\vec{\boldsymbol{\Sigma}}$ is the non-relativistic spin operator (3.41). Note, that the variables t, s, r, w and h are functions with the two parameters $\vec{k}+n\vec{k}_L$ and $\vec{k}+(n-1)\vec{k}_L$. Equation (7.59) rewrites the bi-spinor contractions (4.60c) by converting

$$\sum_{q\neq l} A_0^l r^q(\vec{k},\vec{k}')\boldsymbol{\beta}\boldsymbol{\alpha}_q\boldsymbol{\alpha}_l = \sum_{l,m,q} A_0^l r^q(\vec{k},\vec{k}')\varepsilon_{mql}\mathrm{i}\boldsymbol{\beta}\boldsymbol{\Sigma}_m = \sum_m \left(\vec{r}\times\vec{A}_0\right)_m \mathrm{i}\boldsymbol{\beta}\boldsymbol{\Sigma}_m = \mathrm{i}\boldsymbol{\beta}\vec{\boldsymbol{\Sigma}}\cdot\left(\vec{r}\times\vec{A}_0\right) \tag{7.60}$$

and employs the notion of the the tensor contraction

$$-\vec{A}_0^T\underline{\underline{w}}\,\vec{\boldsymbol{\alpha}} = -\sum_{l,q} A_0^l w^{lq}\boldsymbol{\alpha}_q\,. \tag{7.61}$$

In summary, equation (7.59) introduced the 2×2 matrices

$$\boldsymbol{M}^{uu}_{m,n} = -\boldsymbol{M}^{dd}_{m,n} = \vec{A}_0\cdot\vec{s}(\vec{k}+n\vec{k}_L,\vec{k}+m\vec{k}_L)\,\mathbf{1} + \mathrm{i}\left(\vec{r}(\vec{k}+n\vec{k}_L,\vec{k}+m\vec{k}_L)\times\vec{A}_0\right)\cdot\vec{\boldsymbol{\sigma}} \tag{7.62}$$

$$\boldsymbol{M}^{ud}_{m,n} = \quad \boldsymbol{M}^{du}_{m,n} = t(\vec{k}+n\vec{k}_L,\vec{k}+m\vec{k}_L)\vec{A}_0\cdot\vec{\boldsymbol{\sigma}} - \vec{A}_0^T\underline{\underline{w}}(\vec{k}+n\vec{k}_L,\vec{k}+m\vec{k}_L)\,\vec{\boldsymbol{\sigma}} + \mathrm{i}\vec{A}_0\cdot\vec{h}(\vec{k}+n\vec{k}_L,\vec{k}+m\vec{k}_L)\,\mathbf{1}\,. \tag{7.63}$$

The matrix product in equation (7.58) can be performed with the help of the matrices (7.62) and (7.63).

Only the diffraction of quantum states with positive eigen energy into states of positive eigen energy is of relevance in the case of the Kapitza-Dirac effect, which corresponds to the upper left 2×2 matrix subentry of equation (7.58), which results in

$$\begin{aligned}\boldsymbol{U}_{\mathrm{rd,ul};3,0}(t,t_3) = &-\left(\frac{e}{\mathrm{i}2\hbar}\right)^3 \int_{t_0}^{t} dt_3 \int_{t_0}^{t_3} dt_2 \int_{t_0}^{t_2} dt_1 \sin(\omega t_3)\sin(\omega t_2)\sin(\omega t_1) \\ &\cdot \Big(\mathrm{phase}_1 \boldsymbol{M}^{uu}_{3,2}\boldsymbol{M}^{uu}_{2,1}\boldsymbol{M}^{uu}_{1,0} + \mathrm{phase}_2 \boldsymbol{M}^{ud}_{3,2}\boldsymbol{M}^{du}_{2,1}\boldsymbol{M}^{uu}_{1,0} \\ &+ \mathrm{phase}_3 \boldsymbol{M}^{uu}_{3,2}\boldsymbol{M}^{ud}_{2,1}\boldsymbol{M}^{du}_{1,0} + \mathrm{phase}_4 \boldsymbol{M}^{ud}_{3,2}\boldsymbol{M}^{dd}_{2,1}\boldsymbol{M}^{du}_{1,0} \Big) .\end{aligned} \tag{7.64}$$

The additional "ul" index in $\boldsymbol{U}_{\mathrm{rd,ul};3,0}$ denotes, that only the upper left 2×2 matrix subentry of equation (7.58) is considered. The propagator (7.64) contains the four different phases

$$\begin{aligned}\mathrm{phase}_1 &= \exp\left[-\frac{\mathrm{i}}{\hbar}\left(E_3(t-t_3) + E_2(t_3-t_2) + E_1(t_2-t_1) + E_0(t_1-t_0)\right)\right] \\ &= \exp\left[-\frac{\mathrm{i}}{\hbar}\left(E_3 t - E_0 t_0 + \Delta E^{uu}_{2,3} t_3 + \Delta E^{uu}_{1,2} t_2 + \Delta E^{uu}_{0,1} t_1\right)\right] ,\end{aligned} \tag{7.65}$$

$$\begin{aligned}\mathrm{phase}_2 &= \exp\left[-\frac{\mathrm{i}}{\hbar}\left(E_3(t-t_3) - E_2(t_3-t_2) + E_1(t_2-t_1) + E_0(t_1-t_0)\right)\right] \\ &= \exp\left[-\frac{\mathrm{i}}{\hbar}\left(E_3 t - E_0 t_0 + \Delta E^{du}_{2,3} t_3 + \Delta E^{ud}_{1,2} t_2 + \Delta E^{uu}_{0,1} t_1\right)\right] ,\end{aligned} \tag{7.66}$$

$$\begin{aligned}\mathrm{phase}_3 &= \exp\left[-\frac{\mathrm{i}}{\hbar}\left(E_3(t-t_3) + E_2(t_3-t_2) - E_1(t_2-t_1) + E_0(t_1-t_0)\right)\right] \\ &= \exp\left[-\frac{\mathrm{i}}{\hbar}\left(E_3 t - E_0 t_0 + \Delta E^{uu}_{2,3} t_3 + \Delta E^{du}_{1,2} t_2 + \Delta E^{ud}_{0,1} t_1\right)\right] ,\end{aligned} \tag{7.67}$$

$$\begin{aligned}\mathrm{phase}_4 &= \exp\left[-\frac{\mathrm{i}}{\hbar}\left(E_3(t-t_3) - E_2(t_3-t_2) - E_1(t_2-t_1) + E_0(t_1-t_0)\right)\right] \\ &= \exp\left[-\frac{\mathrm{i}}{\hbar}\left(E_3 t - E_0 t_0 + \Delta E^{du}_{2,3} t_3 + \Delta E^{dd}_{1,2} t_2 + \Delta E^{ud}_{0,1} t_1\right)\right] ,\end{aligned} \tag{7.68}$$

with the abbreviations

$$\Delta E^{uu}_{n,m} = E_n - E_m\,, \quad \Delta E^{ud}_{n,m} = E_n + E_m\,, \quad \Delta E^{du}_{n,m} = -E_n - E_m \text{ and } \quad \Delta E^{dd}_{n,m} = -E_n + E_m\,. \tag{7.69}$$

Note, that the up (u) and down (d) indices of the matrices $\boldsymbol{M}$ coincide with the up and down indices of the energy differences $E_{n,m}$ of the corresponding phases. One may assign some physical interpretation to the product of the 2×2 matrices times the phase. The phase starts out with the positive oscillation energy E_0 times $t_1 - t_0$. At time t_1 either the matrix $\boldsymbol{M}^{uu}_{1,0}$ or the matrix $\boldsymbol{M}^{du}_{1,0}$ is applied. In the case, in which $\boldsymbol{M}^{uu}_{1,0}$ is applied, the phase has again a positive oscillation energy E_1 times $t_2 - t_1$. In the case of the application of $\boldsymbol{M}^{du}_{1,0}$ however, the phase has a negative oscillation energy E_1 times $t_2 - t_1$. In general, the sign of the energy E_{n-1} of the phase before time t_n is related to the upper right index of the matrix $\boldsymbol{M}^{??}_{n,n-1}$ and the sign of energy E_n after the time t_n is related to the upper left index. Therefore, the products of the matrix product $\boldsymbol{M}^{??}_{3,2}\boldsymbol{M}^{??}_{2,1}\boldsymbol{M}^{??}_{1,0}$ times the preceding phase can be interpreted as a

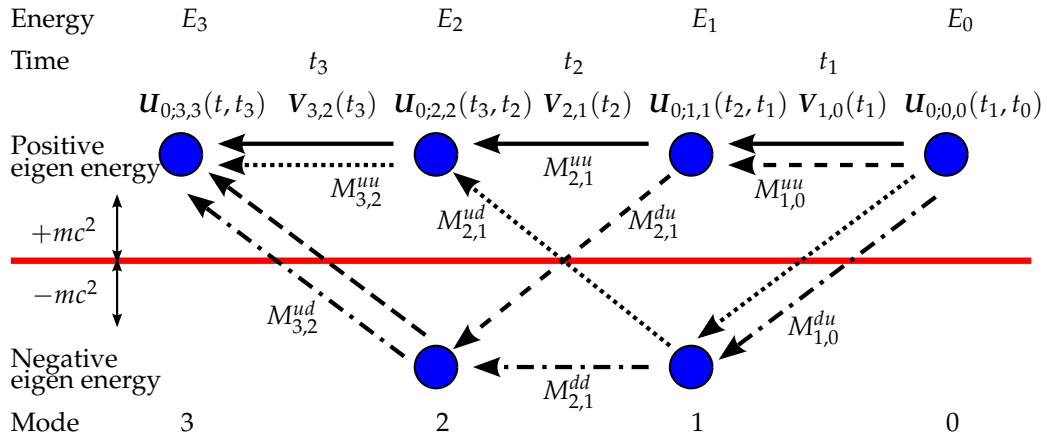

Figure 7.2: This figure illustrates the third order time dependent perturbation theory of equation (7.64) in a similar way as it is presented in figure 7.1. The solid arrows correspond to the contribution, in which the electron propagates in positive energy eigenstates in the whole diffraction process. The dotted arrows correspond to the contribution, in which the electron is scattered to a negative energy eigenstate at time t_1 and is scattered back into a positive energy eigenstate at time t_2. The dashed arrows correspond to the contribution, in which the electron is scattered to a negative energy eigenstate at time t_2 and is scattered back into a positive energy eigenstate at time t_3 and the dash-dotted line corresponds to a contribution, in which the electron is scattered to a negative Energy eigenstate at time t_1 stays a negative energy eigen at t_2 and is scattered back into a positive energy eigenstate at time t_3.

quantum mechanical pathway of an electron which may be scattered into positive or negative energy eigenstates, depending on the upper indices of the matrices $\boldsymbol{M}^{??}_{n,n-1}$. Equation (7.64) contains all four possible combinations of matrix products, which are sketched in figure 7.2. The upper left index of the left matrix and the upper right index of the right matrix is an u, because positive incoming and outgoing electron eigen states are required by considering the upper left 2×2 subentry of equation (7.58).

Similar to section 7.2 a time integration over the vanishing term

$$\Delta E^{uu}_{0,3} + \hbar\omega \tag{7.70}$$

is demanded, because this term will diverge in time and dominate over all other contributions. And similarly to section 7.2, this term occurs in the last integral over t_3, where the former integration times t_1 and t_2 are substituted into t_3 by the upper integration limits. Therefore, the time-dependent phase $\exp(-\mathrm{i}\omega t_3)$ has to be searched in the expansion of $\sin(\omega t_1)\sin(\omega t_2)\sin(\omega t_3)$, in which t_1 and t_2 have to be substituted into t_3. From the expansion of the sine product

$$\begin{aligned}\sin(\omega t_1)\sin(\omega t_2)\sin(\omega t_3) = \frac{\mathrm{i}}{8}\Big[&- \mathrm{e}^{\mathrm{i}\omega(-t_1-t_2-t_3)} + \mathrm{e}^{\mathrm{i}\omega(+t_1-t_2-t_3)} + \mathrm{e}^{\mathrm{i}\omega(-t_1+t_2-t_3)} - \mathrm{e}^{\mathrm{i}\omega(+t_1+t_2-t_3)} \\ &+ \mathrm{e}^{\mathrm{i}\omega(-t_1-t_2+t_3)} - \mathrm{e}^{\mathrm{i}\omega(+t_1-t_2+t_3)} + \mathrm{e}^{\mathrm{i}\omega(-t_1+t_2+t_3)} + \mathrm{e}^{\mathrm{i}\omega(+t_1+t_2+t_3)}\Big]\end{aligned} \tag{7.71}$$

only the terms

$$\frac{\mathrm{i}}{8}\mathrm{e}^{\mathrm{i}\omega(+t_1-t_2-t_3)}, \qquad \frac{\mathrm{i}}{8}\mathrm{e}^{\mathrm{i}\omega(-t_1+t_2-t_3)}, \qquad \frac{\mathrm{i}}{8}\mathrm{e}^{\mathrm{i}\omega(-t_1-t_2+t_3)} \tag{7.72}$$

contribute after the substitution of t_1 and t_2. The time integration over t_1 and t_2 for all three terms times phase_1 will be calculated in the following. The same integration of all three terms times phase_2,

phase$_3$ and phase$_4$ is very similar, except that the u and d indices of the energy differences $\Delta E^{??}_{n,m}$ are different. But Different u and d indices do not affect the calculation.

The integral of the first term of (7.72) times phase$_1$ results in

$$\begin{aligned}
&\frac{\mathrm{i}}{8}\int_{t_0}^{t} dt_3 \int^{t_3} dt_2 \int^{t_2} dt_1 \exp\left[-\frac{\mathrm{i}}{\hbar}\left(E_3 t - E_0 t_0 + (\Delta E^{uu}_{2,3} + \hbar\omega)t_3 + (\Delta E^{uu}_{1,2} + \hbar\omega)t_2 + (\Delta E^{uu}_{0,1} - \hbar\omega)t_1\right)\right] \\
&\quad = -\frac{1}{\Delta E^{uu}_{0,1} - \hbar\omega}\frac{\hbar}{8}\int_{t_0}^{t} dt_3 \int^{t_3} dt_2 \exp\left[-\frac{\mathrm{i}}{\hbar}\left(E_3 t - E_0 t_0 + (\Delta E^{uu}_{2,3} + \hbar\omega)t_3 + \Delta E^{uu}_{0,2} t_2\right)\right] \\
&\quad = -\frac{1}{\Delta E^{uu}_{0,1} - \hbar\omega}\frac{1}{\Delta E^{uu}_{0,2}}\frac{\mathrm{i}\hbar^2}{8}\int_{t_0}^{t} dt_3 \exp\left[-\frac{\mathrm{i}}{\hbar}\left(E_3 t - E_0 t_0 + (\Delta E^{uu}_{0,3} + \hbar\omega)t_3\right)\right].
\end{aligned} \tag{7.73}$$

The integral of the second term of (7.72) times phase$_1$ results in

$$\begin{aligned}
&\frac{\mathrm{i}}{8}\int_{t_0}^{t} dt_3 \int^{t_3} dt_2 \int^{t_2} dt_1 \exp\left[-\frac{\mathrm{i}}{\hbar}\left(E_3 t - E_0 t_0 + (\Delta E^{uu}_{2,3} + \hbar\omega)t_3 + (\Delta E^{uu}_{1,2} - \hbar\omega)t_2 + (\Delta E^{uu}_{0,1} + \hbar\omega)t_1\right)\right] \\
&\quad = -\frac{1}{\Delta E^{uu}_{0,1} + \hbar\omega}\frac{\hbar}{8}\int_{t_0}^{t} dt_3 \int^{t_3} dt_2 \exp\left[-\frac{\mathrm{i}}{\hbar}\left(E_3 t - E_0 t_0 + (\Delta E^{uu}_{2,3} + \hbar\omega)t_3 + \Delta E^{uu}_{0,2} t_2\right)\right] \\
&\quad = -\frac{1}{\Delta E^{uu}_{0,1} + \hbar\omega}\frac{1}{\Delta E^{uu}_{0,2}}\frac{\mathrm{i}\hbar^2}{8}\int_{t_0}^{t} dt_3 \exp\left[-\frac{\mathrm{i}}{\hbar}\left(E_3 t - E_0 t_0 + (\Delta E^{uu}_{0,3} + \hbar\omega)t_3\right)\right].
\end{aligned} \tag{7.74}$$

The integral of the third term of (7.72) times phase$_1$ results in

$$\begin{aligned}
&\frac{\mathrm{i}}{8}\int_{t_0}^{t} dt_3 \int^{t_3} dt_2 \int^{t_2} dt_1 \exp\left[-\frac{\mathrm{i}}{\hbar}\left(E_3 t - E_0 t_0 + (\Delta E^{uu}_{2,3} - \hbar\omega)t_3 + (\Delta E^{uu}_{1,2} + \hbar\omega)t_2 + (\Delta E^{uu}_{0,1} + \hbar\omega)t_1\right)\right] \\
&\quad = -\frac{1}{\Delta E^{uu}_{0,1} + \hbar\omega}\frac{\hbar}{8}\int_{t_0}^{t} dt_3 \int^{t_3} dt_2 \exp\left[-\frac{\mathrm{i}}{\hbar}\left(E_3 t - E_0 t_0 + (\Delta E^{uu}_{2,3} - \hbar\omega)t_3 + (\Delta E^{uu}_{0,2} + 2\omega t)t_2\right)\right] \\
&\quad = -\frac{1}{\Delta E^{uu}_{0,1} + \hbar\omega}\frac{1}{\Delta E^{uu}_{0,2} + 2\omega t}\frac{\mathrm{i}\hbar^2}{8}\int_{t_0}^{t} dt_3 \exp\left[-\frac{\mathrm{i}}{\hbar}\left(E_3 t - E_0 t_0 + (\Delta E^{uu}_{0,3} + \hbar\omega)t_3\right)\right].
\end{aligned} \tag{7.75}$$

Summing up the three integrals (7.73), (7.74) and (7.75) yields

$$PF_1 = \frac{1}{\Delta E^{uu}_{0,1} - \hbar\omega}\frac{1}{\Delta E^{uu}_{0,2}} + \frac{1}{\Delta E^{uu}_{0,1} + \hbar\omega}\frac{1}{\Delta E^{uu}_{0,2}} + \frac{1}{\Delta E^{uu}_{0,1} + \hbar\omega}\frac{1}{\Delta E^{uu}_{0,2} + 2\omega t} \tag{7.76}$$

times

$$\int_{t_0}^{t} dt_3 \exp\left[-\frac{\mathrm{i}}{\hbar}\left(E_3 t - E_0 t_0 + (\Delta E^{uu}_{0,3} + \hbar\omega)t_3\right)\right] \tag{7.77}$$

times $-\mathrm{i}\hbar^2/8$. The integration over the phases (7.66), (7.67) and (7.68) results in the prefactors

$$PF_2 = \frac{1}{\Delta E^{uu}_{0,1} - \hbar\omega}\frac{1}{\Delta E^{ud}_{0,2}} + \frac{1}{\Delta E^{uu}_{0,1} + \hbar\omega}\frac{1}{\Delta E^{ud}_{0,2}} + \frac{1}{\Delta E^{uu}_{0,1} + \hbar\omega}\frac{1}{\Delta E^{ud}_{0,2} + 2\omega t}, \tag{7.78}$$

$$PF_3 = \frac{1}{\Delta E^{ud}_{0,1} - \hbar\omega}\frac{1}{\Delta E^{uu}_{0,2}} + \frac{1}{\Delta E^{ud}_{0,1} + \hbar\omega}\frac{1}{\Delta E^{uu}_{0,2}} + \frac{1}{\Delta E^{ud}_{0,1} + \hbar\omega}\frac{1}{\Delta E^{uu}_{0,2} + 2\omega t}, \tag{7.79}$$

$$PF_4 = \frac{1}{\Delta E^{ud}_{0,1} - \hbar\omega}\frac{1}{\Delta E^{ud}_{0,2}} + \frac{1}{\Delta E^{ud}_{0,1} + \hbar\omega}\frac{1}{\Delta E^{ud}_{0,2}} + \frac{1}{\Delta E^{ud}_{0,1} + \hbar\omega}\frac{1}{\Delta E^{ud}_{0,2} + 2\omega t} \tag{7.80}$$

times equation (7.77) times $-\mathrm{i}\hbar^2/8$. The last integral over t_3 of equation (7.77) is identical to (7.29), if one accounts for the different energy-momentum relation $E^{\mathrm{nr}}_n \rightarrow E_n$ in the Dirac case. Taking together

all calculation results, one obtains

$$\boldsymbol{U}_{\mathrm{rd,ul;3,0}}(t,t_0) = \left(PF_1\boldsymbol{M}^{uu}_{3,2}\boldsymbol{M}^{uu}_{2,1}\boldsymbol{M}^{uu}_{1,0} + PF_2\boldsymbol{M}^{ud}_{3,2}\boldsymbol{M}^{du}_{2,1}\boldsymbol{M}^{uu}_{1,0} + PF_3\boldsymbol{M}^{uu}_{3,2}\boldsymbol{M}^{ud}_{2,1}\boldsymbol{M}^{du}_{1,0} + PF_4\boldsymbol{M}^{ud}_{3,2}\boldsymbol{M}^{dd}_{2,1}\boldsymbol{M}^{du}_{1,0}\right) \cdot \left(-\frac{e^3}{2^6\hbar}\right) e^{-\mathrm{i}(E_3t-E_0t_0)/\hbar} \begin{cases} t-t_0 & \text{on resonance} \\ \frac{\mathrm{i}}{\Delta\omega}\left(e^{-\mathrm{i}\Delta\omega t} - e^{-\mathrm{i}\Delta\omega t_0}\right) & \text{off resonance}\,, \end{cases} \tag{7.81}$$

for equation (7.58). A first order Taylor expansion with respect to k_L and k_3 for vanishing A_2 and vanishing k_2 yields

$$\boldsymbol{U}_{\mathrm{rd,ul;3,0}}(t,t_0) = \frac{1}{12\hbar}\frac{e}{m^2c^3}\left(\frac{5}{\sqrt{2}}A_3\hbar k_3\mathbf{1} - \hbar k_L A_3(\mathrm{i}\sigma_2)\right)\frac{e^2A_3^2}{4mc^2}e^{-\mathrm{i}(E_3t-E_0t_0)/\hbar}(t-t_0)\,, \tag{7.82}$$

where the vector $\vec{k}_L$ is pointing in the x_1-direction. The vanishing A_2, k_2 and the direction of k_L has been chosen, such that a Taylor expansion is feasible with Mathematica. In order to recover an equation, which is independent of this specific geometry, one may perform the following replacements in (7.82). The product A_3k_3 is nothing, but the component $k_{\parallel} = \vec{k}\cdot\vec{A}_0/|\vec{A}_0|$ of the vector $\vec{k}$, parallel to the vector potential direction of the external laser beam times the amplitude of the vector potential $|\vec{A}_0|$, resulting in $A_3k_3 = |\vec{A}_0|k_{\parallel} = \vec{k}\cdot\vec{A}_0$. Similarly, A_3^2 can be written as $\vec{A}_0^2$. The term, containing the σ_2 can be recovered as scalar product of the vector $\vec{\sigma}$ times the cross product of $\vec{k}_L$ with $\vec{A}_0$. Inserting all replacements in (7.82) yields

$$\boldsymbol{U}_{\mathrm{rd,ul;3,0}}(t,t_0) = \frac{1}{12\hbar}\frac{e}{m^2c^3}\left(\frac{5}{\sqrt{2}}\vec{A}_0\cdot\hbar\vec{k}\mathbf{1} + \hbar\vec{k}_L\times\vec{A}_0\cdot(\mathrm{i}\vec{\sigma})\right)\frac{e^2\vec{A}_0^2}{4mc^2}e^{-\mathrm{i}(E_3t-E_0t_0)/\hbar}(t-t_0)\,, \tag{7.83}$$

which is of the same form as the propagator of perturbation theory with the Pauli equation (7.39), except that the prefactors of the 2×2 matrices are different.

7.3.2 Interpretation

Comparison with Pauli theory

There is no non-relativistic limit, in which the propagator of the Dirac equation (7.83) and the propagator of the Pauli equation (7.39) coincide. The reason for this counter-intuitive property is, that there is no configuration for which the laser frequency and initial electron momentum are non-relativistic for the 3-photon Kapitza-Dirac effect. This property is already discussed in section 2.2.4. Therefore, the 3-photon Kapitza-Dirac effect always occurs in a parameter regime, in which the validity of Pauli theory breaks down. Thus, even though the results of Pauli and Dirac theory are similar, it is clear, that they cannot coincide excactly.

Electron spin rotation

Similar to subsection 7.2.2, equation (7.83) has the same form as the proposed $\mathcal{SU}(2)$-ansatz (6.4) for the propagator matrix entry, with vanishing imaginary part of $\vec{n}$. The parameters for this ansatz assume

the values

$$P_{3,0}(t,t_0) = \frac{1}{12\hbar}\frac{e}{m^2c^3}\frac{e^2\vec{A}_0^2}{4mc^2}\left[\left(\frac{5}{\sqrt{2}}\vec{A}_0\cdot\hbar\vec{k}\right)^2 + \left(\hbar\vec{k}_L\times\vec{A}_0\right)^2\right]^{\frac{1}{2}}(t-t_0)\,, \tag{7.84a}$$

$$\phi_{3,0}(t,t_0) = -\mathrm{i}\frac{E_3t - E_0t}{\hbar}\,, \tag{7.84b}$$

$$\cos\left(\frac{\alpha_{3,0}(t,t_0)}{2}\right) = \frac{5}{\sqrt{2}}\vec{A}_0\cdot\hbar\vec{k}\left[\left(\frac{5}{\sqrt{2}}\vec{A}_0\cdot\hbar\vec{k}\right)^2 + \left(\hbar\vec{k}_L\times\vec{A}_0\right)^2\right]^{-\frac{1}{2}}, \tag{7.84c}$$

$$\vec{n}_{3,0}(t,t_0)\sin\left(\frac{\alpha_{3,0}(t,t_0)}{2}\right) = -\hbar\vec{k}_L\times\vec{A}_0\left[\left(\frac{5}{\sqrt{2}}\vec{A}_0\cdot\hbar\vec{k}\right)^2 + \left(\hbar\vec{k}_L\times\vec{A}_0\right)^2\right]^{-\frac{1}{2}}. \tag{7.84d}$$

Like in subsection 7.2.2, the four equations (7.84) are unique, because of the unitarity of the $\mathcal{SU}(2)$ representation.

One analogously concludes as in subsection 7.2.2, that the rotation angle $\alpha_{3,0}(t,t_0)$ and the rotation axis $\vec{n}_{3,0}(t,t_0)$ are constant in time. The unit vector

$$\vec{n}_{3,0} = -\frac{\vec{k}_L\times\vec{A}_0}{|\vec{k}_L\times\vec{A}_0|} = \frac{\vec{B}_0}{|\vec{B}_0|} \tag{7.85}$$

of the rotation axis of the electron spin points in the direction of the magnetic field $\vec{B}_0$ of the laser beam, too.

The rotation angle $\alpha_{3,0}$ is again computed by multiplying equation (7.84d) with equation (7.85) and dividing it by equation (7.84c), resulting in

$$\tan\left(\frac{\alpha_{3,0}}{2}\right) = \frac{\sqrt{2}}{5}\frac{|\vec{k}_L\times\vec{A}_0|}{\vec{A}_0\cdot\vec{k}}\,. \tag{7.86}$$

Rabi frequency

The quantity

$$\boldsymbol{U}_{\mathrm{nd,ul};3,0}(T,0)\boldsymbol{U}^{\dagger}_{\mathrm{nd,ul};3,0}(T,0) = \left(\frac{1}{12\hbar}\right)^2\left(\frac{e}{m^2c^3}\right)^2\left[\left(\frac{5}{\sqrt{2}}\vec{A}_0\cdot\hbar\vec{k}\right)^2 + \left(\hbar\vec{k}_L\times\vec{A}_0\right)^2\right]\left(\frac{e^2\vec{A}_0^2}{4mc^2}\right)^2 T^2\mathbf{1}\,, \tag{7.87}$$

originating from propagator subentry (7.83) is of the same form as the Taylor expansion (7.46). Therefore one may conclude the Rabi frequency

$$\Omega_R = \frac{1}{6\hbar}\frac{e}{m^2c^3}\frac{e^2\vec{A}_0^2}{4mc^2}\sqrt{\left(\frac{5}{\sqrt{2}}\vec{A}_0\cdot\hbar\vec{k}\right)^2 + \left(\hbar\vec{k}_L\times\vec{A}_0\right)^2}\,. \tag{7.88}$$

of the 3-photon Kapitza-Dirac effect, similarly to subsection 7.2.2.

Spin-flip probability

Similarly to subsection 7.2.2, the time evolution of the expansion coefficients c_n^{σ} can be computed by equation (6.1). If one assumes an initial configuration, in which only the 0 mode with spin up is occupied, one may compute

$$c_3^{+\uparrow}(t) = (\boldsymbol{U}_{\mathrm{nd};a,b})^{(+\uparrow,+\uparrow)}(t,t_0)c_0^{+\uparrow}(t_0) = \frac{1}{12\hbar}\frac{5e\vec{A}_0\cdot\hbar\vec{k}}{\sqrt{2}m^2c^3}\frac{e^2\vec{A}_0^2}{4mc^2}e^{-\mathrm{i}(E_3^{\mathrm{nr}}t - E_0^{\mathrm{nr}}t_0)/\hbar}(t-t_0)c_0^{+\uparrow}(t_0)\,, \tag{7.89a}$$

$$c_3^{+\downarrow}(t) = (\boldsymbol{U}_{\mathrm{nd};a,b})^{(+\downarrow,+\uparrow)}(t,t_0)c_0^{+\uparrow}(T) = \frac{1}{12\hbar}\frac{e\hbar\vec{k}_L\times\vec{A}_0}{m^2c^3}\frac{e^2\vec{A}_0^2}{4mc^2}e^{-\mathrm{i}(E_3^{\mathrm{nr}}t - E_0^{\mathrm{nr}}t_0)/\hbar}(t-t_0)c_0^{+\downarrow}(t_0)\,. \tag{7.89b}$$

With the more specific initial condition $c_0^{+\uparrow}(0) = 1$ one obtains

$$|c_3^{+\uparrow}(T)|^2 = \left(\frac{1}{12\hbar}\right)^2 \left(\frac{5e\vec{A}_0 \cdot \hbar\vec{k}}{\sqrt{2}m^2c^3}\right)^2 \left(\frac{e^2\vec{A}_0^2}{4mc^2}\right)^2 T^2 \quad \text{and} \tag{7.90a}$$

$$|c_3^{+\downarrow}(T)|^2 = \left(\frac{1}{12\hbar}\right)^2 \left(\frac{e\hbar\vec{k}_L \times \vec{A}_0}{m^2c^3}\right)^2 \left(\frac{e^2\vec{A}_0^2}{4mc^2}\right)^2 T^2 . \tag{7.90b}$$

after time T. Analogous to subsection 7.2.2 one can compute the non-spin-flip and spin-flip probabilities

$$P_{\text{noflip}} = \frac{(5e\vec{A}_0 \cdot \hbar\vec{k}/\sqrt{2})^2}{(5e\vec{A}_0 \cdot \hbar\vec{k}/\sqrt{2})^2 + (e\hbar\vec{k}_L \times \vec{A}_0)^2} = \frac{(5k_\parallel/\sqrt{2})^2}{(5k_\parallel/\sqrt{2})^2 + (k_L)^2} = \frac{1}{1 + 2k_L^2/(25k_\parallel^2)} \quad \text{and} \tag{7.91a}$$

$$P_{\text{flip}} = \frac{(e\hbar\vec{k}_L \times \vec{A}_0)^2}{(5e\vec{A}_0 \cdot \hbar\vec{k}/\sqrt{2})^2 + (e\hbar\vec{k}_L \times \vec{A}_0)^2} = \frac{(k_L)^2}{(5k_\parallel/\sqrt{2})^2 + (k_L)^2} = \frac{1}{25k_\parallel^2/(2k_L^2) + 1} . \tag{7.91b}$$

Chapter 8

Electron spin dynamics: Numerical results

In this chapter, the quantum dynamics of the 3-photon Kapitza-Dirac effect is solved by numerical application of the quantum wave equations in chapter 4, in analogy to the 2-photon Kapitza-Dirac effect of chapter 5. A focus is on the spin properties, which clearly shows up in the 3-photon Kapitza-Dirac effect, in contrast to the 2-photon Kapitza-Dirac effect. The considerations on the general electron spin properties of chapter 6, together with the perturbative short-time solution of chapter 7 are verified with the numerical simulations in this chapter.

The chapter starts with the detailed presentation of the 3-photon Kapitza-Dirac effect of reference [25]. After that, the spin-flip probability and the spin rotation properties of the 3-photon Kapitza-Dirac effect are discussed in section 8.2. The properties of a slower turn on and turn off of the laser field amplitude are considered similarly to section 5.2. At the end, the resonance peak structure of the diffraction probability is discussed (section 8.5) and the Rabi frequencies from the perturbative solution 7 are verified (section 8.6).

8.1 Setup

One may use the resonance condition (2.17) from energy and momentum conservation for the determination of the initial momentum $\vec{p}_{1,\text{in}}$ of the 3-photon Kapitza-Dirac effect, similarly to chapter 5. The number of absorbed photons is 2 and the number of emitted photons is 1. The photon energy of $3.1\,\text{keV} = 6.1 \cdot 10^{-3}\, mc^2$ of the laser beam is adopted from [25], as well as the initial electron momentum in laser polarization direction of $2\hbar k_L/5$. Equation (2.17) yields a value of $176\,\text{keV}/c = 0.347mc$ for the initial momentum of the electron in laser propagation direction. The ponderomotive amplitude is chosen to be $1.16 \cdot 10^{-2}\, mc^2$, as it is used in [25].

The resulting quantum dynamics is shown in figure 8.1. The initial condition of the simulation is $c_0^{+\uparrow}(0) = 1$ and all other expansion coefficients are 0. The amplitude of the vector potential is turned on for 10 laser cycles and off for 10 laser cycles, according to the envelope function (5.4). One can identify Rabi oscillations in the quantum dynamics and may use the Rabi frequencies and spin-flip probabilities from perturbation theory of section 7.3 for expressing the curves with sine and cosine functions as it is done for the 2-photon Kapitza-Dirac effect in section 5. For the chosen parameters, the spin-flip probability (7.91b) evaluates to $1/3$ and the probability of no spin-flip (7.91a) evaluates to

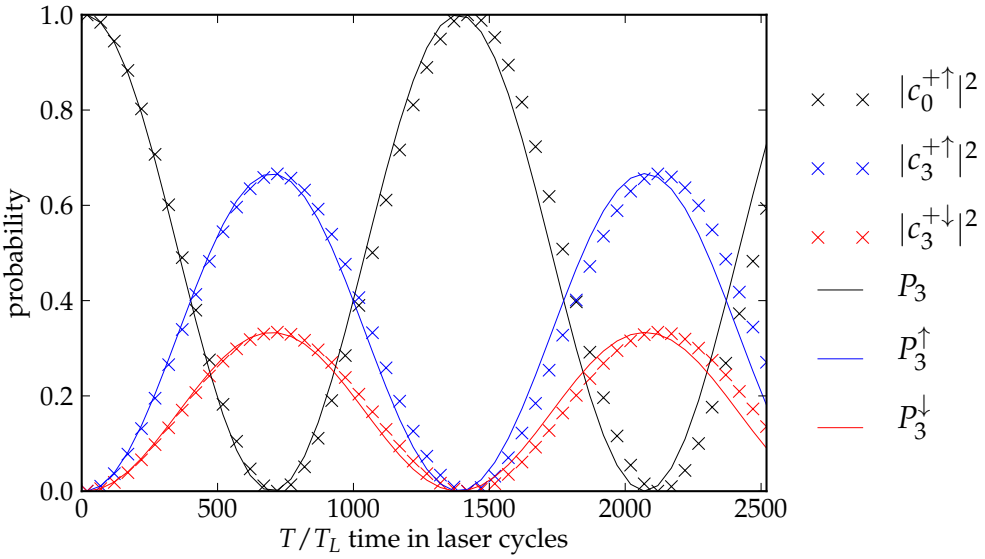

Figure 8.1: This figure shows a similar time evolution of the Dirac equation (4.64), as in figure 5.2, but this time for the case of the 3-photon Kapitza-Dirac effect. The corresponding parameters of the laser and the electron are introduced in section 8.1. The laser intensity of this simulation corresponds to $2.0 \cdot 10^{23}\,\mathrm{W/cm^2}$, with a laser wave length of 0.4 nm. The electron momentum is $176\,\mathrm{keV}/c$ in laser propagation direction and $1.2\,\mathrm{keV}/c$ in laser polarization direction. The solid lines are the analytical estimate (8.1) and the crosses are data points of the numerical simulation [25]. The Rabi transition evolves between mode 0 and 3, implying 3 transferred photon momenta, in contrast to the two photon momenta of the 2-photon Kapitza-Dirac effect in section 5. Furthermore, the diffraction probability of the electron beam consists of a spin-flipped part $|c_3^{+\downarrow}|^2$ and a not spin-flipped part $|c_3^{+\uparrow}|^2$.

2/3. Therefore, one may assume

$$P_0(T) = \cos^2\left(\frac{\Omega_R}{2}T - \frac{\Omega_R}{2}13.75\,T_L\right), \tag{8.1a}$$

$$P_3^{\uparrow}(T) = \frac{2}{3}\sin^2\left(\frac{\Omega_R}{2}T - \frac{\Omega_R}{2}13.75\,T_L\right), \tag{8.1b}$$

$$P_3^{\downarrow}(T) = \frac{1}{3}\sin^2\left(\frac{\Omega_R}{2}T - \frac{\Omega_R}{2}13.75\,T_L\right), \tag{8.1c}$$

where $P_0(T)$, $P_3^{\uparrow}(T)$ and $P_3^{\downarrow}(T)$ should approximate the probabilities $|c_0^{+\uparrow}(T)|^2$, $|c_3^{+\uparrow}(T)|^2$ and $|c_3^{+\downarrow}(T)|^2$ in figure 8.1. The frequency Ω_R is the Rabi frequency (7.88), derived from perturbation theory of the Dirac equation and T_L is the time of one laser period $T_L = 2\pi/ck_L$. The number of 13.75 laser periods accounts for the turn on and turn off time of the external laser field and is determined according to the considerations of section 8.4.

Figure 8.1 may mislead the reader to assume, that the quantum dynamics of the 3-photon Kapitza-Dirac effect only takes place in the 0^{th} and the 3^{rd} mode and all other modes are not occupied. However, figures 8.2, 8.3 and 8.4 show, that the opposite is the case. If the external laser field is turned on, the occupation probability distributes over many neighboring modes and rejoins back in mode 3 after the interaction of 700 laser periods. This is a remarkable property, because there is a priori no reason that quantum dynamics oscillates according to the sine shaped Rabi oscillations (8.1) and that parameters like the Rabi frequency and the spin-flip probability agree with the perturbatively derived values. In particular, the spread of the occupation probability over many neighboring modes implies, that higher order terms of time-dependent perturbation theory need to be accounted for, in order to

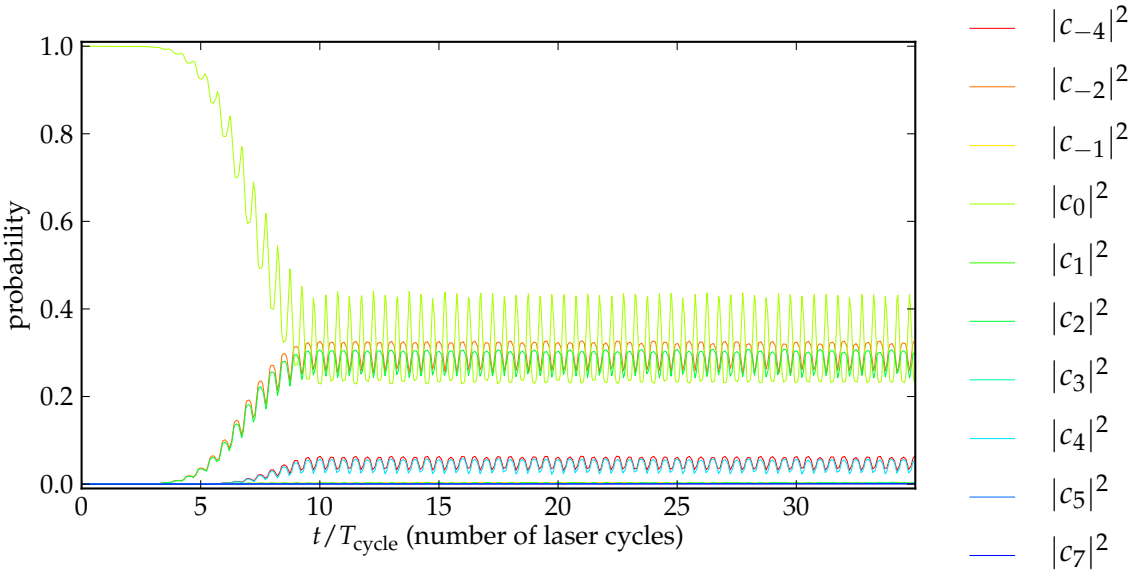

Figure 8.2: This figure shows the same time evolution as in figure 8.1 for the duration of the first 35 laser periods. The difference is that the occupation probability $\sum_\sigma |c_n^\sigma|^2$ for each mode n is plotted while the external field amplitude is not turned off. In contrast to that, a turn off of 10 laser cycles is propagated for each data point in figure 8.1. One can see, that the occupation probability of the 0 mode decreases and the probability is distributed over the neighboring modes during the turn on phase of the interaction.

assure validity of perturbation theory. However, the results in this, the next section and in section 8.6 indicate, that the predictions of third order time-dependent perturbation theory are applicable even in a non-perturbative parameter space.

It should be pointed out that the numerical results in figure 8.2, 8.3 and 8.4 demonstrate impressively, that the numerical solution of the quantum wave equation is a powerful tool to prove the analytical estimations of chapter 7. Even though, the perturbative solutions of chapter 7 provide useful equations for describing the 3-photon Kapitza-Dirac effect, only a numerical solution can answer, how quantum dynamics evolves without approximations.

8.2 Spin properties of the 3-photon Kapitza-Dirac effect

Figure 8.1 contains the probability that an initial electron with spin up is diffracted to a final electron with spin down, where the spin quantization axis points in x_3-direction. In general, the initial electron spin could point in any direction $\vec{n}$, with polar coordinates θ, φ and one may detect, if the final spin points in the $\vec{n}'$ direction, with polar coordinates θ', φ'. If the initial quantum state is parameterized by the Bloch state $c_0(\theta, \varphi)$ of equation (6.16) and the final quantum state, on which the wave function is projected to, is parameterized by the similar Bloch state $c_3(\theta', \varphi')$ with different angles θ' and φ', then the transition probability from $c_0(\theta, \varphi)$ to $c_3(\theta', \varphi')$ is given by the matrix element

$$c_3(\theta', \varphi')^\dagger \boldsymbol{U}_{3,0}(t, t_0) c_0(\theta, \varphi)\,. \tag{8.2}$$

This matrix element can be reasoned with the scalar product of $c_3^+(\theta', \varphi')$ with c_3^+ of equation (6.7b), which is the spin-dependent transition probability. The scalar product of $c_3^+(\theta', \varphi')$ with the right-hand side of equation (6.7b) yields the matrix element (8.2). Therefore, the knowledge of the matrix $\boldsymbol{U}_{3,0}(t, t_0)$ can answer the above question of a spin dependent diffraction probability for a general incoming spin direction and a general outgoing spin direction. Chapter 6 assumes, that this propagator subentry $\boldsymbol{U}_{3,0}(t, t_0)$ should be of the form (6.4), with the $\mathcal{SU}(2)$ representation (6.5) and vanishing

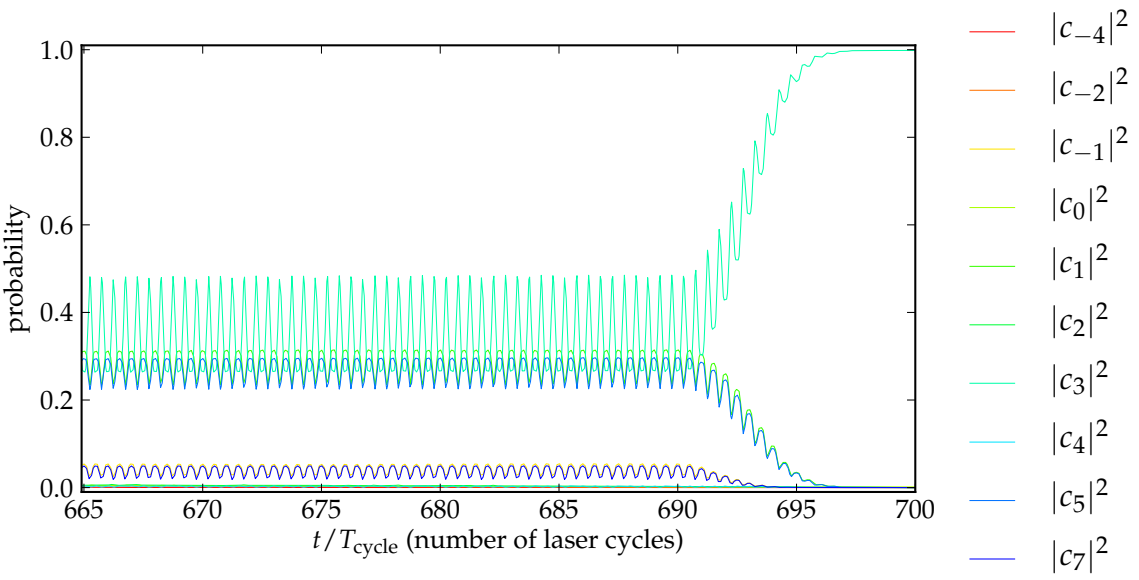

Figure 8.3: This figure shows the same time evolution as in figure 8.1 for the duration of the last 35 laser periods of the interaction time of 700 laser periods. Similarly to figure 8.2, the occupation probability $\sum_\sigma |c_n^\sigma|^2$ for each mode n is plotted while the external field amplitude is not turned off. When the external laser field is smoothly turned off all the distributed occupation probability joins back into mode 3 at time $t = 700T_L$.

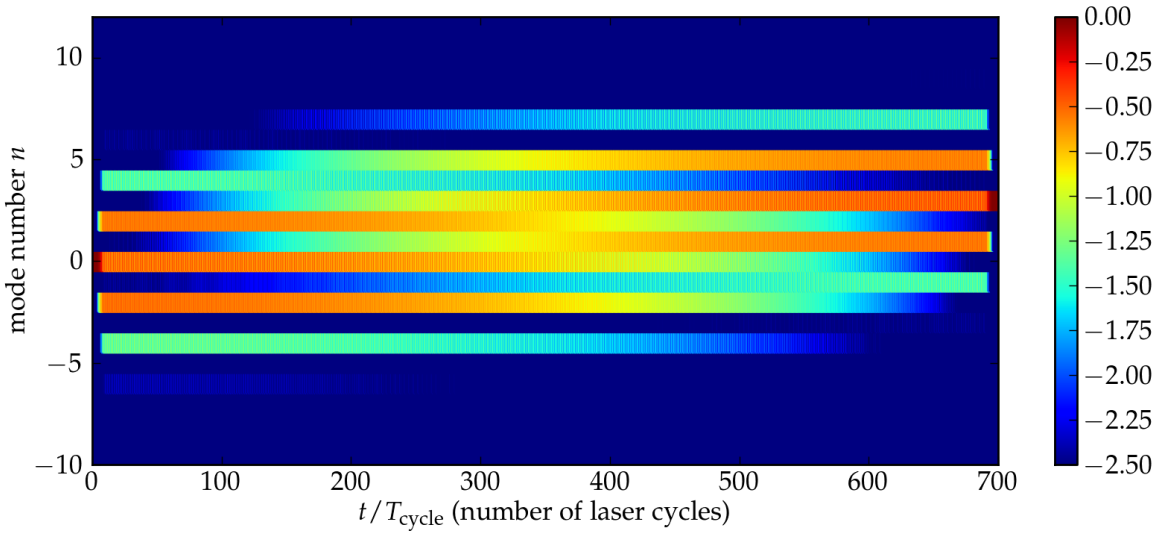

Figure 8.4: This figure shows exactly the same data as in the figures 8.2 and 8.3, but for the whole interaction time of 700 laser periods and in a rainbow colored density plot. The color coding is the logarithm to base 10 of the occupation density $\sum_\sigma |c_n^\sigma|^2$ of each mode at time t. Occupation probabilities lower than $10^{-2.5}$ are represented in dark blue. One can see, that the probability density distributes in momentum space during the interaction. The modes -4, -2, 0, 2 and 4 exchange their occupation probability with the modes -1, 1, 3, 5 and 7 in the interacting process. In the turn off phase of the last 10 laser cycles, the occupation probability accumulates to mode 3, resulting in the data point at interaction time $T = 700T_L$ in figure 8.1.

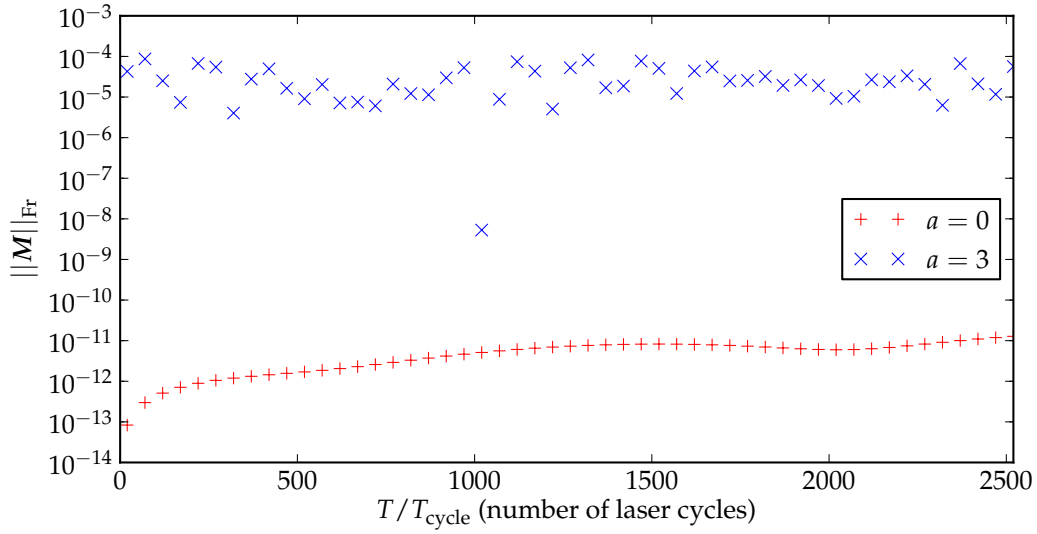

Figure 8.5: This figure shows the Frobenius norm (8.3) of the propagator subentry $\boldsymbol{U}_{a,b}(t,t_0)$, subtracted by its approximation (6.4) for the data of the simulation, which is described in section 8.1. The data with $a = 0$ originates from the propagator $\boldsymbol{U}_{0,0}(t,t_0)$, which describes the quantum dynamics of the undiffracted beam, whereas $a = 3$ corresponds to the propagator $\boldsymbol{U}_{3,0}(t,t_0)$ of the diffracted beam. The propagator entry of the undiffracted beam is approximated well. In the case of the diffracted beam, the value between 10^{-4} till 10^{-5} means, that the parameters P, Φ, α and $\vec{n}$ are approximated well up to 4 till 5 decimal places, in the case of a full diffraction probability $P \approx 1$.

imaginary part of $\vec{n}_{3,0}$. This property would be quite useful, because the diffraction properties, which are encoded in $\boldsymbol{U}_{3,0}(t,t_0)$ are reduced to the degrees of freedom of a diffraction probability, a complex phase, a rotation angle and a rotation direction, where the rotation refers to the rotation of the spin expectation value of the Foldy-Wouthuysen spin operator (3.40). In order to check, whether the approximation (6.4) can be applied to the simulated propagator subentry, the parameters $P_{3,0}$, $\phi_{3,0}$, $\alpha_{3,0}$ and $\vec{n}_{3,0}$ are determined numerically and the Frobenius norm

$$||\boldsymbol{M}||_{\mathrm{Fr}} = \left(\sum_{i,j} |\boldsymbol{M}_{i,j}|^2 \right)^{\frac{1}{2}} \tag{8.3}$$

of the matrix

$$\boldsymbol{M} = \boldsymbol{U}_{a,b}(t,t_0) - \sqrt{P_{a,b}(t,t_0)} \mathrm{e}^{\mathrm{i}\phi_{a,b}(t,t_0)} \left[\cos\left(\frac{\alpha_{a,b}(t,t_0)}{2} \right) \mathbf{1} - \mathrm{i} \sin\left(\frac{\alpha_{a,b}(t,t_0)}{2} \right) \vec{n}_{a,b}(t,t_0) \cdot \vec{\boldsymbol{\sigma}} \right] \tag{8.4}$$

is computed in figure 8.5. The Frobenius norm is used, because it is a matrix norm, which is compatible to the euclidean scalar product $||\cdot||_2$ and it is easy to compute. Figure 8.5 tells, that the propagator subentry $\boldsymbol{U}_{3,0}$ can be approximated with a precision of 4 to 5 decimal places and $\boldsymbol{U}_{0,0}$ can be approximated even better. The successful approximation of the propagator by the parameters P, ϕ, α and $\vec{n}$, with vanishing imaginary part $\vec{n}$ implies already, that the electron spin is rotated by the angle α around the direction $\vec{n}$. The question arises, how these parameters evolve in time in the case of Kapitza-Dirac scattering. The figures 8.6 and 8.7 present the relevant data over the interaction time T. According to figure 8.6(a), the spin of the undiffracted beam remains unchanged. The figures 8.6(b) and 8.7 tell, that the electron spin is rotated by an angle of 70.6 degrees around the direction of the magnetic field of the counterpropagating laser beam.

As stated above, the spin-flip probability of the diffracted beam can be deduced from the matrix element of the $\mathcal{SU}(2)$ representation of rotations (6.5). If the initial electron points in the x_3-direction

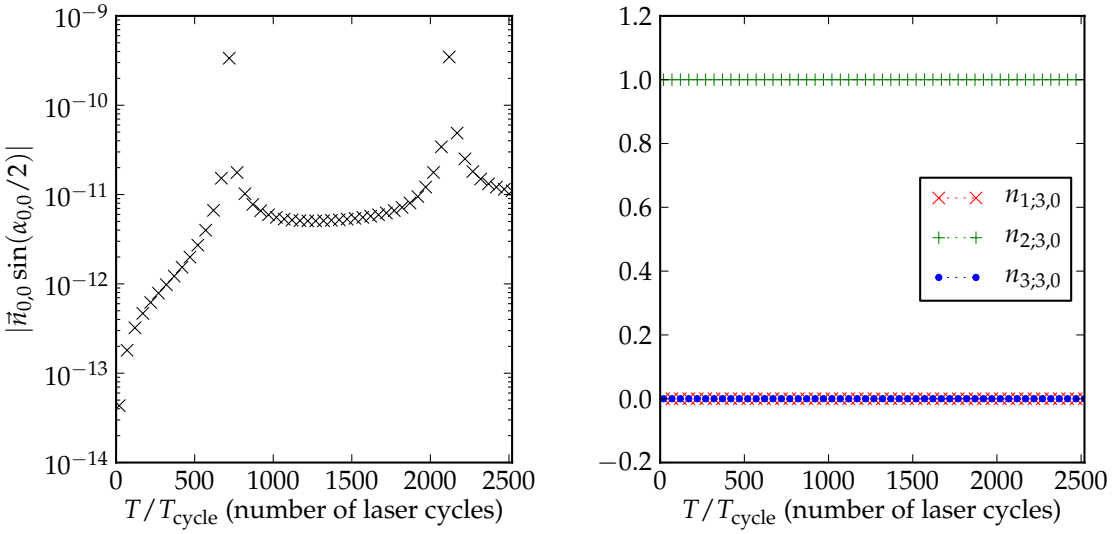

Figure 8.6: (a) *Left figure.* The value $|\vec{n}_{0,0}\sin(\alpha_{0,0}/2)|$ is plotted for the data of the simulation, which is described in section 8.1. Since this value is below 10^{-9}, the angle $\alpha_{0,0}$ is also below 10^{-9}, which means, that the change of the electron spin of the undiffracted beam is negligible. (b) *Right figure.* The three components of the unit vector $\vec{n}_{3,0}$ are plotted for the data of the simulation, which is described in section 8.1. The vector points precisely in the x_2-direction for all interaction times T, which is the direction of the magnetic field of the external vector potential (2.1b).

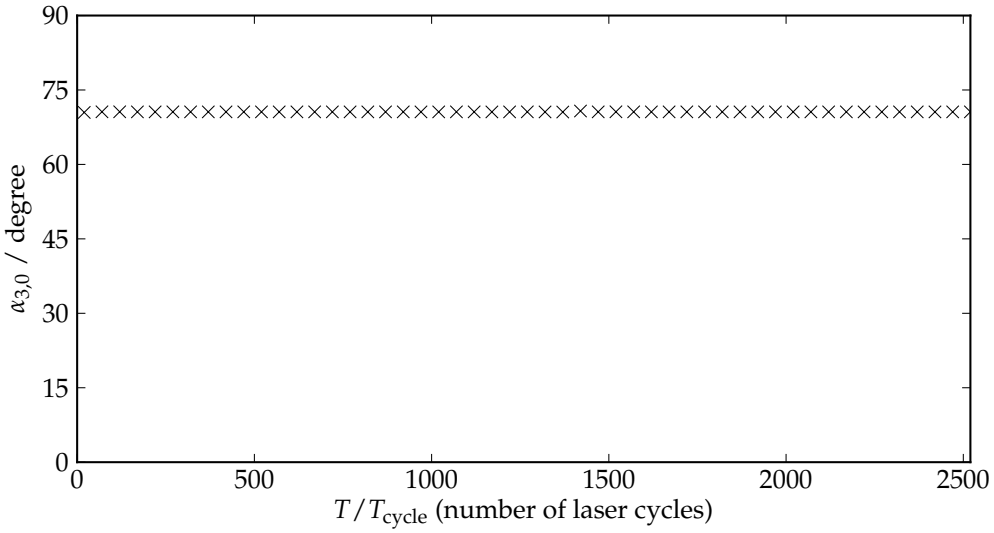

Figure 8.7: The rotation angle $\alpha_{3,0}$ is plotted for the simulation data, shown in figure 8.1. The value of this angle is 70.6° independent of the interaction time T.

($\theta = 0, \phi = 0$), as well as the final projecting state ($\theta' = 0, \phi' = 0$) and the rotation axis was pointing in x_2-direction ($\vec{n}_{3,0} = (0,1,0)^T$), the matrix element (8.2) evaluates to

$$c_3(0,0)^\dagger \boldsymbol{S}\, c_0(0,0) = \begin{pmatrix} 1 \\ 0 \end{pmatrix}^\dagger \begin{pmatrix} \cos(\alpha/2) & -\sin(\alpha/2) \\ \sin(\alpha/2) & \cos(\alpha/2) \end{pmatrix} \begin{pmatrix} 1 \\ 0 \end{pmatrix} = \cos\left(\frac{\alpha}{2}\right) . \tag{8.5}$$

If the final projecting state was pointing in the $-x_3$-direction ($\theta' = \pi, \phi' = 0$), the matrix element evaluates to

$$c_3(\pi,0)^\dagger \boldsymbol{S}\, c_0(0,0) = \begin{pmatrix} 0 \\ 1 \end{pmatrix}^\dagger \begin{pmatrix} \cos(\alpha/2) & -\sin(\alpha/2) \\ \sin(\alpha/2) & \cos(\alpha/2) \end{pmatrix} \begin{pmatrix} 1 \\ 0 \end{pmatrix} = \sin\left(\frac{\alpha}{2}\right) . \tag{8.6}$$

Note, that the two matrix elements (8.5) and (8.6) correspond to the observables $|c_3^{+\uparrow}|^2$ and $|c_3^{+\downarrow}|^2$ of figure 8.1 at the initial condition $c_0^{+\uparrow}(0) = 1$. The absolute square of these matrix elements with the angle $\alpha = 70.6$ results in $|\cos(\alpha/2)|^2 = 0.666$ and $|\sin(\alpha/2)|^2 = 0.334$, which is consistent with the spin-flip probabilities (7.91a) and (7.91b). This demonstrates, that the knowledge of the parameters P, ϕ, α and $\vec{n}$ of the propagator subentry $\boldsymbol{U}_{3,0}(t,t_0)$ is sufficient for computing the spin-flip probability in figure 8.1 and any other directed spin change probability.

The rotation angle and the rotation axis of the propagator of the diffracted and the undiffracted electron beam do not depend on the interaction time. This means, that the electron spin of the undiffracted beam never changes its direction. Similarly, the electron spin of the diffracted beam is always rotated by the angle 70.6 degrees around the y direction for all times T. The only property, which evolves in time (and oscillates in Rabi cycles) is the diffraction probability of the diffracted and the undiffracted beam.

8.3 Variation of the spin rotation

The spin-flip probability of the numerical results in figure 8.1 is deduced from perturbation theory by using the equations (7.91a) and (7.91b). Both probabilities depend on the parameters k_L and $k_\parallel$. If these parameters are changed, the spin-flip probability changes, which implies, that also the angle of the electron spin rotation changes. This is tested by varying the electron momentum in laser polarization direction $\hbar k_\parallel$ in figure 8.8. The spin-flip probability changes indeed according to (7.91b). The parameters of the propagator subentries $\boldsymbol{U}_{0,0}(t,t_0)$ and $\boldsymbol{U}_{3,0}(t,t_0)$ are determined from the simulation data, similarly to section 8.2. Figure 8.9 shows, that the propagator is approximated well by the $\mathcal{SU}(2)$ ansatz (6.4). Therefore, one may proceed in interpreting the parameters of the propagator approximation. Figure 8.10(a) tells, that the spin of the undiffracted electron beam remains unchanged, analogously to section 8.2. One concludes from figure 8.10(b), that the vector $\vec{n}_{3,0}$ points in the x_2-direction, which means that the spin of the diffracted electron is rotated around the magnetic field axis of the laser beam. Figure 8.11 tells, that the rotation angle of the of the electron spin rotation can be varied by varying $k_\parallel$, according to equation (7.86).

8.4 The beam envelope in the 3-photon Kapitza-Dirac effect

Like in chapter 5, the amplitude of the external vector potential is turned on and turned off in a very short time, as compared to the full interaction time of the electron with the laser beam. And like in section 5.3, it is of interest to consider a more realistic time-dependent envelope of the external potential. This section considers the same envelope function (5.4), as in section 5.3.

In order to treat the delay of the Rabi cycle, caused by the lower potential amplitude during the

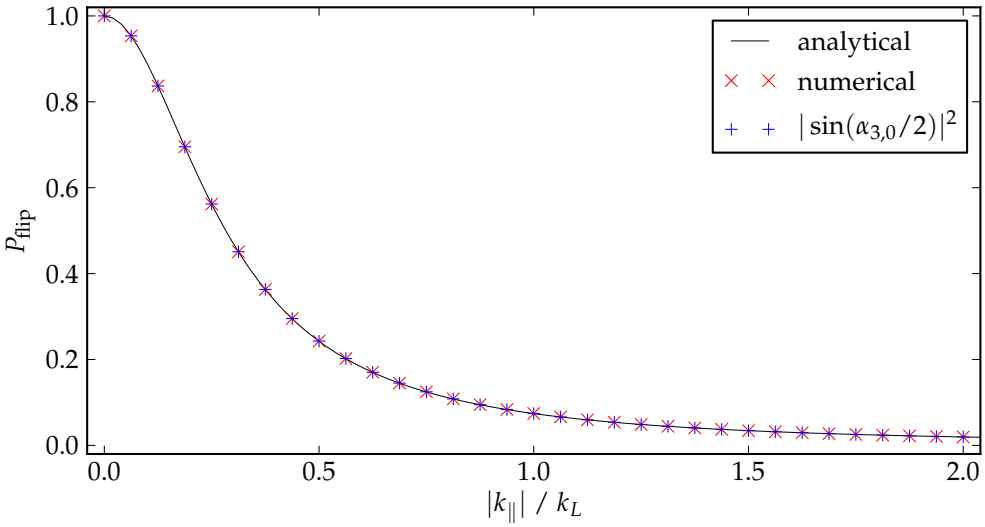

Figure 8.8: This figure shows the spin-flip probability of the diffracted beam for the data of the simulation, which is described in section 8.1 at the interaction time of one half Rabi period π/Ω_R. The only parameter, which is varied, is the electron momentum in laser polarization direction $\hbar k_\parallel$. The solid, analytical line originates from equation (7.91b), the red crosses represent the spin-flip probability from numerical simulation (see also reference [25]) and the blue pluses are the absolute value squared matrix elements (8.6). The angle alpha in (8.6) is the rotation angle of figure 8.11. All three methods for determining the electron spin-flip probability agree well with each other.

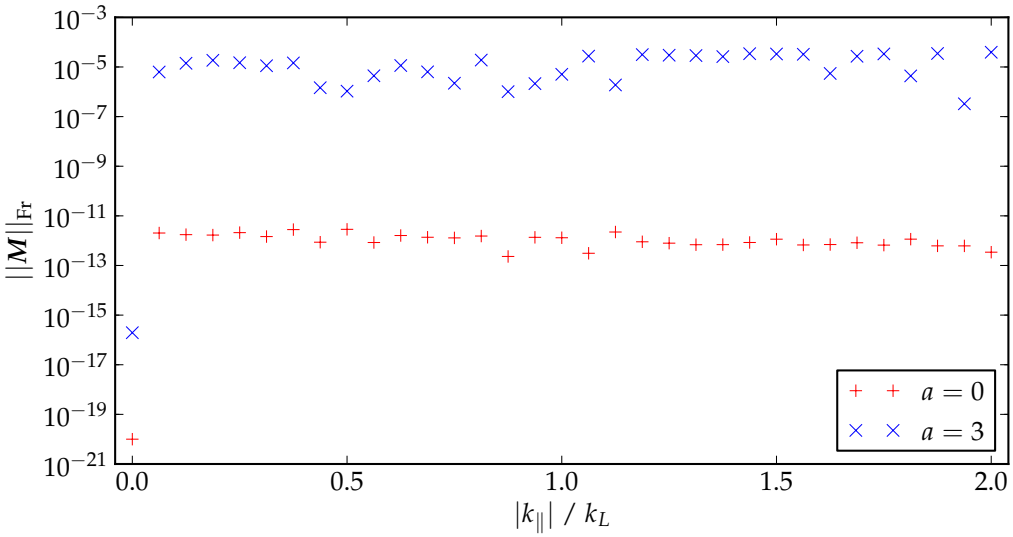

Figure 8.9: This figure shows the same Frobenius norm plot as in figure 8.5, but now for the data set presented in figure 8.8. Similarly to the conclusion of figure 8.5 the parameters P, Φ, α and $\vec{n}$ are approximated well up to 4 or 5 decimal places in the case of the diffracted beam and are determined even more accurately for the undiffracted beam.

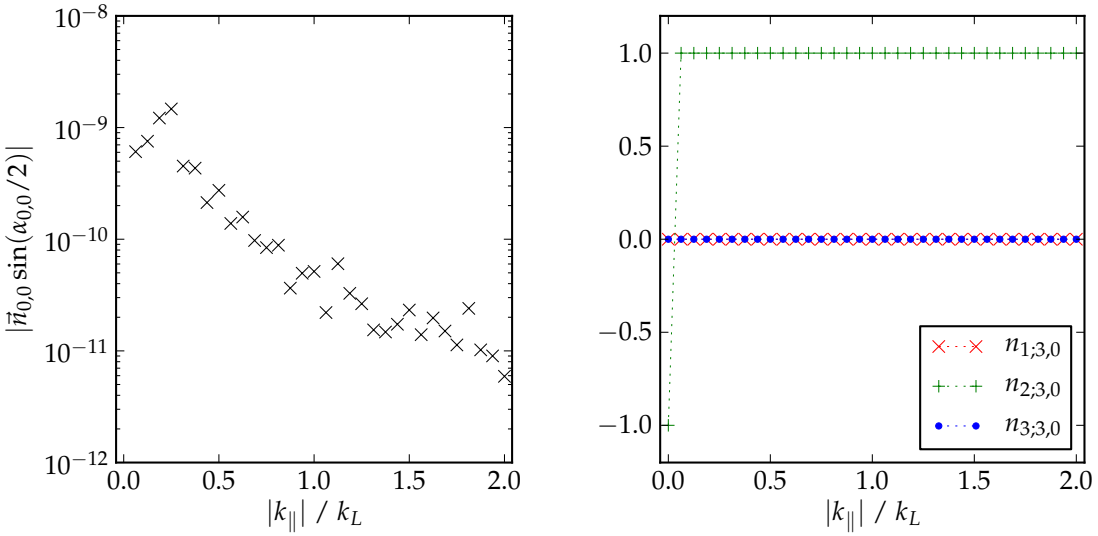

Figure 8.10: (a) *Left figure* This figure shows the same $|\vec{n}_{0,0}\sin(\alpha_{0,0}/2)|$ as in figure 8.6, but for a variation with respect to $k_\parallel$. One similarly concludes, that the spin of the undiffracted beam remains unchanged. (b) *Right figure* This figure shows the same $\vec{n}_{3,0}$ as in figure 8.6(b) but also for a variation with respect to $k_\parallel$. Similarly, the electron spin is rotated around the x_2-direction of the magnetic field of the laser beam.

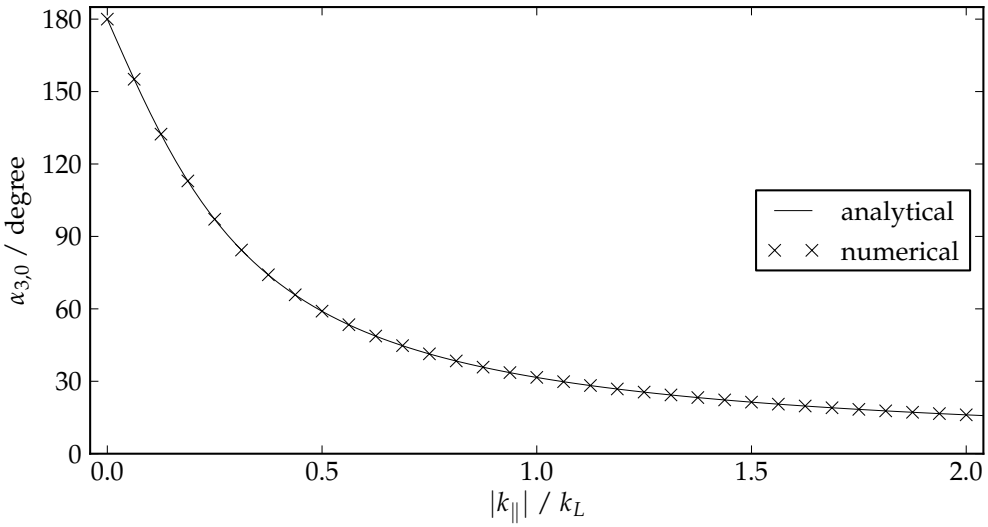

Figure 8.11: This figure shows the $\alpha_{3,0}$ parameter of the $\mathcal{SU}(2)$ ansatz (6.4), which has been determined for the numerical data of figure 8.8. The solid line corresponds to the analytical property (7.86), which has been derived by applying third order, time-dependent perturbation theory at the Dirac equation. The numerical data agrees well with the analytical derivation.

turn on and turn off, the Rabi transition is modeled by the differential equation

$$\dot{c}_0 = \mathrm{i}\frac{\Omega_R(t)}{2}c_3 \tag{8.7a}$$

$$\dot{c}_3 = \mathrm{i}\frac{\Omega_R(t)}{2}c_0\,, \tag{8.7b}$$

similarly to the system of ordinary differential equations (5.5). The Rabi frequency (7.88) of the 3-photon Kapitza-Dirac effect scales with the third power of the potential amplitude, such that one may write

$$\Omega_R(A_3) = \Omega_{R,\max}\frac{(A_3)^3}{(A_{3,\max})^3}\,. \tag{8.8}$$

The Rabi frequency $\Omega_{R,\max}$ is the frequency (7.88) with the maximal field amplitude $A_{3,\max}$. Analogously to section 5.3, the differential equation (8.7) is solved by the solution

$$c_0(t) = \cos(t') \tag{8.9a}$$

$$c_3(t) = \mathrm{i}\sin(t')\,, \tag{8.9b}$$

with the warped time parameter

$$t'(t) = \int_0^t \frac{\Omega_R(\tau)}{2}d\tau\,. \tag{8.10}$$

Like in section 5.3, one may compute this integral and solve the requirement $t'(T) \stackrel{!}{=} \pi/2$ for T, resulting in

$$T = \frac{\pi}{\Omega_{R,\max}}\frac{16}{16-11f}\,. \tag{8.11}$$

Figure 8.12 tests, whether the quantum system undergoes a full Rabi cycle, if the fraction f is varied. For large f the diffraction probability decreases. This may be attributed to the small resonance peak, which is described in the next section. If one compares the Rabi frequencies of the 2-photon Kapitza-Dirac effect with the 3-photon Kapitza-Dirac effect, one obtains

$$\frac{\Omega_{R,3\text{photon}}}{\Omega_{R,2\text{photon}}} = \frac{1}{6\hbar}\frac{e}{m^2c^3}\sqrt{\left(\frac{5}{\sqrt{2}}\vec{A}_0\cdot\hbar\vec{k}\right)^2 + \left(\hbar\vec{k}_L\times\vec{A}_0\right)^2}\,. \tag{8.12}$$

This means, that the Rabi frequency of the 3-photon Kapitza-Dirac effect is a factor $3.8\cdot10^{-4}$ times smaller than the Rabi frequency of the 2-photon Kapitza-Dirac effect, for the chosen parameters of figure 8.12. A high amplitude of the external potential detunes the laser frequency of the resonance peak slightly. If the external potential is detuned during the turn on and turn off, the transition of the 3-photon Kapitza-Dirac effect may not take place to 100%, because there will always be a time, in which the Rabi transition is off-resonant.

8.5 The resonance peak

Within this thesis, the resonance peak is referred to as the property, that the Kapitza-Dirac effect takes place only, if constraint of energy- and momentum conservation (see section 2.2) are fulfilled. If the laser frequency or the electron momentum are not fine tuned to each other no diffraction takes place. Of course, the parameter range for diffraction is not of measure zero, which means that there is a smooth transition between resonant parameters and off-resonant parameters and the diffraction probability smoothly decreases, if the parameters of the laser and the electron smoothly deviate from the resonance condition. It should be mentioned, that these peak properties have already been illustrated by Gush and Gush [31] for the case of the 2-photon Kapitza-Dirac effect.

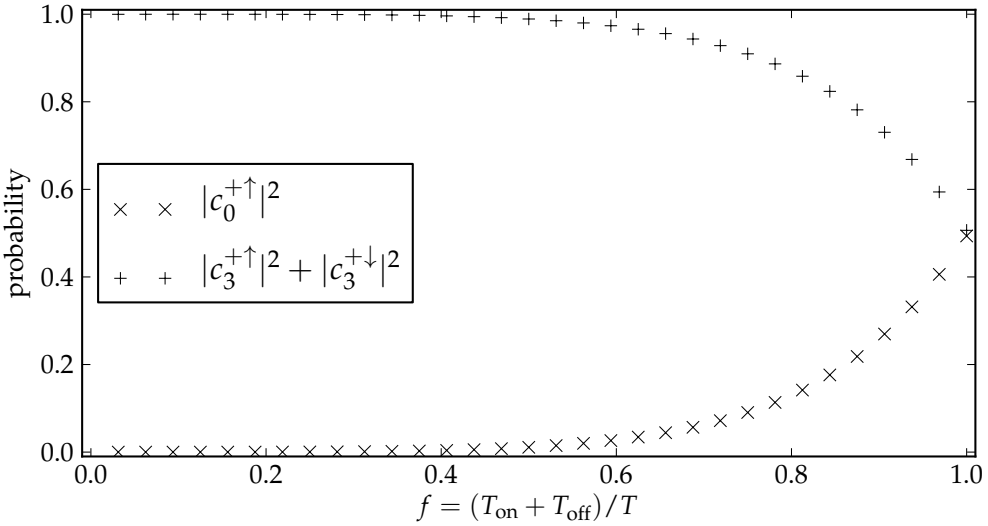

Figure 8.12: This figure shows the final transition probability of the 3-photon Kapitza-Dirac effect, if the fraction $\Delta T = fT$ of the turn on and turn off is varied, according to the envelope function (5.4). All simulation parameters are the same as in figure 8.1. The interaction time is extended by the factor $16/(16 - 11f)$ of equation (8.11), in order to compensate for the lower Rabi transition time. One can see, that the diffraction probability decreases for an increasing fraction of turn on and turn off duration.

The resonance peak can be described by off-resonant Rabi cycles. Therefore, it is worth to exploit the theory of Rabi transitions of a two-level quantum system. The differential equation, which describes Rabi transitions is a more sophisticated version of the differential equation (8.7) and can be found for example in subsection 5.2.1 in the book of Scully and Zubairy [52].

$$\dot{c}_0 = \mathrm{i}\frac{\Omega_R}{2}\mathrm{e}^{-\mathrm{i}\phi+\Delta\omega t}c_3 \tag{8.13a}$$

$$\dot{c}_3 = \mathrm{i}\frac{\Omega_R}{2}\mathrm{e}^{\mathrm{i}\phi-\mathrm{i}\Delta\omega t}c_0\,. \tag{8.13b}$$

This is a simple differential equation of a two level quantum system with detuning $\Delta\omega$, which evolves in Rabi cycles. The analytical solution of equation (8.13) can also be found in [52].

$$c_0(t) = \left\{c_0(0)\left[\cos\left(\frac{\Omega t}{2}\right) - \frac{\mathrm{i}\Delta\omega}{\Omega}\sin\left(\frac{\Omega t}{2}\right)\right] + c_3(0)\mathrm{i}\frac{\Omega_R}{\Omega}\mathrm{e}^{-\mathrm{i}\phi}\sin\left(\frac{\Omega t}{2}\right)\right\}e^{\mathrm{i}\frac{\Delta\omega t}{2}} \tag{8.14a}$$

$$c_3(t) = \left\{c_3(0)\left[\cos\left(\frac{\Omega t}{2}\right) + \frac{\mathrm{i}\Delta\omega}{\Omega}\sin\left(\frac{\Omega t}{2}\right)\right] + c_0(0)\mathrm{i}\frac{\Omega_R}{\Omega}\mathrm{e}^{\mathrm{i}\phi}\sin\left(\frac{\Omega t}{2}\right)\right\}e^{-\mathrm{i}\frac{\Delta\omega t}{2}} \tag{8.14b}$$

The frequency

$$\Omega = \sqrt{\Omega_R^2 + \Delta\omega^2} \tag{8.15}$$

is the oscillation frequency of the off-resonant transition probability and is always larger or equal to the Rabi frequency Ω_R. Similar to the initial condition of figure 8.1, the initial condition $c_0(0) = 1$ and $c_3(0) = 0$ may be inserted in the solution (8.14b), resulting in the time-dependent transition probability

$$|c_3(t)|^2 = \frac{\Omega_R^2}{\Omega^2}\sin^2\left(\frac{\Omega t}{2}\right)\,. \tag{8.16}$$

This equation is not only to be seen as function of the time t, but also implicitly as function of the detuning $\Delta\omega$. The structure of equation (8.16) tells, that the transition probability would be peaked for zero detuning. Figure 8.13 shows a similar peak also for the case of the 3-photon Kapitza-Dirac effect, if the off-resonant frequency peak was adapted by a scaling of the detuning $\Delta\omega$.

$$\Omega = \sqrt{\Omega_R^2 + \frac{\Delta\omega^2}{b^2}} \tag{8.17}$$

If one accounts for the effective peak-broadening parameter $b = 45.7$, which is obtained by a fit to the numerical data, equation (8.16) seems to approximate the resonance peak well. From the variation of the resonance condition (2.17), one also expects a detuning by changing the initial momentum of the electron, which should be related to the energy detuning by

$$|\Delta p_{1,\mathrm{in}}| = \left|\frac{\partial p_{1,\mathrm{in}}}{\partial\omega}\right| \Delta\omega \approx \frac{|n_a + n_e|}{2c}\hbar\Delta\omega = \frac{3}{2c}\hbar\Delta\omega\,. \tag{8.18}$$

Therefore, one would expect the off-resonant frequency

$$\Omega = \sqrt{\Omega_R^2 + \left(\frac{2c\Delta k_1}{3b}\right)^2} \tag{8.19}$$

in dependence of the momentum $\hbar k_1$ of the electron in laser propagation direction. Figure 8.14 verifies this property.

It should be mentioned, that the resonance condition (2.17) yields the momentum $p_1 = 0.344468mc$, which corresponds to $176.022\,\mathrm{keV}/c$, but the position of zero detuning in figure 8.14 has the momentum $p_1 = 0.347017mc$, corresponding to $177.325\,\mathrm{keV}/c$. One may assume, that this detuning originates from the coupling of mode 0 and mode 3 to the neighboring modes. Since the classically expected and the numerically found momenta of the resonance peak differ by $1.303\,\mathrm{keV}/c$, either the initial electron momentum or the laser frequency must be tuned. Otherwise, the diffraction probability would be negligibly small.

8.6 Rabi frequency of the 3-photon Kapitza-Dirac effect

The Rabi frequency Ω_R depends on various parameters of the laser and the electron, according to subsection (7.3.2). Figure 8.15 tests the dependency of Ω_R on the momentum $\hbar k_{\parallel}$ in laser polarization direction of the electron. The Rabi frequency can be measured, by fitting the function

$$\sin^2\left(\frac{\Omega_R T}{2} + \phi\right) \tag{8.20}$$

at the time evolution of the numerical data $|c_3^{+\uparrow}|^2 + |c_3^{+\downarrow}|^2$. One can see, that the numerical data agrees with the analytical model (7.88), of third order time-dependent perturbation theory. There is a small deviation, which can also be found in the plot of the time-dependent dynamics 8.1. This deviation can be attributed to the interactions of the modes 0 and 3 with the neighboring modes.

One may also vary the frequency ck_L or the potential amplitude $|\vec{A}_0|$ of the laser beam, which is shown in figure 8.16 and 8.17. The setups of both figures differ from the setup, which is described in section 8.1. The reason is, that if the interaction parameter and in particular the laser frequency are changed by orders of magnitudes, the quantum dynamics of the 3-photon Kapitza-Dirac effect may interfere with other quantum dynamical effects, for example the 2-photon Kapitza-Dirac effect. Therefore, even though there always exists an analytical short-time propagator from perturbation theory and therewith a Rabi-frequency, there is no guarantee, that a well-formed 3-photon Kapitza-Dirac transition, as it is shown in figure 8.1, takes place in the quantum system. In order to fit at least the short-time time evolution of the diffraction probability, it is useful to start with the mode of the higher

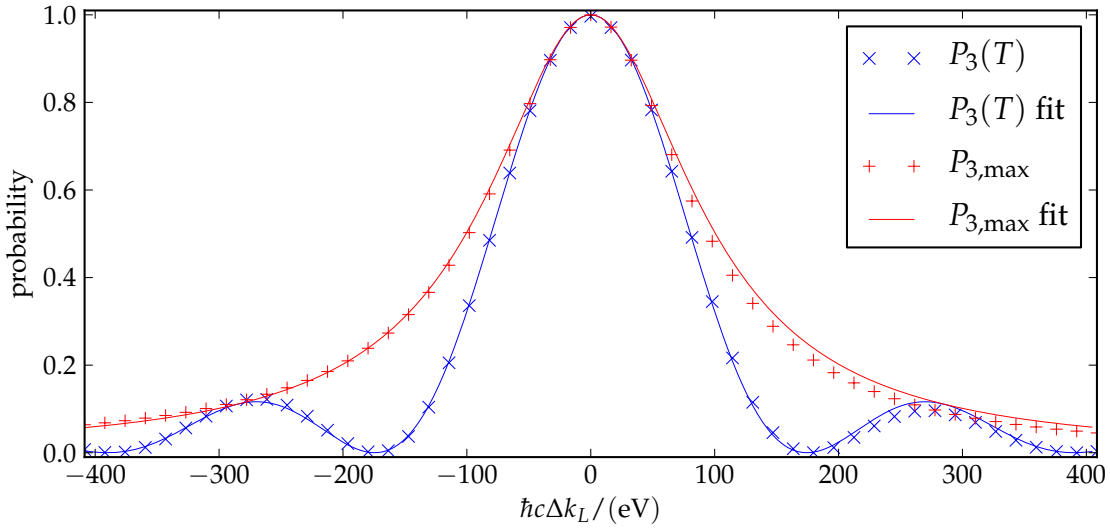

Figure 8.13: This figure shows the diffraction probability $P_3 = |c_3^{\uparrow}|^2 + |c_3^{\downarrow}|^2$, for the setup of section 8.1, but for a variation of the laser frequency ck_L by $c\Delta k_L$. The interaction time T is one half Rabi cycle π/Ω_R. P_3 is fitted at the function (8.16) with off-resonant frequency (8.17) and fit parameter $b = 45.7$. The maximum diffraction probability, independent of interaction time T is also plotted, with the corresponding function (8.16), in which the sine is set to 1.

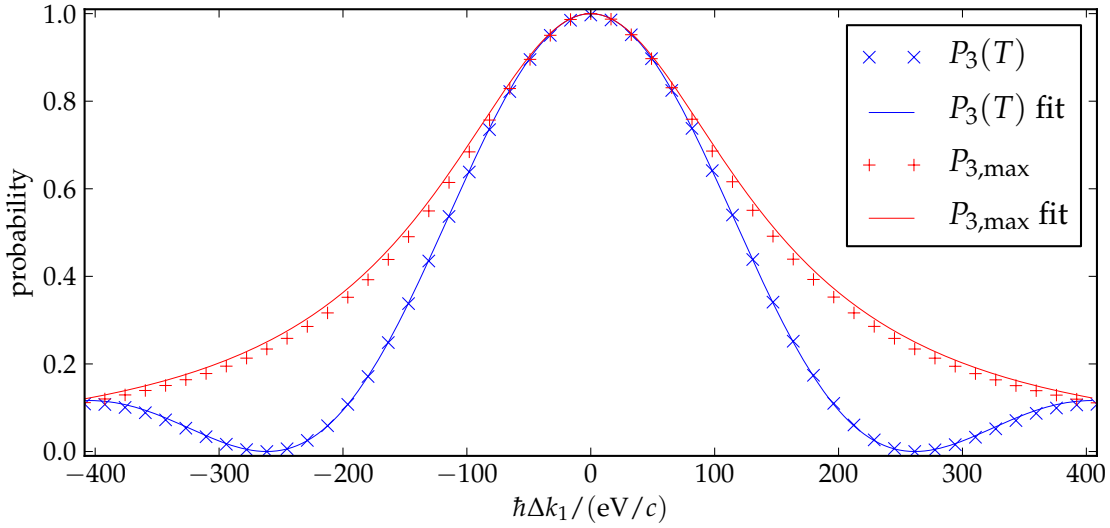

Figure 8.14: This figure shows the same variation of the diffraction probability $P_3 = |c_3^{\uparrow}|^2 + |c_3^{\downarrow}|^2$ as figure 8.13, but this time with respect to the variation of the initial electron momentum $\hbar k_1$ in laser propagation direction. Equation (8.16) also applies for the parameter variation with respect to $\hbar k_1$ in the case of the detuning (8.19) and peak-broadening parameter $b = 45.7$.

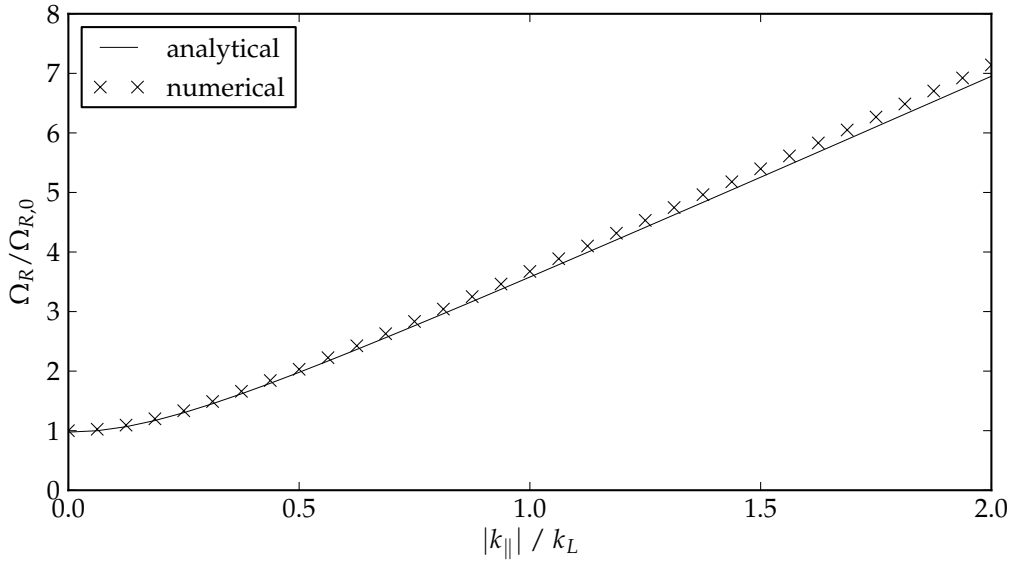

Figure 8.15: This figure shows the Rabi frequency Ω_R of the 3-photon Kapitza-Dirac effect, for the variation of the momentum $\hbar k_\parallel$ in laser polarization direction of the electron. The numerical points are fits of the function (8.20) at the numerical data, presented in figure 8.8. The analytical line originates from equation (7.88) of time-dependent perturbation theory of the Dirac equation. The numerical data is in good agreement with the analytical prediction.

momentum (3-mode) and to evaluate the mode with lower momentum. The Rabi frequency from mode 3 to mode 0 should be the same as from mode 0 to mode 3. Since there might not occur a full Rabi cycle, it might not be possible, to find a resonance peak, as described in section 8.5 and the off-resonant quantum dynamics, described by equation (8.16) is fitted. However, in the case of a very small detuning, the fit parameters Ω_R and Ω are almost degenerate and equation (8.16) is no longer a good fitting function. Therefore, depending on the dynamics, the short time evolution of mode 0 may only be fitted at the fourth order Taylor expansion of equation (8.16) with respect to t

$$\frac{\Omega_R^2}{4}t^2 - \frac{1}{3}\frac{\Omega_R^2}{4}\frac{\Omega^2}{4}t^4 + \mathcal{O}(t^5)\,. \tag{8.21}$$

The turn-on and turn-off time of the external potential is zero in the case of the figures 8.16 and 8.17. This is reasoned by the amplitude of the external potential, which is much lower that the one in figure 8.1. Therefore, the approximation of the quantum dynamics with an infinite short turn-on and turn-off does not affect the diffraction probability very much. Since there is no turn on and no turn off time, the ϕ-offset in the time argument is omitted in the fitting functions, which are used for the figures 8.16 and 8.17.

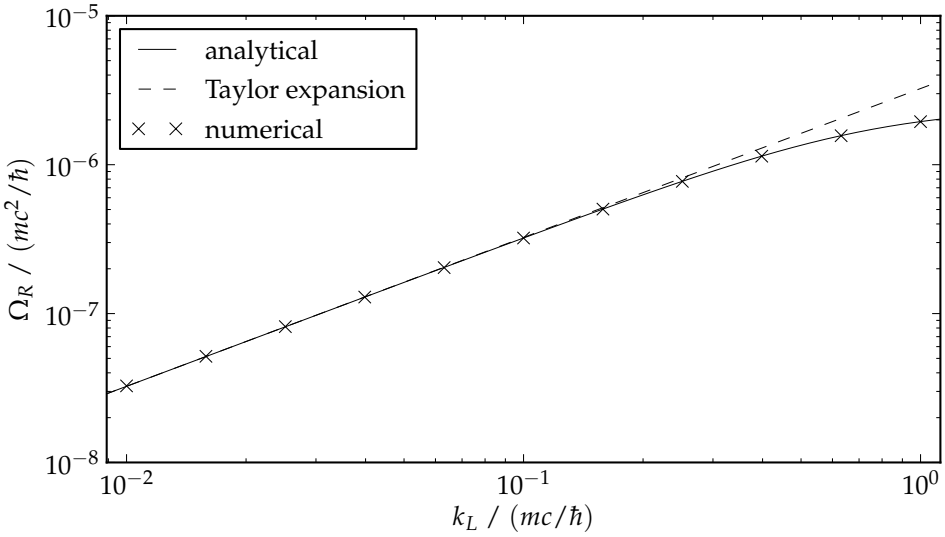

Figure 8.16: This figure shows the Rabi frequency of the 3-photon Kapitza-Dirac effect for an electron, which moves collinear to the laser propagation direction. The amplitude of the external potential is $A_2 = 0$ and $A_3 = 0.5\,mc^2/\sqrt{\hbar c}$. The final electron momentum in laser propagation direction is given by equation (2.17). The analytical curve is from the evaluation of $\boldsymbol{U}_{0,3}$ in equation (7.81), whereas the dashed line originates from the Taylor expansion of the propagator (7.82). The crosses of the fits of the numerical time-evolution data agree well with the analytical curve.

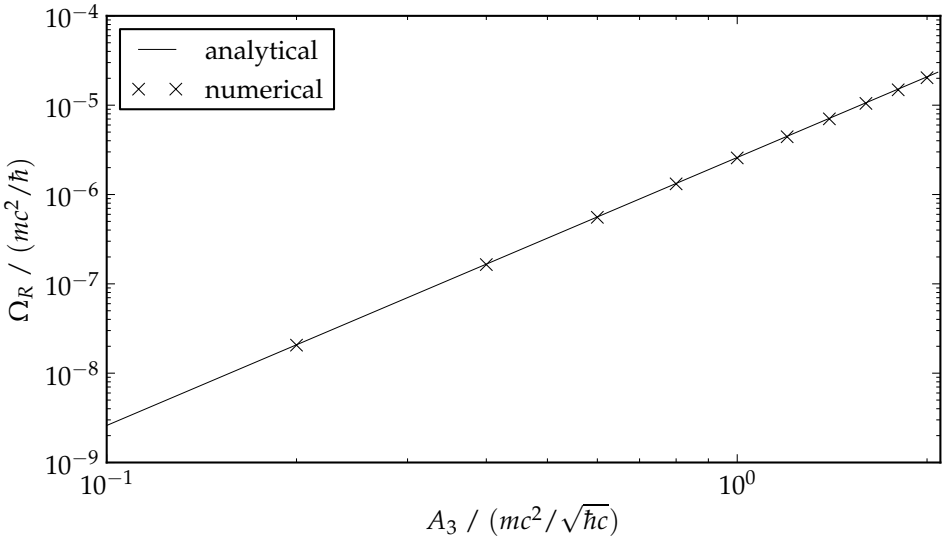

Figure 8.17: This figure shows the same, as figure 8.16, but this time for a variation of the potential amplitude A_3 of the external laser field. The laser wave number is $0.1mc/\hbar$, which corresponds to a photon energy of 51.1 keV or a laser wave length of 24.3 pm. The solid line is the Rabi frequency Ω_R of equation (7.88) and it agrees well with the crosses of the fits of the numerical time-evolution data.

Chapter 9

Conclusions and Outlook

9.1 Conclusions

The main result of this thesis is the discovery and characterization of a Kapitza-Dirac effect, in which a diffracted electron interacts with 3 laser photons. A special feature of this 3-photon Kapitza-Dirac effect is the influence of the diffraction process on the electron spin.

The 3-photon Kapitza-Dirac effect only appears, if the initial electron momentum and the frequency of the standing light wave are tuned with respect to each other. This resonance condition originates from conservation of energy and momentum of the combined system of the electron and the laser photons it interacts with. Section 2.2 provides a graphical interpretation of this energy- and momentum conservation, which allows a more intuitive understanding of the scaling of the resonance condition. One can infer from this resonance condition, that there is no non-relativistic limit for the 3-photon Kapitza-Dirac effect, which demands for a relativistic description of the effect. Even the resonance condition from the relativistic energy-momentum relation itself differs from the resonance condition from the non-relativistic energy-momentum relation in the case of the 3-photon Kapitza-Dirac effect.

The quantum dynamics in this thesis is described by the Schrödinger equation, the Pauli equation, the Klein-Gordon equation, and the Dirac equation which are introduced in chapter 3. All four quantum wave equations are transformed into momentum space in chapter 4. Chapter 4 thereby makes use of the bi-scalar and bi-spinor matrix contractions of the appendices A and B. The quantum dynamics of the Kapitza-Dirac effect is solved numerically in the chapters 5 and 8. The quantum dynamics of the 2-photon Kapitza-Dirac effect is verified in chapter 5 with the numerical solution of the quantum wave equations in momentum space. The quantum dynamics of the 3-photon Kapitza-Dirac effect is elaborately discussed in section 8. The numeric solution is able to prove that a full Rabi cycle of the diffraction probability takes place for the 3-photon Kapitza-Dirac effect, and shows that the quantum dynamics features an in-field interaction of the electron with many neighboring modes in momentum space. A full Rabi transition is possible, even for a sine-shaped time-dependent envelope of the laser amplitude, in the case of the 2-photon Kapitza-Dirac effect. In the case of the 3-photon Kapitza-Dirac effect, the diffraction probability decreases to 50% for a sine-shaped laser envelope.

A short time solution of the 3-photon Kapitza-Dirac effect is also provided in chapter 7 by applying time-dependent perturbation theory to the full Pauli equation (section 7.2) and the full Dirac equation (section 7.3). The derivation of the perturbative solution of the Dirac equation thereby takes advantage of the matrix notation of the bi-spinor matrix contractions in appendix B. A low laser frequency solution is obtained by a Taylor expansion of the perturbative solution. The perturbative solutions of the Pauli equation and the Dirac equation differ from each other even for the low frequency limit. This discrepancy is reasoned by the inapplicability of Pauli theory in the case of the always relativistic parameters of the 3-photon Kapitza-Dirac effect. The solution of time-dependent perturbation theory allows for the analytical derivation of the Rabi frequency, the spin-flip probability, and also the parameters of the $\mathcal{SU}(2)$-rotation of the electron spin. These analytical parameters of the 3-photon

Kapitza-Dirac effect are verified by the numerical solution of the Dirac equation in section 8. The Rabi frequency of the 3-photon Kapitza-Dirac effect is, in contrast to the 2-photon Kapitza-Dirac effect, low and demands for high laser field strengths, which in turn require a relativistic description of the effect.

Even though high laser intensities and short wavelengths in the X-ray regime are required for an experimental realization, a detection of the 3-photon Kapitza-Dirac appears feasible in the near future. Reference [25] discusses the implementation of such an experiment at the European X-ray free electron laser facility.

A special property of the 3-photon Kapitza-Dirac effect is the rotation of the electron spin, when the electron is diffracted. The rotation angle of the electron spin depends on the electron momentum in laser propagation direction. This property opens the possibility to tune the spin-flip probability of the diffracted electron. The spin properties of the electron and the diffraction pattern are inferred from the propagator of the electron wave function. It is important to mention, that only the diffraction probability of the electron varies in time, whereas the spin properties and, in particular, the spin-flip probability of the diffracted electron are time-independent.

The theoretical framework and the concepts which are introduced in this thesis open a precise understanding of the 3-photon Kapitza-Dirac effect and its spin properties. The methods presented can be generalized to n-photon Kapitza-Dirac effects.

9.2 Outlook

This work considers the standard field configuration of the Kapitza-Dirac effect with two counter-propagating linearly polarized laser beams of equal laser frequency. This standard scenario may be modified and extended towards more general geometries such as unequal laser frequencies and different laser polarizations. In this way the understanding of the effect could be deepened further.

The whole setup of the 3-photon Kapitza-Dirac effect may be Lorentz transformed into a frame, in which the absolute value of the incoming electron momentum equals the outgoing one. In this frame the two counter-propagating laser fields have unequal frequencies. As a consequence, according to the graphical considerations in section 2.2, the initial and final electron momentum and the laser frequency can be reduced at the same time for this configuration. This means that the 3-photon Kapitza-Dirac effect in a two color laser field has a non-relativistic limit in this inertial frame. This opens the possibility to compare the quantum dynamics of the Pauli equation and the dynamics of the Dirac equation in the non-relativistic limit, which would be an important consistency check for the theory of Kapitza-Dirac scattering.

The investigation of the Kapitza-Dirac effect is based on two counter-propagating laser beams with equal linear polarization in this thesis. One may study the quantum dynamics of the Kapitza-Dirac effect also for different light polarizations. It is possible that the quantum dynamics is completely different from that of linearly polarized light and therefore new effects are expected.

The change of the electron spin is of essential interest because the 3-photon Kapitza-Dirac effect explicitly demonstrates a change of the electron spin in the laser polarization direction, while the laser photons only carry an angular momentum in their propagation direction. An intuitive description of the angular momentum transfer from the laser photons to the electrons would be highly desirable, in particular for various laser polarizations.

Appendix A

Bi-scalar matrix relations

The contraction of the identity matrix with the bi-scalar matrices (3.25) yields

$$\begin{aligned}\boldsymbol{u}^{\mathrm{KG}}(\vec{k})\boldsymbol{u}^{\mathrm{KG}}(\vec{k}')^{\dagger} &= \left(d_{+}^{\mathrm{KG}}(\vec{k})\mathbf{1} + d_{-}^{\mathrm{KG}}(\vec{k})\sigma_1\right)\left(d_{+}^{\mathrm{KG}}(\vec{k}')\mathbf{1} + d_{-}^{\mathrm{KG}}(\vec{k}')\sigma_1\right) \\ &= \left(d_{+}^{\mathrm{KG}}(\vec{k})d_{+}^{\mathrm{KG}}(\vec{k}') + d_{-}^{\mathrm{KG}}(\vec{k})d_{-}^{\mathrm{KG}}(\vec{k}')\right)\mathbf{1} + \left(d_{+}^{\mathrm{KG}}(\vec{k})d_{-}^{\mathrm{KG}}(\vec{k}') + d_{-}^{\mathrm{KG}}(\vec{k})d_{+}^{\mathrm{KG}}(\vec{k}')\right)\sigma_1 \\ &= t^{\mathrm{KG}}(\vec{k},\vec{k}')\mathbf{1} + s^{\mathrm{KG}}(\vec{k},\vec{k}')\sigma_1\,. \end{aligned} \tag{A.1}$$

The contraction of the σ_1 matrix yields

$$\boldsymbol{u}^{\mathrm{KG}}(\vec{k})\sigma_1\boldsymbol{u}^{\mathrm{KG}}(\vec{k}')^{\dagger} = \boldsymbol{u}^{\mathrm{KG}}(\vec{k})\boldsymbol{u}^{\mathrm{KG}}(\vec{k}')^{\dagger}\sigma_1 = \left(t^{\mathrm{KG}}(\vec{k},\vec{k}')\mathbf{1} + s^{\mathrm{KG}}(\vec{k},\vec{k}')\sigma_1\right)\sigma_1 = s^{\mathrm{KG}}(\vec{k},\vec{k}')\mathbf{1} + t^{\mathrm{KG}}(\vec{k},\vec{k}')\sigma_1\,. \tag{A.2}$$

The contraction of the σ_3 matrix yields

$$\begin{aligned}\boldsymbol{u}^{\mathrm{KG}}(\vec{k})\sigma_3\boldsymbol{u}^{\mathrm{KG}}(\vec{k}')^{\dagger} &= \sigma_3\left(d_{+}^{\mathrm{KG}}(\vec{k})\mathbf{1} - d_{-}^{\mathrm{KG}}(\vec{k})\sigma_1\right)\left(d_{+}^{\mathrm{KG}}(\vec{k}')\mathbf{1} + d_{-}^{\mathrm{KG}}(\vec{k}')\sigma_1\right) \\ &= \left(d_{+}^{\mathrm{KG}}(\vec{k})d_{+}^{\mathrm{KG}}(\vec{k}') - d_{-}^{\mathrm{KG}}(\vec{k})d_{-}^{\mathrm{KG}}(\vec{k}')\right)\sigma_3 + \left(d_{+}^{\mathrm{KG}}(\vec{k})d_{-}^{\mathrm{KG}}(\vec{k}') - d_{-}^{\mathrm{KG}}(\vec{k})d_{+}^{\mathrm{KG}}(\vec{k}')\right)\mathrm{i}\sigma_2 \\ &= f^{\mathrm{KG}}(\vec{k},\vec{k}')\sigma_3 + r^{\mathrm{KG}}(\vec{k},\vec{k}')\mathrm{i}\sigma_2\,. \end{aligned} \tag{A.3}$$

If $\vec{k}$ equals $\vec{k}'$, the functions $t^{\mathrm{KG}}, s^{\mathrm{KG}}, f^{\mathrm{KG}}$ and r^{KG} of equation (4.43) simplify to

$$t^{\mathrm{KG}}(\vec{k},\vec{k}) = d_{+}^{\mathrm{KG}}(\vec{k})^2 + d_{-}^{\mathrm{KG}}(\vec{k})^2 = \frac{\left(mc^2 + E(\vec{k})\right)^2 + \left(mc^2 - E(\vec{k})\right)^2}{4E(\vec{k})mc^2} = \frac{(mc^2)^2 + E(\vec{k})^2}{2E(\vec{k})mc^2} \tag{A.4a}$$

$$s^{\mathrm{KG}}(\vec{k},\vec{k}) = 2d_{+}^{\mathrm{KG}}(\vec{k})d_{-}^{\mathrm{KG}}(\vec{k}) = \frac{\left(mc^2 + E(\vec{k})\right)\left(mc^2 - E(\vec{k})\right)}{2E(\vec{k})mc^2} = \frac{(mc^2)^2 - E(\vec{k})^2}{2E(\vec{k})mc^2} = -\frac{c^2\vec{p}^2}{2E(\vec{k})mc^2} \tag{A.4b}$$

$$f^{\mathrm{KG}}(\vec{k},\vec{k}) = d_{+}^{\mathrm{KG}}(\vec{k})^2 - d_{-}^{\mathrm{KG}}(\vec{k})^2 = \frac{\left(mc^2 + E(\vec{k})\right)^2 - \left(mc^2 - E(\vec{k})\right)^2}{4E(\vec{k})mc^2} = \frac{4mc^2E(\vec{k}}{4E(\vec{k})mc^2} = 1 \tag{A.4c}$$

$$r^{\mathrm{KG}}(\vec{k},\vec{k}) = 0\,. \tag{A.4d}$$

Therefore, the contraction of σ_3 in equation (A.3) turns into the property of $u^{\mathrm{KG},\sigma}(\vec{k})$ beeing pseudo orthonormal

$$\boldsymbol{u}(\vec{k})\sigma_3\boldsymbol{u}(\vec{k})^{\dagger} = \sigma_3\,. \tag{A.5}$$

Furthermore, the pseudo-orthonormal contracted free Hamiltonian turns into the relativistic energy-momentum relation. This can be seen by expanding the pseudo-orthonormal contracted free Klein-Gordon Hamiltonian (3.18) into

$$\begin{aligned}\boldsymbol{u}^{\mathrm{KG}}(\vec{k})\sigma_3\boldsymbol{H}_0(\vec{k})\boldsymbol{u}^{\mathrm{KG}}(\vec{k})^\dagger &= \boldsymbol{u}^{\mathrm{KG}}(\vec{k})\sigma_3\left((\sigma_3+\mathrm{i}\sigma_2)\frac{\vec{p}^2}{2m}+\sigma_3 mc^2\right)\boldsymbol{u}^{\mathrm{KG}}(\vec{k})^\dagger \\ &= \boldsymbol{u}^{\mathrm{KG}}(\vec{k})\left(\mathbf{1}\frac{\vec{p}^2+2m^2c^2}{2m}+\sigma_1\frac{\vec{p}^2}{2m}\right)\boldsymbol{u}^{\mathrm{KG}}(\vec{k})^\dagger \\ &= \left(t^{\mathrm{KG}}(\vec{k},\vec{k})\frac{\vec{p}^2+2m^2c^2}{2m}+s^{\mathrm{KG}}(\vec{k},\vec{k})\frac{\vec{p}^2}{2m}\right)\mathbf{1} \\ &\quad+\left(s^{\mathrm{KG}}(\vec{k},\vec{k})\frac{\vec{p}^2+2m^2c^2}{2m}+t^{\mathrm{KG}}(\vec{k},\vec{k})\frac{\vec{p}^2}{2m}\right)\sigma_1\,.\end{aligned} \tag{A.6}$$

The prefactors of the $\mathbf{1}$ matrix simplify into the relativistic energy-momentum relation

$$\begin{aligned}t^{\mathrm{KG}}(\vec{k},\vec{k})\frac{\vec{p}^2+2m^2c^2}{2m}+s^{\mathrm{KG}}(\vec{k},\vec{k})\frac{\vec{p}^2}{2m} &= \frac{\left((mc^2)^2+E(\vec{k})^2\right)\left(\vec{p}^2+2m^2c^2\right)+\left((mc^2)^2-E(\vec{k})^2\right)\vec{p}^2}{4E(\vec{k})m^2c^2} \\ &= \frac{2(mc^2)^2\vec{p}^2+\left((mc^2)^2+E(\vec{k})^2\right)2(mc^2)^2}{4E(\vec{k})(mc^2)^2} = \frac{2(mc^2)^2\left(2c^2\vec{p}^2+2(mc^2)^2+2E(\vec{k})^2\right)}{4E(\vec{k})(mc^2)^2} \\ &= \frac{4(mc^2)^2E(\vec{k})^2}{4E(\vec{k})(mc^2)^2} = E(\vec{k})\end{aligned} \tag{A.7}$$

and the prefactor of the σ_1 matrix vanishes.

$$\begin{aligned}s^{\mathrm{KG}}(\vec{k},\vec{k})\frac{\vec{p}^2+2m^2c^2}{2m}+t^{\mathrm{KG}}(\vec{k},\vec{k})\frac{\vec{p}^2}{2m} &= \frac{-c^2\vec{p}^2\left(\vec{p}^2+2m^2c^2\right)+\left((mc^2)^2+E(\vec{k})^2\right)\vec{p}^2}{4E(\vec{k})m^2c^2} \\ &= \frac{-\vec{p}^2\left(c^2\vec{p}^2+2(mc^2)^2\right)+\left(2(mc^2)^2+c^2\vec{p}^2\right)\vec{p}^2}{4E(\vec{k})m^2c^2} = 0\end{aligned} \tag{A.8}$$

Taking together both results (A.7) and (A.8) yields

$$\boldsymbol{u}^{\mathrm{KG}}(\vec{k})\sigma_3\boldsymbol{H}_0(\vec{k})\boldsymbol{u}^{\mathrm{KG}}(\vec{k})^\dagger = E(\vec{k})\mathbf{1}\,, \tag{A.9}$$

for equation (A.6).

Appendix B

Bi-spinor matrix relations

B.1 Calculation of bi-spinor contractions

The calculations in this subsection make use of the commutation relations (3.28) of the Dirac matrices. The product of two spinor matrices $\boldsymbol{u}(\vec{k})\boldsymbol{u}(\vec{k}')^\dagger$ in equation (4.60a) may be expanded to:

$$\begin{aligned}
\boldsymbol{u}(\vec{k})\boldsymbol{u}(\vec{k}')^\dagger &= \sum_{l,q} \left(d_+(\vec{k})\mathbf{1} + k_l d_-(\vec{k})\boldsymbol{\beta}\boldsymbol{\alpha}_l \right) \cdot \left(d_+(\vec{k}')\mathbf{1} + k'_q d_-(\vec{k}')\boldsymbol{\alpha}_q\boldsymbol{\beta} \right) \\
&= \left(d_+(\vec{k})d_+(\vec{k}') + \vec{k}\cdot\vec{k}'\, d_-(\vec{k})d_-(\vec{k}') \right)\mathbf{1} \\
&\quad + \sum_l \left(k_l d_-(\vec{k})d_+(\vec{k}') - k'_l d_+(\vec{k})d_-(\vec{k}') \right)\boldsymbol{\beta}\boldsymbol{\alpha}_l \\
&\quad + \sum_{l\neq q} k_l k'_q d_-(\vec{k})d_-(\vec{k}')\boldsymbol{\alpha}_l\boldsymbol{\alpha}_q \\
&= \left(d_+(\vec{k})d_+(\vec{k}') + \vec{k}\cdot\vec{k}'\, d_-(\vec{k})d_-(\vec{k}') \right)\mathbf{1} \\
&\quad + \sum_l \left(k_l d_-(\vec{k})d_+(\vec{k}') - k'_l d_+(\vec{k})d_-(\vec{k}') \right)\boldsymbol{\beta}\boldsymbol{\alpha}_l \\
&\quad + \sum_{\substack{1\le l<q \\ l<q\le 3}} \left(k_l k'_q - k_q k'_l \right) d_-(\vec{k})d_-(\vec{k}')\boldsymbol{\alpha}_l\boldsymbol{\alpha}_q \\
&= t(\vec{k},\vec{k}')\mathbf{1} + \sum_l r^l(\vec{k},\vec{k}')\boldsymbol{\beta}\boldsymbol{\alpha}_l + \sum_{\substack{1\le l<q \\ l<q\le 3}} g^{lq}(\vec{k},\vec{k}')\boldsymbol{\alpha}_l\boldsymbol{\alpha}_q \,.
\end{aligned} \tag{B.1}$$

The contraction of $\boldsymbol{\beta}$, namly $\boldsymbol{u}(\vec{k})\boldsymbol{\beta}\boldsymbol{u}(\vec{k}')^\dagger$ of equation (4.60b) can be split up into three terms. Note, that the parameters of the left and right spinor matrix have the same parameter $\vec{k}$, because different parameters are not required.

$$\begin{aligned}
\boldsymbol{u}(\vec{k})\boldsymbol{\beta}\boldsymbol{u}(\vec{k})^\dagger &= \sum_{l,q} \left(d_+(\vec{k})\mathbf{1} + k_l d_-(\vec{k})\boldsymbol{\beta}\boldsymbol{\alpha}_l \right) \boldsymbol{\beta} \left(d_+(\vec{k})\mathbf{1} + k_q d_-(\vec{k})\boldsymbol{\alpha}_q\boldsymbol{\beta} \right) \\
&= d_+(\vec{k})^2\boldsymbol{\beta} && \text{(B.2a)} \\
&\quad + \sum_{l,q} k_l d_+(\vec{k})d_-(\vec{k})\boldsymbol{\beta}\boldsymbol{\alpha}_l\boldsymbol{\beta} + k_q d_+(\vec{k})d_-(\vec{k})\boldsymbol{\beta}\boldsymbol{\alpha}_q\boldsymbol{\beta} && \text{(B.2b)} \\
&\quad + \sum_{l,q} k_l k_q d_-(\vec{k})d_-(\vec{k})\boldsymbol{\beta}\boldsymbol{\alpha}_l\boldsymbol{\beta}\boldsymbol{\alpha}_q\boldsymbol{\beta} && \text{(B.2c)}
\end{aligned}$$

The second term (B.2b) can be simplified by using $\boldsymbol{\beta}\boldsymbol{\alpha}_l\boldsymbol{\beta} = -\boldsymbol{\beta}\boldsymbol{\beta}\boldsymbol{\alpha}_l = -\boldsymbol{\alpha}_l$ and noticing that the sum over the indices q and l yields the same term twice. The third term (B.2c) is a doubled sum consisting of

$3 \times 3 = 9$ terms. The three terms with equal index $l = q$ can be simplified by $\boldsymbol{\beta}\boldsymbol{\alpha}_q\boldsymbol{\beta}\boldsymbol{\alpha}_q\boldsymbol{\beta} = -\boldsymbol{\beta}\boldsymbol{\beta}\boldsymbol{\alpha}_q\boldsymbol{\alpha}_q\boldsymbol{\beta} = -\boldsymbol{\beta}$ and summed up, yielding $-\vec{k}^2 d_-(\vec{k})^2\boldsymbol{\beta}$. The six terms with unequal indices $l \neq q$ are a sum over anti-symmetric matrices $\boldsymbol{\beta}\boldsymbol{\alpha}_l\boldsymbol{\beta}\boldsymbol{\alpha}_q\boldsymbol{\beta} = -\boldsymbol{\beta}\boldsymbol{\alpha}_q\boldsymbol{\beta}\boldsymbol{\alpha}_l\boldsymbol{\beta}$ multiplied with symmetric factors $k_l k_q$. Therefore, these six terms vanish and the sum of (B.2a) and (B.2c) yields

$$\left(d_+(\vec{k})^2 - \vec{k}^2 d_-(\vec{k})^2\right)\boldsymbol{\beta} = \frac{mc^2}{E(\vec{k})}\boldsymbol{\beta}\,. \tag{B.3}$$

Therefore, the matrix (B.2) can be rewritten into

$$\boldsymbol{u}(\vec{k})\boldsymbol{\beta}\boldsymbol{u}(\vec{k})^\dagger = \frac{mc^2}{E(\vec{k})}\boldsymbol{\beta} - \frac{c\hbar k_l}{E(\vec{k})}\boldsymbol{\alpha}_l\,. \tag{B.4}$$

The contraction of $\boldsymbol{\alpha}_l$, namly $\boldsymbol{u}(\vec{k})\boldsymbol{\alpha}_l\boldsymbol{u}(\vec{k}')^\dagger$ of equation (4.60c) splits up into three terms too.

$$\begin{aligned}
\boldsymbol{u}(\vec{k})\boldsymbol{\alpha}_l\boldsymbol{u}(\vec{k}')^\dagger &= \sum_{q,j}\left(d_+(\vec{k})\mathbf{1} + k_q d_-(\vec{k})\boldsymbol{\beta}\boldsymbol{\alpha}_q\right)\boldsymbol{\alpha}_l\left(d_+(\vec{k}')\mathbf{1} + k'_j d_-(\vec{k}')\boldsymbol{\alpha}_j\boldsymbol{\beta}\right) \\
&= d_+(\vec{k})d_+(\vec{k}')\boldsymbol{\alpha}_l && \text{(B.5a)} \\
&+ \sum_{q,j} k_q d_-(\vec{k})d_+(\vec{k}')\boldsymbol{\beta}\boldsymbol{\alpha}_q\boldsymbol{\alpha}_l + k'_j d_+(\vec{k})d_-(\vec{k}')\boldsymbol{\alpha}_l\boldsymbol{\alpha}_j\boldsymbol{\beta} && \text{(B.5b)} \\
&+ \sum_{q,j} k_q k'_j d_-(\vec{k})d_-(\vec{k}')\boldsymbol{\beta}\boldsymbol{\alpha}_q\boldsymbol{\alpha}_l\boldsymbol{\alpha}_j\boldsymbol{\beta} && \text{(B.5c)}
\end{aligned}$$

The line (B.5b) consists of a sum of six different terms. In the case of equal indices $q = l$ and $j = l$ of the $\boldsymbol{\alpha}$ matrices, line (B.5b) simplifies to

$$k_q d_-(\vec{k})d_+(\vec{k}')\boldsymbol{\beta} + k'_j d_+(\vec{k})d_-(\vec{k}')\boldsymbol{\beta} = s^l(\vec{k},\vec{k}')\boldsymbol{\beta}\,. \tag{B.6}$$

If the indices of the $\boldsymbol{\alpha}$ matricies in the sum are not equal ($q \neq l$ and $j \neq l$), they need to be commuted, resulting in another minus sign.

$$\sum_{\substack{q\neq l\\ j\neq l}} k_q d_-(\vec{k})d_+(\vec{k}')\boldsymbol{\beta}\boldsymbol{\alpha}_q\boldsymbol{\alpha}_l + k'_j d_+(\vec{k})d_-(\vec{k}')\boldsymbol{\alpha}_l\boldsymbol{\alpha}_j\boldsymbol{\beta} = \sum_{q\neq l} k_q d_-(\vec{k})d_+(\vec{k}')\boldsymbol{\beta}\boldsymbol{\alpha}_q\boldsymbol{\alpha}_l - k'_q d_+(\vec{k})d_-(\vec{k}')\boldsymbol{\beta}\boldsymbol{\alpha}_q\boldsymbol{\alpha}_l \tag{B.7}$$

Therefore, line (B.5b) can be reformulated into

$$\sum_{q,j} k_q d_-(\vec{k})d_+(\vec{k}')\boldsymbol{\beta}\boldsymbol{\alpha}_q\boldsymbol{\alpha}_l + k'_j d_+(\vec{k})d_-(\vec{k}')\boldsymbol{\alpha}_l\boldsymbol{\alpha}_j\boldsymbol{\beta} = s^l(\vec{k},\vec{k}')\boldsymbol{\beta} + \sum_{q\neq l} r^q(\vec{k},\vec{k}')\boldsymbol{\beta}\boldsymbol{\alpha}_q\boldsymbol{\alpha}_l\,. \tag{B.8}$$

Line (B.5c) consists of a doubled sum containing $3 \times 3 = 9$ terms. In contrast to (B.2) the calculation depends additionally one the index l of the $\boldsymbol{\alpha}_l$ matrix. Therefore the nine terms in (B.5b) can be divided in

- one term consisting of three identical $\boldsymbol{\alpha}$ matricies ($q = l = j$),
- two terms for which the indices of $\vec{k}$ and $\vec{k}'$ are the same but not equal to the contracted $\boldsymbol{\alpha}_l$ ($q = j \neq l$),
- four terms for which $\vec{k}$ or $\vec{k}'$ have the same index of the contracted $\boldsymbol{\alpha}_l$, but not the same index as the other $\vec{k}'$ or $\vec{k}$ ($q \neq l = j$ or $q = l \neq j$),
- and two terms in which all three $\boldsymbol{\alpha}$ have different indices ($q \neq l \neq j$,$q \neq j$) .

If all three $\boldsymbol{\alpha}$ are the same ($q = l = j$), the matricies in line (B.5c) simplify to $\boldsymbol{\beta\alpha}_l\boldsymbol{\alpha}_l\boldsymbol{\alpha}_l\boldsymbol{\beta} = \boldsymbol{\beta\alpha}_l\boldsymbol{\beta} = -\boldsymbol{\beta\beta\alpha}_l = -\boldsymbol{\alpha}_l$, yielding

$$- k_l k'_l d_-(\vec{k}) d_-(\vec{k}')\boldsymbol{\alpha}_l \,. \tag{B.9}$$

In the case ($q = j \neq l$) there is another minus sign from the commutation of alphas $\boldsymbol{\beta\alpha}_q\boldsymbol{\alpha}_l\boldsymbol{\alpha}_q\boldsymbol{\beta} = -\boldsymbol{\beta\beta\alpha}_q\boldsymbol{\alpha}_l\boldsymbol{\alpha}_q = \boldsymbol{\alpha}_q\boldsymbol{\alpha}_q\boldsymbol{\alpha}_l = \boldsymbol{\alpha}_l$, resulting in the expression

$$\sum_{q\neq l} k_q k'_q d_-(\vec{k}) d_-(\vec{k}')\boldsymbol{\alpha}_l \tag{B.10}$$

for line (B.5c). If the indices are ($q \neq l = j$ or $q = l \neq j$) the matrices turn into $\boldsymbol{\beta\alpha}_q\boldsymbol{\alpha}_l\boldsymbol{\alpha}_l\boldsymbol{\beta} = -\boldsymbol{\beta\beta\alpha}_q = -\boldsymbol{\alpha}_q$, which yields

$$\begin{aligned}\sum_{q\neq l} k_q k'_l d_-(\vec{k}) d_-(\vec{k}')\boldsymbol{\beta\alpha}_q\boldsymbol{\alpha}_l\boldsymbol{\alpha}_l\boldsymbol{\beta} + \sum_{j\neq l} k_l k'_j d_-(\vec{k}) d_-(\vec{k}')\boldsymbol{\beta\alpha}_l\boldsymbol{\alpha}_l\boldsymbol{\alpha}_j\boldsymbol{\beta}& \\ = -\sum_{q\neq l}\left(k_l k'_q d_-(\vec{k}) d_-(\vec{k}') + k_q k'_l d_-(\vec{k}) d_-(\vec{k}')\right)\boldsymbol{\alpha}_q = -\sum_{q\neq l} w^{lq}(\vec{k},\vec{k}')\boldsymbol{\alpha}_q \,.&\end{aligned} \tag{B.11}$$

The terms which consist of three different $\boldsymbol{\alpha}$ matricies can be reduced by $\boldsymbol{\beta\alpha}_q\boldsymbol{\alpha}_l\boldsymbol{\alpha}_j\boldsymbol{\beta} = -\boldsymbol{\beta\beta\alpha}_q\boldsymbol{\alpha}_l\boldsymbol{\alpha}_j = -\boldsymbol{\alpha}_q\boldsymbol{\alpha}_l\boldsymbol{\alpha}_j$. The remaining three $\boldsymbol{\alpha}$ matricies anti-commute with each other and are totally anti-symmetric with respect to their indices. Since this is a property of the totally anti-symmetric Levi-Civita tensor, one may write $\boldsymbol{\alpha}_q\boldsymbol{\alpha}_l\boldsymbol{\alpha}_j = \varepsilon_{qlj}\boldsymbol{\alpha}_1\boldsymbol{\alpha}_2\boldsymbol{\alpha}_3$. Furthermore, ε_{qlj} is zero if two indices are equal. Therefore, the sum over the terms in line (B.5c) with three different indices can be rewritten into

$$\begin{aligned}\sum_{\text{(see text)}} k_q k'_j d_-(\vec{k}) d_-(\vec{k}')\boldsymbol{\beta\alpha}_q\boldsymbol{\alpha}_l\boldsymbol{\alpha}_j\boldsymbol{\beta} = -\sum_{q,j} k_q k'_j d_-(\vec{k}) d_-(\vec{k}')\varepsilon_{qlj}\boldsymbol{\alpha}_1\boldsymbol{\alpha}_2\boldsymbol{\alpha}_3& \\ = \vec{e}_l\cdot(\vec{k}\times\vec{k}') d_-(\vec{k}) d_-(\vec{k}')\boldsymbol{\alpha}_1\boldsymbol{\alpha}_2\boldsymbol{\alpha}_3 = h^l(\vec{k},\vec{k}')\boldsymbol{\alpha}_1\boldsymbol{\alpha}_2\boldsymbol{\alpha}_3 \,,&\end{aligned} \tag{B.12}$$

where only terms with three different indices are counted in the sum of the first line. The identity $\vec{k}\times\vec{k}' = \varepsilon_{lqj}\vec{k}_q\vec{k}_j\vec{e}_l$ was used in the last but one step. Note, that $\boldsymbol{\alpha}_1\boldsymbol{\alpha}_2\boldsymbol{\alpha}_3$ equals $\mathrm{i}\boldsymbol{\gamma}^5$ of the Lorentz-kovariant Clifford algebra representation γ^μ. The results (B.5a), (B.9), (B.10) and (B.11) can be combined to

$$\begin{aligned}d_+(\vec{k}) d_+(\vec{k}')\boldsymbol{\alpha}_l - k_l k'_l d_-(\vec{k}) d_-(\vec{k}')\boldsymbol{\alpha}_l + \sum_{q\neq l} k_q k'_q d_-(\vec{k}) d_-(\vec{k}')\boldsymbol{\alpha}_l - \sum_{q\neq l} w^{lq}(\vec{k},\vec{k}')\boldsymbol{\alpha}_q& \\ = d_+(\vec{k}) d_+(\vec{k}')\boldsymbol{\alpha}_l - 2k_l k'_l d_-(\vec{k}) d_-(\vec{k}')\boldsymbol{\alpha}_l + \sum_q k_q k'_q d_-(\vec{k}) d_-(\vec{k}')\boldsymbol{\alpha}_l - \sum_{q\neq l} w^{lq}(\vec{k},\vec{k}')\boldsymbol{\alpha}_q& \\ = t(\vec{k},\vec{k}')\boldsymbol{\alpha}_l - \sum_q w^{lq}(\vec{k},\vec{k}')\boldsymbol{\alpha}_q \,.&\end{aligned} \tag{B.13}$$

The sum of the terms (B.8), (B.12) and (B.13) results in a transformed equation (B.5).

$$\boldsymbol{u}(\vec{k})\boldsymbol{\alpha}_l\boldsymbol{u}(\vec{k}')^\dagger = t(\vec{k},\vec{k}')\boldsymbol{\alpha}_l - \sum_q w^{lq}(\vec{k},\vec{k}')\boldsymbol{\alpha}_q + s^l(\vec{k},\vec{k}')\boldsymbol{\beta} + \sum_{q\neq l} r^q(\vec{k},\vec{k}')\boldsymbol{\beta\alpha}_q\boldsymbol{\alpha}_l + h^l(\vec{k},\vec{k}')\boldsymbol{\alpha}_1\boldsymbol{\alpha}_2\boldsymbol{\alpha}_3 \tag{B.14}$$

B.2 Verification of spinor properties

The spinors (3.37) are orthogonal and are eigen vectors of the free Dirac Hamiltonian $\boldsymbol{H}_0(\vec{k})$. This property is shown in terms of matrix relations in this section. In order to do so, the matrix relations (4.60) are employed with $\vec{k} = \vec{k}'$ for the left and right spin matrix. Therefore, the functions (4.59) need

to be evaluated for $\vec{k} = \vec{k}'$, resulting in

$$t(\vec{k},\vec{k}) = d_+(\vec{k})^2 + \vec{k}^2 d_-(\vec{k})^2 = 1\,, \tag{B.15a}$$

$$s^l(\vec{k},\vec{k}) = 2k_l d_+(\vec{k}) d_-(\vec{k}) = \frac{c\hbar k_l}{E(\vec{k})}\,, \tag{B.15b}$$

$$r^l(\vec{k},\vec{k}) = 0\,, \tag{B.15c}$$

$$w^{lq}(\vec{k},\vec{k}) = 2k_l k_q d_-(\vec{k}) d_-(\vec{k}) = w^{ql}(\vec{k},\vec{k})\,, \tag{B.15d}$$

$$g^{lq}(\vec{k},\vec{k}) = 0\,, \tag{B.15e}$$

$$h^l(\vec{k},\vec{k}) = 0\,. \tag{B.15f}$$

Inserting these coefficients into (4.60a) yields the orthonormality property of spinors in matrix notation.

$$\boldsymbol{u}(\vec{k})\boldsymbol{u}(\vec{k})^\dagger = \mathbf{1} \tag{B.16}$$

The contraction of the free Dirac Hamiltonian requires the evaluation of the term

$$\begin{aligned}
\sum_l \boldsymbol{u}(\vec{k})\boldsymbol{\alpha}_l\boldsymbol{u}(\vec{k})^\dagger k_l &= \sum_{l,q} k_l\boldsymbol{\alpha}_l t(\vec{k},\vec{k}) - k_l 2k_l k_q d_-(\vec{k})^2\boldsymbol{\alpha}_q + k_l\frac{c\hbar k_l}{E(\vec{k})}\boldsymbol{\beta} \\
&= \sum_l k_l\boldsymbol{\alpha}_l t(\vec{k},\vec{k}) - 2k_l\vec{k}^2 d_-(\vec{k})^2\boldsymbol{\alpha}_l + \frac{c\hbar\vec{k}^2}{E(\vec{k})}\boldsymbol{\beta} \\
&= \left(d_+(\vec{k})^2 - \vec{k}^2 d_-(\vec{k})^2\right)\vec{k}\cdot\vec{\boldsymbol{\alpha}} + \frac{c\hbar\vec{k}^2}{E(\vec{k})}\boldsymbol{\beta} = \frac{mc^2}{E(\vec{k})}\vec{k}\cdot\vec{\boldsymbol{\alpha}} + \frac{c\hbar\vec{k}^2}{E(\vec{k})}\boldsymbol{\beta}\,.
\end{aligned} \tag{B.17}$$

With this and equation (4.60b), the contraction of the free Hamiltonian $\boldsymbol{H}_0(\vec{k})$ results in the signed relativistic energy-momentum relation.

$$\begin{aligned}
\boldsymbol{u}(\vec{k})\boldsymbol{H}_0(\vec{k})\boldsymbol{u}(\vec{k})^\dagger &= \boldsymbol{u}(\vec{k})\left(c\hbar\vec{k}\cdot\vec{\boldsymbol{\alpha}} + \boldsymbol{\beta}mc^2\right)\boldsymbol{u}(\vec{k})^\dagger \\
&= c\left(\frac{mc^2}{E(\vec{k})}\hbar\vec{k}\cdot\vec{\boldsymbol{\alpha}} + \frac{c\hbar^2\vec{k}^2}{E(\vec{k})}\boldsymbol{\beta}\right) + mc^2\left(\frac{mc^2}{E(\vec{k})}\boldsymbol{\beta} - \frac{c}{E(\vec{k})}\hbar\vec{k}\cdot\vec{\boldsymbol{\alpha}}\right) \\
&= \boldsymbol{\beta}\left(\frac{c^2\hbar^2\vec{k}^2 + m^2c^4}{E(\vec{k})}\right) = E(\vec{k})\boldsymbol{\beta}\,.
\end{aligned} \tag{B.18}$$

Appendix C

Energy-momentum conservation

This appendix derives analytical formulas for the resonance condition from energy and momentum conservation, which is discussed geometrically in section 2.2. The conservation of energy of the incoming and outgoing electron, together with the absorbed and emitted photons can be written as

$$E(\vec{p}_{\text{out}}) = E(\vec{p}_{\text{in}}) + n_a\hbar\omega - n_e\hbar\omega\,. \tag{C.1}$$

The corresponding conservation of momentum reads

$$c\vec{p}_{\text{out}} = c\vec{p}_{\text{in}} + n_a\hbar\omega\vec{e}_1 + n_e\hbar\omega\vec{e}_1\,. \tag{C.2}$$

C.1 Non-relativistic energy-momentum conservation

If (C.2) is inserted in (C.1) and the non-relativistic energy-momentum relation (3.4) is used, one obtains

$$\left[\left(\frac{\hbar\omega}{c}(n_a+n_e)+p_{1,\text{in}}\right)^2 + p_{2,\text{in}}^2 + p_{3,\text{in}}^2\right]\frac{1}{2m} = \frac{p_{1,\text{in}}^2 + p_{2,\text{in}}^2 + p_{3,\text{in}}^2}{2m} + (n_a-n_e)\hbar\omega\,. \tag{C.3}$$

This can be rearranged to

$$\frac{\hbar^2\omega^2}{2mc^2}(n_a+n_e)^2 + \frac{\hbar\omega(n_a+n_e)p_{1,\text{in}}}{mc} = \hbar\omega\,(n_a-n_e)\;, \tag{C.4}$$

and devided by $\hbar\omega$

$$\frac{\hbar\omega}{2mc^2}(n_a+n_e)^2 + \frac{(n_a+n_e)p_{1,\text{in}}}{mc} = (n_a-n_e)\;. \tag{C.5}$$

A further rearrangement yields

$$\frac{\hbar\omega}{mc^2} = \left[-(n_a+n_e)\frac{p_{1,\text{in}}}{mc} + (n_a-n_e)\right]\frac{2}{(n_a+n_e)^2} \tag{C.6}$$

for the dimensionless energy or

$$\frac{p_{1,\text{in}}}{mc} = -\frac{n_a+n_e}{2}\frac{\hbar\omega}{mc^2} + \frac{n_a-n_e}{n_a+n_e}\,. \tag{C.7}$$

for the dimensionless initial electron momentum in laser propagation direction.

C.2 Relativistic energy-momentum conservation

One may also use the relativistic energy-momentum relation (3.22) in the combination of equation (C.1) and (C.2), resulting in

$$\sqrt{m^2c^4 + ((n_a + n_e)\hbar\omega + cp_{1,\mathrm{in}})^2 + c^2p_2^2 + c^2p_3^2} = \sqrt{m^2c^4 + c^2p_{1,\mathrm{in}}^2 + c^2p_2^2 + c^2p_3^2} + n_a\hbar\omega - n_e\hbar\omega \tag{C.8}$$

The momentum in 2 and 3-direction is absorbed in the increased mass

$$m'c^2 = \sqrt{m^2c^4 + c^2p_2^2 + c^2p_3^2}\,, \tag{C.9}$$

which is already introduced in section 2.2. The square of equation (C.8) is

$$\begin{aligned} m'^2c^4 + ((n_a + n_e)\hbar\omega + cp_{1,\mathrm{in}})^2 \\ = m'^2c^4 + c^2p_{1,\mathrm{in}}^2 + (n_a - n_e)^2\hbar^2\omega^2 + 2(n_a - n_e)\hbar\omega\sqrt{m'^2c^4 + c^2p_{1,\mathrm{in}}^2}\,. \end{aligned} \tag{C.10}$$

It is useful to perform the following side calculations for a further transformation of this equation.

$$((n_a + n_e)\hbar\omega + cp_{1,\mathrm{in}})^2 = n_a^2\hbar^2\omega^2 + n_e^2\hbar^2\omega^2 + c^2p_{1,\mathrm{in}}^2 + 2n_an_e\hbar^2\omega^2 + 2cp_{1,\mathrm{in}}(n_a + n_e)\hbar\omega \tag{C.11}$$

$$c^2p_{1,\mathrm{in}}^2 + (n_a - n_e)^2\hbar^2\omega^2 = c^2p_{1,\mathrm{in}}^2 + n_a^2\hbar^2\omega^2 + n_e^2\hbar^2\omega^2 - 2n_an_e\hbar^2\omega^2 \tag{C.12}$$

Inserting these side calculations in equation (C.10) results in

$$4n_an_e\hbar^2\omega^2 + 2cp_{1,\mathrm{in}}(n_a + n_e)\hbar\omega = 2(n_a - n_e)\hbar\omega\sqrt{m'^2c^4 + c^2p_{1,\mathrm{in}}^2}\,. \tag{C.13}$$

Dividing this by $2\hbar\omega$ yields

$$2n_an_e\hbar\omega + cp_{1,\mathrm{in}}(n_a + n_e) = (n_a - n_e)\sqrt{m'^2c^4 + c^2p_{1,\mathrm{in}}^2}\,. \tag{C.14}$$

This equation is squared again.

$$4n_a^2n_e^2\hbar^2\omega^2 + 4n_an_e\hbar\omega cp_{1,\mathrm{in}}(n_a + n_e) + c^2p_{1,\mathrm{in}}^2(n_a + n_e)^2 = (n_a - n_e)^2\left(m'^2c^4 + c^2p_{1,\mathrm{in}}^2\right) \tag{C.15}$$

Rearranging and dividing by $4n_a^2n_e^2m'^2c^4$ yields

$$\frac{\hbar^2\omega^2}{m'^2c^4} + \frac{\hbar\omega}{m'c^2}\frac{p_{1,\mathrm{in}}}{m'c}\frac{n_a + n_e}{n_an_e} + \frac{p_{1,\mathrm{in}}^2}{m'^2c^2}\frac{1}{n_an_e} - \frac{(n_a - n_e)^2}{4n_a^2n_e^2} = 0\,. \tag{C.16}$$

The dimensionless energy $\hbar\omega/m'c^2$ in this equation has the two solutions

$$\frac{\hbar\omega}{m'c^2} = \left[-(n_a + n_e)\frac{p_{1,\mathrm{in}}}{m'c} \pm |n_a - n_e|\frac{\sqrt{c^2p_{1,\mathrm{in}}^2 + m'^2c^4}}{m'c^2}\right]\frac{1}{2n_an_e}\,, \tag{C.17}$$

where the following expression appears in the square-root and is simplified to

$$\begin{aligned} &\left(c^2p_{1,\mathrm{in}}^2(n_a + n_e)^2 - 4n_en_ac^2p_{1,\mathrm{in}}^2 + (n_a - n_e)^2m'^2c^4\right)/4n_a^2n_e^2m'^2c^4 \\ &= \left(c^2p_{1,\mathrm{in}}^2(n_a - n_e)^2 + (n_a - n_e)^2m'^2c^4\right)/4n_a^2n_e^2m'^2c^4 \\ &= (n_a - n_e)^2\left(c^2p_{1,\mathrm{in}}^2 + m'^2c^4\right)/4n_a^2n_e^2m'^2c^4\,. \end{aligned} \tag{C.18}$$

Equation (C.16) has also two solutions for the dimensionless momentum $p_{1,\mathrm{in}}/m'c$

$$\frac{p_{1,\mathrm{in}}}{m'c} = -\frac{n_a + n_e}{2}\frac{\hbar\omega}{m'c^2} \pm \frac{|n_a - n_e|}{2}\sqrt{\frac{\hbar^2\omega^2}{m'^2c^4} + \frac{1}{n_a n_e}}\,, \tag{C.19}$$

where the following expression appears in the square-root and is simplified to

$$\begin{aligned}
&\left(\hbar^2\omega^2\left(n_a + n_e\right)^2 - 4n_e n_a\hbar^2\omega^2 + \frac{\left(n_a - n_e\right)^2}{n_a n_e}m'^2c^4\right)/4m'^2c^4 \\
&= \left(\hbar^2\omega^2\left(n_a - n_e\right)^2 + \frac{\left(n_a - n_e\right)^2}{n_a n_e}m'^2c^4\right)/4m'^2c^4 \\
&= \left(n_a - n_e\right)^2\left(\hbar^2\omega^2 + \frac{m'^2c^4}{n_a n_e}\right)/4m'^2c^4\,.
\end{aligned} \tag{C.20}$$

Bibliography

[1] Roberto Cecchini and Guiseppe Pelosi. Diffraction: The first recorded observation. *Antennas and Propagation Society, IEEE*, 32(2):27–30, Apr. 1990.

[2] Thomas Young. The Bakerian lecture. Experiments and calculations relative to physical optics. *Philosophical transactions of the Royal Society of London*, 94:1–16, Nov. 1803.

[3] Isaac Barrow, John Flamsteed, John Wallis, Sir Isaac Newton, and Augustus De Morgan. *Correspondence of Scientific Men of the Seventeenth Century*, volume 2. Oxford University Press, 1841. The letter from James Gregory to Collins, on 13th May 1673, at pages 251 to 255.

[4] Clinton Joseph Davisson and Lester Halbert Germer. The scattering of electrons by a single crystal of nickel. *Nature*, 119:558–560, Apr. 1927.

[5] George Paget Thomson and A. Reid. Diffraction of cathode rays by a thin film. *Nature*, 119:890–890, Jun. 1927.

[6] P. L. Kapitza and P. A. M. Dirac. The reflection of electrons from standing light waves. *Math. Proc. Cambridge Philos. Soc.*, 29(2):297–300, 1933.

[7] Klaus Hornberger, Stefan Gerlich, Hendrik Ulbricht, Lucia Hackermüller, Stefan Nimmrichter, Ilya V. Goldt, Olga Boltalina, and Markus Arndt. Theory and experimental verification of Kapitza-Dirac-Talbot-Lau interferometry. *New Journal of Physics*, 11(4):043032, 2009.

[8] H. Schwarz, H. A. Tourtellotte, and W. W. Gaertner. Direct observation of nonlinear scattering of electrons by laser beam. *Physics Letters*, 19(3):202–203, 1965.

[9] H. Chr. Pfeiffer. Experimentelle Prüfung der Streuwarscheinlichkeit für Elektronen beim Kapitza-Dirac-Effekt. *Physics Letters A*, 26(8):362–363, 1968.

[10] Yasutugu Takeda and Isao Matsui. Electron reflection by standing wave of giant pulse laser. *Journal of the Physical Society of Japan*, 25(8):1202–1202, 1968.

[11] Phillip L. Gould, George A. Ruff, and David E. Pritchard. Diffraction of atoms by light: The near-resonant Kapitza-Dirac effect. *Physical Review Letters*, 56(8):827–830, 1986.

[12] Peter J. Martin, Bruce G. Oldaker, Andrew H. Miklich, and David E. Pritchard. Bragg scattering of atoms from a standing light wave. *Physical Review Letters*, 60(6):515–518, 1986.

[13] P. H. Bucksbaum, D. W. Schumacher, and M. Bashkansky. High-intensity Kapitza-Dirac effect. *Physical Review Letters*, 61(10):1182–1185, 1988.

[14] Daniel L. Freimund, Kayvan Aflatooni, and Herman Batelaan. Observation of the Kapitza-Dirac effect. *Nature*, 413(6852):142–143, 2001.

[15] T. H. Maiman. Stimulated optical radiation in ruby. *Nature*, 187:493–494, 1960.

[16] Donna Strickland and Gerard Mourou. Compression of amplified chirped optical pulses. *Optics Communications*, 56(3):219–221, 1985.

[17] V. Yanovsky, V. Chvykov, G. Kalinchenko, P. Rousseau, T. Planchon, T. Matsuoka, A. Maksimchuk, J. Nees, G. Cheriaux, G. Mourou, and K. Krushelnick. Ultra-high intensity- 300-TW laser at 0.1 Hz repetition rate. *Optics Express*, 16(3):2109–2114, 2008.

[18] Th. Kuehl, R. Bock, and S. Borneis. PHELIX – status and first experiments. *Hyperfine Interactions*, 162:55–62, 2005.

[19] F. Amiranoff, F. Augé, H. Backe, et al. Proposal for a european extreme light infrastructure. Technical report, The extreme light infrastructure, Oct 2010. http://www.extreme-light-infrastructure.eu/pictures/ELI-scientific-case-id17.pdf.

[20] Y. Nomura, R. Hörlein, P. Tzallas, B. Dromey, S. Rykovanov, Zs. Major, J. Osterhoff, S. Karsch, L. Veisz, M. Zepf, D. Charalambidis, F. Krausz, and G. D. Tsakiris. Attosecond phase locking of harmonics emitted from laser-produced plasmas. *Nature physics*, 5(2):124–128, 2009.

[21] George D. Tsakiris, Klaus Eidmann, and Jürgen Meyer ter Vehn. Route to intense single attosecond pulses. *New Journal of Physics*, 8(1), Jan. 2006.

[22] L. Young, E. P. Kanter, B. Krässig, et al. Femtosecond electronic response of atoms to ultra-intense X-rays. *Nature*, 466:56 – 61, 2010.

[23] Massimo Altarelli, Reinhard Brinkmann, Majed Chergui, Winfried Decking, Barry Dobson, Stefan Düsterer, Gerhard Grübel, Walter Graeff, Heinz Graafsma, Janos Hajdu, Jonathan Marangos, Joachim Pflüger, Harald Redlin, David Riley, Ian Robinson, Jörg Rossbach, Andreas Schwarz, Kai Tiedtke, Thomas Tschentscher, Ivan Vartaniants, Hubertus Wabnitz, Hans Weise, Riko Wichmann, Karl Witte, Andreas Wolf, Michael Wulff, and Mikhail Yurkov, editors. *The European X-Ray Free-Electron Laser Technical design report*. DESY XFEL Project Group European XFEL Project Team Deutsches Elektronen-Synchrotron Member of the Helmholtz Association, Hamburg, 2007.

[24] Dan Freimund. *Electron matter optics and the Kapitza-Dirac effect*. PhD thesis, The Graduate College at the University of Nebraska, May 2003. http://www.unl.edu/amop/pdf_files/Daniel_L_Freimund_Dissertation.pdf.

[25] Sven Ahrens, Heiko Bauke, Christoph H. Keitel, and Carsten Müller. Spin dynamics in the Kapitza-Dirac effect. *Physical Review Letters*, 109(4):043601, 2012.

[26] V. G. Minogin, M. V. Fedorov, and V. S. Letokohov. Formation of ultrashort electron pulses on scattering of an electron beam by a standing laser wave of ultrashort duration. *Optics Communitations*, 140:250–254, Aug. 1997.

[27] H. Batelaan. The Kapitza-Dirac effect. *Contemporary Physics*, 41(6):369–381, 2000.

[28] M. V. Fedorov. Stimulated scattering of electrons by photons and adiabatic switching on hypothesis. *Optics Communitations*, 12(2):205–209, 1974.

[29] M. A. Efremov und M. V. Fedorov. Classical and quantum versions of the Kapitza-Dirac effect. *Journal of Experimental and Theoretical Physics*, 89(3):460–467, 1999.

[30] M. A. Efremov and M. V. Fedorov. Wavepacket theory of the Kapitza-Dirac effect. *Journal of Physics B*, 33(20):4535–4550, 2000.

[31] R. Gush and H. P. Gush. Electron scattering from a standing light wave. *Physical Review D*, 3(8):1712–1721, Apr 1971.

[32] Leonard Rosenberg. Effect of virtual Compton scattering on electron propagation in a laser field. *Physical Review A*, 49(2):1122–1130, 1994.

[33] Dong-Sheng Guo. Theory of the Kapitza-Dirac effect in strong radiation fields. *Physical Review A*, 53(6):4311–4319, 1996.

[34] Xiaofeng Li, Jingtao Zhang, Zhizhan Xu, Panming Fu, Dong-Sheng Guo, and R. R. Freeman. Theory of the Kapitza-Dirac diffraction effect. *Physical Review Letters*, 92(23):233603, 2004.

[35] V. M. Haroutunian and H. K. Avetissian. An analogue of the Kapitza-Dirac effect. *Physics Letters*, 51(6):320–322, 1975.

[36] M. V. Federov and J. K. McIver. Multiphoton stimulated compton scattering. *Optics Communications*, 32(1):179–182, 1980.

[37] Pedro Sancho. Two-particle Kapitza-Dirac diffraction. *Physical Review A*, 82(3):033814, 2010.

[38] D. L. Freimund and H. Batelaan. A microscopic Stern-Gerlach magnet for electrons? *Laser Physics*, 13(6):892–896, 2003.

[39] Leonard Rosenberg. Extended theory of Kapitza-Dirac scattering. *Physical Review A*, 70(6):023401, 2004.

[40] L. D. Landau and E. M. Lifshitz. *Mechanics*, volume 1. Elsevier, 3 edition, 1976.

[41] Paul Gibbon. *Short Pulse Laser Interactions with matter, An Introduction*. Imperial College Press, 2 edition, 2007.

[42] Arthur H. Compton. Secondary rediations produced by x-rays and some of their applications to physical problems. *Bulletin of the National Research Council*, 4(20), 1922.

[43] Louis de Broglie. *Recherches sur la théorie des quanta*. PhD thesis, La Sorbonne Paris, 1924.

[44] Franz Schwabl. *Quantenmechanik*, volume 1. Springer, 6 edition, 2002.

[45] Armin Wachter. *Relativistische Quantenmechanik*. Springer, 2005.

[46] Bernd Thaller. *Advanced Visual Quantum Mechanics*. Springer, 2005.

[47] Leslie L. Foldy and Siegfried A. Wouthuysen. On the Dirac theory of spin 1/2 particles and its non-relativistic limit. *Physical Review*, 78(1):29–36, 1950.

[48] E. de Vries. Foldy-Wouthuysen transformations and related problems. *Fortschritte der Physik*, 18(4):149–182, 1970.

[49] Silvan S. Schweber. *An introduction to relativistic quantum field theory*. Dover, 2005.

[50] Daniel L. Freimund and Herman Batelaan. Bragg scattering of free electrons using the Kapitza-Dirac effect. *Physical Review Letters*, 89(28):283602, 2002.

[51] Christof Wetterich. Theoretische quantenmechanik. Lecture notes, 2009. Department of physics and astronomy, Heidelberg.

[52] Marlan O. Scully and M. Suhail Zubairy. *Quantum Optics*. Cambridge University Press, 1997.

Danksagung

Zu allererst möchte ich meinem Betreuer Prof. Christoph H. Keitel herzlich danken, dass er mir die Möglichkeit gegeben hat, in seiner Arbeitsgruppe zu promovieren. Dies umfasst auch die vielen Tagungen und Konferenzen, die Sommer- und Winterschulen und Graduiertenseminare, die mein Verständnis von der Welt erweitert haben. Ich danke Prof. Keitel auch für den offenen und einfachen Umgangston, den ich sehr schätze.

Ich danke auch meinem Mitbetreuer Prof. Carsten Müller, der immer Zeit für mich hatte und mir mit ruhiger und besonnener Stimme in allen Lagen weiter geholfen und Mut zugesprochen hat. Ich danke ihm für das aufmerksame Zuhören, seine aufgeschlossene Art ohne die ich meine Arbeit wohl nur schwer hätte zu Ende führen können.

Ich danke zudem auch meinem Mitbetreuer Heiko Bauke, der immer Rücksprache mit mir gehalten hat und mir viele Möglichkeiten aufgezeigt hat, meine Arbeit zu verbessern. Seine Ratschläge haben die Struktur meiner Arbeit und auch die Struktur meines eigenen Arbeitens verbessert.

Herzlichen Dank möchte ich auch an Prof. Rainer Grobe und die Kollaboration mit ihm richten. Ich danke ihm für die freundlichen und aufgeschlossenen Diskussionen, die er mit mir geführt hat.

Ich danke auch meinen Eltern Gotthelf Ahrens und Marion Ahrens, die zwar physisch weit weg, aber im Geiste immer bei mir waren. Danke, dass ihr immer für mich da wart. Ebenso danke auch meinem Bruder Marco Ahrens, seiner Freundin Lena und meiner kleinen, lieben Nichte Klara.

Einen ganz besonderen Dank möchte ich auch meinem freundlichen Kollegen Matthias Ruf zusprechen, der mich auf seine erfrischende Art in schwierigen Phasen meiner Promotion immer wieder aufgepäppelt und einen lebensfrohen Menschen aus mir gemacht hat.

Einen großen Dank möchte ich auch an meinen Bürokollegen Wen-Te Liao richten, der mit der Reise nach Taiwan und vielen anderen Ausflügen in mir die wohl wertvollste Erinnerung in meiner Promotionszeit hinterlassen hat.

Ich danke auch meinen beiden anderen Bürokollegen Enderalp Yakaboylu and Felix Mackenroth für die schöne Arbeitsatmosphäre in meinem Büro.

Ein besonderes Dankeschön möchte ich auch an die Computeradministratoren Dominik Hertel, Peter Brunner und Frank Köck richten. Zum Einen für die Hilfestellung bei Computerproblemen aller Art, deren Lösung sie jeder Zeit bereitwillig in Angriff genommen haben, zum Anderen für die interessanten und unterhaltsamen Gespräche, die wir geführt haben.

Ich danke auch Markus Kohler für viele wichtige Tipps und Einsichten rund ums promovieren und die vielen Wettläufe.

Zudem danke ich Benjamin Galow, Kilian Heeg, Jonas Gunst und Carmen Leimer für das Korrekturlesen meiner Arbeit.

Ich möchte auch all meinen anderen Kollegen danken, insbesondere Sebastian Meuren, Martin Gärtner, Stefano Cavaletto, Sven Augustin, Stephan Helmrich, Norman Neitz, Anton Wöllert, Andreas

Reichegger, Lida Zhang, Huayu Hu, Sarah Müller, Michael Klaiber, Matteo Tamburini und Jörg Evers.

Außerdem danke ich meinen WG-Mitbewohnern insbesondere Philipp Paa, Kai Becker und Sebastian Richtarsky, deren Gespräche mich und meine Weltsicht während meiner Promotionszeit nachhaltig geprägt haben. Auch meine Freunde vom Tanzsport, vor allem Andre, Jürgen und Katja seien in diesem Zusammenhang dankend erwähnt.

Zudem auch großen Dank an meine ehemaligen Kommilitonen von der TU-Darmstadt. Es war insbesondere schön, einige von meinem Jahrgang des Sommersemesters 2004 auch während meiner Promotionszeit wieder gesehen zu haben – Hinter der grünen Tür!

Und natürlich danke ich auch meinen Rollenspielfreunden aus Wiesbaden, die seit meinem Studium einen wichtigen Ankerpunkt in meinem Leben bilden.

Zu guter Letzt möchte ich auch Marius Schollmeier danken, ohne welchem die vergangen drei Jahre meiner Promotion gar nicht erst stattgefunden hätten. Danke Marius!